Arnold Schwarzenegger
Governor

FIFTY-SEVEN YEAR CALIFORNIA REANALYSIS DOWNSCALING AT 10 KILOMETERS (CaRD10)

PIER PROJECT REPORT

Prepared For:
California Energy Commission
Public Interest Energy Research Program

Prepared By:
Masao Kanamitsu and Hideki Kanamaru
Scripps Institution of Oceanography
University of California, San Diego

March 2007
CEC-500-2006-071

California Climate Change Center
Report Series Number 2006-009

Prepared By:
Masao Kanamitsu and Hideki Kanamaru
Scripps Institution of Oceanography
University of California, San Diego

Corresponding author: Dr. Masao Kanamitsu, Mail Code 0224; CRD/SIO/UCSD; 9500 Gilman Drive; La Jolla, CA 92093-0224. E-mail: mkanamitsu@ucsd.edu

Contract No. 500-02-004
Work Authorization No. MR-025

Prepared For:
California Energy Commission
Public Interest Energy Research (PIER) Program

Guido Franco,
Contract Manager

Kelly Birkinshaw,
Program Area Manager
Energy-Related Environmental Research

Martha Krebs, Ph.D.
Deputy Director
ENERGY RESEARCH AND DEVELOPMENT DIVISION

B. B. Blevins
Executive Director

DISCLAIMER
This report was prepared as the result of work sponsored by the California Energy Commission. It does not necessarily represent the views of the Energy Commission, its employees or the State of California. The Energy Commission, the State of California, its employees, contractors and subcontractors make no warrant, express or implied, and assume no legal liability for the information in this report; nor does any party represent that the uses of this information will not infringe upon privately owned rights. This report has not been approved or disapproved by the California Energy Commission nor has the California Energy Commission passed upon the accuracy or adequacy of the information in this report.

Acknowledgments

This work was funded by the California Energy Commission Public Interest Energy Research (PIER) program, which supports the California Climate Change Center (Award Number MGC-04-04). The authors sincerely thank Guido Franco for his assistance in performing this research. We also would like to thank Dr. Dan Cayan for continuous encouragement throughout this study. We also thank Drs. Henry Juang and Yi-Feng Cui for converting the regional code to parallel machine. Without their contribution, this project would have been impossible. We also thank Ms. Mary Tyree and Mr. Steve Taylor for providing us observational data, and Drs. Marty Ralph and Paul Neiman for providing observational diurnal variation data from Piedras Blancas. The computations were performed at the National Center for Atmospheric Research, San Diego Supercomputer Center and University of Illinois Super Computing Center. The assistance of Ms. Diane Boomer in refining the writing is appreciated.

Please cite this report as follows:

Kanamitsu, M., and H. Kanamaru. 2007. *Fifty-Seven Year California Reanalysis Downscaling at 10 Kilometers (CaRD10).* Scripps Institution of Oceanography for the California Energy Commission, PIER Energy-Related Environmental Research. CEC-500-2006-071.

Preface

The Public Interest Energy Research (PIER) Program supports public interest energy research and development that will help improve the quality of life in California by bringing environmentally safe, affordable, and reliable energy services and products to the marketplace.

The PIER Program, managed by the California Energy Commission (Energy Commission), annually awards up to $62 million to conduct the most promising public interest energy research by partnering with Research, Development, and Demonstration (RD&D) organizations, including individuals, businesses, utilities, and public or private research institutions.

PIER funding efforts are focused on the following RD&D program areas:

- Buildings End-Use Energy Efficiency
- Energy-Related Environmental Research
- Energy Systems Integration
- Environmentally Preferred Advanced Generation
- Industrial/Agricultural/Water End-Use Energy Efficiency
- Renewable Energy Technologies

The California Climate Change Center (CCCC) is sponsored by the PIER program and coordinated by its Energy-Related Environmental Research area. The Center is managed by the California Energy Commission, Scripps Institution of Oceanography at the University of California at San Diego, and the University of California at Berkeley. The Scripps Institution of Oceanography conducts and administers research on climate change detection, analysis, and modeling; and the University of California at Berkeley conducts and administers research on economic analyses and policy issues. The Center also supports the Global Climate Change Grant Program, which offers competitive solicitations for climate research.

The California Climate Change Center Report Series details ongoing Center-sponsored research. As interim project results, the information contained in these reports may change; authors should be contacted for the most recent project results. By providing ready access to this timely research, the Center seeks to inform the public and expand dissemination of climate change information; thereby leveraging collaborative efforts and increasing the benefits of this research to California's citizens, environment, and economy.

The work described in this report was conducted under the Climate Data Collection, Analysis, and Modeling - Phase II contract, contract number 500-02-004, work authorization MR-025 by the Scripps Institution of Oceanography at the University of California, San Diego.

For more information on the PIER Program, please visit the Energy Commission's website www.energy.ca.gov/pier/ or contract the Energy Commission at (916) 654-5164.

Table of Contents

Preface.. ii
Abstract viii
Executive Summary 1
1.0 Introduction 3
2.0 Model and Dynamical Downscaling Procedure 4
2.1. The Regional Spectral Model 4
2.2. Model Domain and Topography 6
2.3. Scale Selective Bias Correction 6
2.4. Lateral Forcing, SST and Land Characteristics 9
2.5. Integration Procedure 10
3.0 Validation of the Downscaled Analysis Against Station Observations 14
3.1. Daily Scale 14
3.1.1. Wind over coastal ocean 14
3.1.2. Wind over Land 17
3.1.3. Daily Mean and Max/Min Temperature over Land 19
3.1.4. Precipitation over Land 26
3.2. Hourly Scale 26
3.3. Synoptic Examples 32
3.4. Monthly Averages 34
3.5. Trend 37
4.0 Comparison with North American Regional Reanalysis 46
5.0 Comparison of Precipitation with Gridded Analysis 56
6.0 Conclusions 63
7.0 Data Archive and Availability 65
8.0 References 70

List of Figures

Figure 1. CaRD10 domain and surface elevation 7

Figure 2. Vegetation type used in the downscaling. The color below the numbers on the color bar differentiate the vegetation classification (for example, classification number 10 as light yellow). See text for vegetation classification. 11

Figure 3. Soil type used in the downscaling 12

Figure 4. An example of vegetation cover used in downscaling (August). The color bar indicates vegetation cover in fraction. 13

Figure 5. Observation station locations used in downscaling validation. The stations in blue with circles are buoy observation (names begin with *b*; courtesy of Steve Taylor). The stations in black with square mark are the USHCN stations (names begin with *c, v, or m*) and the stations in brown with plus signs are from NCDC (three-letter abbreviation). The color bar indicates altitude in meters..... 15

Figure 6. Comparisons of the vector correlation on the left panels and vector root mean square error (RMSE) on the right panels of daily near surface wind analysis with buoy observations, for January (upper panels) and August (lower panels) of 2000. Note the significant increase (decrease) in the correlation (RMSE) from NNR (blue) to CaRD10 (green). 18

Figure 7. Same as Figure 5, but for land stations 19

Figure 8. Comparisons of the correlation (left panels) and root mean square error (RMSE) (right panels) of CaRD10 daily near surface temperature with station observations in January (upper panels) and August (lower panels) during 2000 20

Figure 9. Same as Figure 8, but for daily maximum temperature 21

Figure 10. Same as Figure 8, but for daily minimum temperature 22

Figure 11. CaRD10 bias of near surface daily mean (top), daily maximum (middle), and daily minimum (bottom) temperature at various observation stations for January (left) and Aug (right) during 2000. Station locations are shown in Figure 7. Note that max/min temperature information was not available for NARR. 24

Figure 12. Comparison of daily temperature range for January (upper panels) and July (lower panels) 1996. Left observation (courtesy of Mary Tyree), and right CaRD10. 25

Figure 13. Comparison of the monthly composited diurnal variation of near surface winds for each month in 2000 and 2001 at buoy station b25. Black lines are observation and red lines are CaRD10 27

Figure 14. Same as Figure 13 but for buoy b42 28

Figure 15. Same as Figure 13, but for buoy b47 28

Figure 16. Same as Figure 13, but for buoy b63 29

Figure 17. Comparison of the monthly composited diurnal variation of near surface wind vector for each month in 2000 at buoy station b25. Black arrows are observation and red arrows are CaRD10. 29

Figure 18. Same as Figure 17, but for buoy b42 30

Figure 19. Same as Figure 17, but for buoy b47 30

Figure 20. Same as Figure 17, but for buoy b63 31

Figure 21. Validation of composite diurnal variation of wind and wind speed at Piedras Blancas (35N, 121.3W) 31

Figure 22. An example of the Catalina Eddy appeared in the CaRD10 at 1500UTC on May 22, 1984 33

Figure 23. An example of the evolution of Coastally Trapped Wind Reversal on July 21 to 22, 1996 34

Figure 24. An example of Santa Ana events, 00Z October 26, 2003 35

Figure 25. Correlation of monthly mean daily mean temperature with observation for the period 1948–1996 36

Figure 26. Correlation of monthly mean daily maximum temperature with observation for the period 1948–1996 36

Figure 27. Correlation of monthly mean precipitation with observation for the period 1948–1996 37

Figure 28. Variation of correlation of monthly mean temperature with observation for the period 1948–1996 at coastal (c1 to c3), central valley (v1 to v6), and mountain (m1 and m2) stations 39

Figure 29. Variation of correlation of monthly mean daily max temperature with observation for the period 1948–1996 at coastal (c1 to c3), central valley (v1 to v6), and mountain (m1 and m2) stations 40

Figure 30. Variation of correlation of monthly mean precipitation with observation for the period 1948–1996 at coastal (c1 to c3), central valley (v1 to v6), and mountain (m1 and m2) stations 41

Figure. 31. CaRD10 1950–1996 trend of 2-meter temperature for January (left) and July (right) 42

Figure 32. Comparison of 1950–1997 trend of near surface temperature between CaRD10 (left) and R1 (right) for January (bottom) and August (top) 43

Figure 33a. Seasonal variation of monthly averaged precipitation in CaRD10 at 11 selected observation locations. Black lines are for the period 1950–1974 and red lines for 1975–1996. The horizontal lines are the annual averages. 44

Figure 33b. Same as Figure 332a, but from station observation 45

Figure 34a. Comparison of January mean 2-meter temperature between CaRD10 (left) and NARR (right) 47

Figure 34b. Same as Figure 34a, but for July..... 47

Figure 35a. Comparison of January mean 10-meter wind vector between CaRD10 (left) and NARR (right) 48

Figure 35b. Same as Figure 35a, but for July..... 48

Fig**ure** 36a. Comparison of January mean precipitation between CaRD10 (left) and NARR (right)..... 49

Figure 36b. Same as Figure 36a, but for July..... 50

Figure 37a. Comparison of January mean soil moisture between CaRD10 (left) and NARR (right)..... 51

Figure 37b. Same as Figure 37a, but for July..... 51

Figure 38a. Comparison of surface evaporation (January) between CaRD10 (left) and NARR (right)..... 52

Figure 38b. Same as Figure 38a, but for July..... 53

Figure 39. Comparison of mean diurnal variation of near surface winds in July between CaRD10 (left) and NARR (right) 54

Figure 40a. Comparison of 1979–2002 trend between CaRD10 (left), NARR (center) and R1 (right) in January..... 55

Figure 40b. Same as Figure 40a, but for August..... 55

Figure 41. Comparison of the precipitation bias against PRISM analysis for CaRD10 (top), NARR (middle), and NRR (bottom) in January (left column) and August (right column). Unit in mm/day. **57**

Figure 42. Comparison of the temporal correlations of monthly mean precipitation against PRISM analysis in January (left column) and August (right column) for CaRD10 (top), NARR (middle), and NRR (bottom) computed for 1979–2002 period 60

Figure 43. RMS difference of monthly average precipitation between CaRD10 (top), NARR (middle), and R1 (bottom) with PRISM analysis. Left column is for January and right column is for August. 61

Figure 44. Comparison of 1950–1997 trend in January mean precipitation rate, PRISM (left), and CaRD10 (right). Unit is in mm/day/decade. 62

List of Tables

Table 1. Physics of the regional spectral model 5

Table 2.a Buoy station locations 16

Table 2.b Stations for monthly analysis (data obtained from United States Historical Climatology Network) 16

Table 2.c Airport stations for daily analysis (data obtained from NCDC) 17

Table 3. Mean vector anomaly correlation and RMSE of winds of three analyses and fifteen buoy observations during 2000 17

Table 4. Mean vector anomaly correlation and RMSE of winds of three analyses and twelve land station observations during 2000 18

Table 5. Mean correlation and RMSE of daily mean temperature and max/min temperature of three analyses and twelve land station observations during 2000 ... 23

Table 6. Mean bias of daily mean temperature and max/min temperature of three analyses and twelve land station observations during 2000 23

Table 7. Correlation and bias (in mm/day) between CaRD10 and daily station observation of precipitation for 6 selected stations in California in January and August for the period 1948–2003 26

Table 8. Comparison of 1950–1996 trend in monthly mean near surface temperature between observation and CaRD10 38

Table 9. Daily precipitation skill scores of NARR and CaRD10 in January and August of 1998 against Higgins analysis 59

Table 10. List of pressure level variables in the output file 65

Table 11. List of pressure levels 66

Table 12. List of non-pressure level variables in the output file 67

Table 13. Data volumes for various types of outputs 69

Abstract

For the purpose of producing datasets for regional-scale global change research and application, the National Centers for Environmental Prediction (NCEP)/National Center for Atmospheric Research (NCAR) Reanalysis for the period 1948–2005 was dynamically downscaled to hourly, 10 kilometer (km) resolution over California using the Regional Spectral Model. In order to maintain the large-scale features of the Reanalysis, the Scale Selective Bias Correction has been applied to minimize the large-scale errors. Extensive validation of the downscaled analysis was performed using station observations and gridded precipitation analyses. The downscaled near-surface wind, temperature, and precipitation fit better with regional-scale station observations than the Reanalysis used to force the regional model. This advantage of the downscaling was found on all time scales, ranging from hourly to decadal scales. The 10 km resolution made the analysis over land fit even better than North American Regional Reanalysis, which is performed with 32 km resolution with observations assimilated. However, the downscaling suffers from positive bias in precipitation for heavy precipitation. The analyses are also inaccurate near the lateral boundary. The apparent advantage of the dynamical downscaling upon the statistical downscaling method is that all variables in the downscaled analysis are dynamically, physically, and hydrologically consistent. The dataset is freely available to the public.

Keywords: Reanalysis, downscaling, NCEP, NCAR, CaRD10, regional spectral model, RSM, PRISM, NARR

Executive Summary

Introduction

The PIER Climate Change Research Center (Center) plans to develop probabilistic climate projections for California at adequate levels of temporal and geographical resolution for both impacts and adaptation studies and long-term state planning, such as the State Water Plan. Before these projections can be developed, however, it is necessary to determine the performance of the tools used to translate the results from global climate models to regional scales such as California. The Regional Spectral Model (RSM), a regional climate model, is one of the tools that the Center will use to develop climate projections for California.

Regional Climate Models such as RSM are able to simulate historical weather conditions extremely well when they assimilate or use meteorological observations from ground-level stations and satellites. However, observations are not available to simulate future climate conditions in California, so it is also necessary to ensure that the regional climate models also perform reasonably well without the guidance of measured meteorological observations.

Project Objectives

Project objectives were to:

- Conduct a path-breaking, long-term simulation for California for the last 57 years at a very high resolution (10 kilometers, km) to determine how well the RSM simulate historical conditions.
- Verify that the model is able to simulate historical conditions fairly well without using meteorological observations to fine-tune it.
- Determine any model deficiencies that should be corrected before the model is used to estimate future climatic conditions in the state.

Project Approach

The research team used the RSM model to recreate California's climate for the time period of 1948 to 2005. Various climatic parameters such as temperature, wind speed and direction, and precipitation were compared with observations from that time period and with the output of another meteorological model that was fine-tuned to replicate historical observations, to determine the accuracy of the RSM's downscaled meteorological outputs.

Project Outcomes

The data from the 10 km, hourly downscaling of the RSM model over the West Coast from 1948 to 2005 agree well with the available observations, with the exception of large precipitation events, where the model overestimates precipitation amounts.

The downscaled RSM meteorological model fits the observations better than the coarse-resolution meteorological model that is currently available. The RSM model's 10 km downscaling is now available for the period 1948 to 2005. The outputs contain various meteorological values (such as temperature, wind speed, direction, and precipitation) and land values (such as soil temperature and moisture) that were estimated for every hour of that period. These data are publicly accessible through the Internet.

Conclusions

This downscaled analysis is considered to be useful for regional climate research and application, and its use is highly encouraged, with the caveat that the downscaled analysis is not perfect (especially for large precipitation events). Because this model reproduced the historical climate of California so well, it should be ideal for use in predicting California's future climate.

Recommendations

It is recommended that the downscaled analysis be further refined to reduce the errors observed in the precipitation values. This work is under way.

Benefits for California

This is the first time that a high-resolution, long-period "analysis" of a large number of meteorological and surface variables over California is available. Because this downscaled analysis has shown that it can reproduce historical climatic variables as well as or better than the current coarse-grid climate models, it will enable researchers to more fully investigate the affects of greenhouse gas emissions on California's future climate.

1.0 Introduction

Climate research, particularly the application studies for water, agriculture, forestry, fishery, and energy management require fine-scale, multi-decadal information of meteorological, oceanographic, and land states. Unfortunately, spatially and temporally homogeneous multi-decadal observations of these variables in high horizontal resolution are nonexistent. Some long-term surface records of temperature and precipitation exist, but the number of observation are very limited and the measurements are often contaminated by the changes in instrumentation over time. Some climatologically important variables, such as soil moisture, surface evaporation, and radiation are not even measured on most of the continental United States and around the globe.

Reanalysis is one way to obtain long term homogeneous analysis of needed variables. Unfortunately, the horizontal resolution of reanalysis is on the order of 100 to 200 kilometers (km)—too coarse for many application studies. Recently, regional reanalysis over the continental United States was conducted (North American Regional Reanalysis, NARR) (Mesinger et al. 2006). The horizontal resolution of 32 km and the duration of 25 years used in that study are still not completely satisfactory for application requirements, but the product is definitely valuable. Exciting results are expected soon from studies using the NARR.

This paper presents another attempt to produce even higher resolution regional reanalysis over a longer period for the State of California, using a dynamical downscaling technique. This method (hereafter called *CaRD10*) is based on the concept that small-scale detail can be attained by laterally forcing a high-resolution regional model with large-scale analysis. The major assumptions in this process are that the small-scale features are purely forced by large-scale motions and that the small-scale motions never feed back to the large scale. This assumption holds well when the large scale forcing is strong (e.g., during winter and transient seasons), but may fail when the forcing is weak (e.g., during summer). The essential difference between the dynamical downscaling method and data assimilation, which is used in NARR and in all the global reanalyses, is that dynamical downscaling does not utilize station observations to correct model forecast error. In this context, the dynamical downscaling can be referred to as "regional data assimilation without observation" (von Storch et al. 2000). As described later, dynamical downscaling can be improved by forcing the large scale part of the field *within* the regional domain. This process reduces the forecast error of the "large scale" part of the regional model. Therefore, the dynamical downscaling can better be referred to as "regional data assimilation without *regional* scale observation."

This paper is organized as follows: Section 2 discusses details of the model and downscaling procedures. Section 3 presents validation of the analysis based on station observation. Section 4 discusses comparison to NARR. Section 5 compares precipitation with gridded observed precipitation analysis, PRISM (Precipitation-elevation Regression Independent Slopes Model) and Higgins data (Higgins et al. 2000). Section 6 concludes the paper, and Section 7 describes data availability.

2.0 Model and Dynamical Downscaling Procedure

2.1. The Regional Spectral Model

The Regional Spectral Model (RSM) (Juang and Kanamitsu 1994) is used in this study. The model originates from the one used at the National Centers for Environmental Prediction (NCEP), but the code was updated with greater flexibility and much higher efficiency (Kanamitsu et al. 2005). The RSM utilizes a spectral method (with sine and cosine series) in two dimensions. A unique aspect of the model is that the spectral decomposition is applied to the difference between the full field and the time-evolving background global analysis field. Hereafter, this difference is called *perturbation*, and the background global analysis is called *base*. The horizontal derivatives that appear in the dynamical forcing terms in the prediction equations are computed for perturbation spectral coefficients and the base field separately, and are summed to obtain the total forcing. The transform method of Orszak (1970) is used to evaluate quadratic nonlinear terms for both perturbation and the base field. For the forcing due to nonlinear physical processes, the sum of the perturbation and base field (total field) on the transform grid is used. After the time derivative is computed as a sum of dynamical and physical forcing terms, the perturbation tendency is computed as a difference between total tendency and the base field tendency (assumed to be constant for the available time interval of the back ground field, namely six hours). This perturbation tendency is numerically filtered using sine and cosine series, and then is used to advance the spectral coefficients of perturbation in time. This procedure mimics the prediction of perturbations, but it is not the perturbation equation that is integrated in time. The procedure is probably better named the *optimum spectral perturbation filtering method*, in which full field minus base field (both of which are defined within the domain) is used to apply sine and cosine filter.

The model equations consist of a momentum equation, a thermodynamic equation, a mass conservation equation, and a moisture equation. The primitive equation system is used, in which vertical motion is diagnosed rather than predicted. This system of equations is based on an approximation that the horizontal scale is larger than the vertical scale. This approximation places a limit to the use of horizontal resolution depending on the vertical scale of the phenomena. The regional scale phenomena, such as sea breeze, mountain-valley breeze, and many of the flow regimes appearing along the coast of California are confined within the marine boundary layer and have the vertical scale of 1–3 km. Therefore, the horizontal grid size of the quasi-hydrostatic equation model can be as small as 5–10 km. On the contrary, the deep convective system which appears in the summertime over the Midwest has a vertical scale of more than 10 km and therefore, the horizontal resolution of 50 km or larger is preferred. For the downscaling performed in this study, a horizontal resolution of 10 km is used. Because of the use of Mercator projection, the physical grid size varies with latitude, and the smallest grid distance can be as short as 7 km in the domain chosen for this study. The use of this rather high resolution is based on the dominance of a relatively small vertical scale of phenomena in the region of interest. The choice is also based on the more practical desire for water management application that will resolve complex topography in California as much as possible.

The only difference in the dynamical core used in this study from the original RSM is the application of a process-splitting time scheme (Williamson 2002), in which physical processes are computed in parallel with the dynamical forcing terms, as opposed to computing them in a serial manner. This scheme saves considerable computational time for parallel computing because it reduces the communication between the processors by as much as a factor of two. The time-scheme slightly increases precipitation, but the difference is found to be sufficiently small. Other details of the parallelization and optimization of the model are described in Kanamitsu et al. (2005).

The physical processes included in the model are listed in Table 1. Among these processes, particular mention will be given to the Oregon State University Land Scheme (Pan and Mahrt 1987) and the radiation. The land scheme consists of two soil layers, 10 centimeters (cm) and 190 cm thick, where soil moisture and soil temperature are predicted. Evaporation from the land surface is divided into two parts: direct evaporation and transpiration. The formula of Chen and Dudhia (2001a, b) is used for direct evaporation (Kanamitsu and Mo 2003). The snow model is a simple 1-layer energy balance model. Specifications of the land surface characteristics are described in Section 2.4. Other details of the scheme are described in Chen et al. (1996).

Table 1. Physics of the regional spectral model

	Parameterization	Reference
Convection	Relaxed Arakawa Schubert	Moorthi and Suarez (1992)
Large scale condensation	Evaporation of rain included	
Shallow Convection	Tiedtke scheme	Tiedtke (1983)
Boundary Layer	Non-Local scheme	Hong and Pan (1996)
Surface Layer	Monin-Obukhov	
Long wave radiation	M.-D. Chou	Chou and Suarez (1994)
Short wave radiation	M.-D. Chou	Chou and Lee (1996)
Cloud	Slingo	Slingo (1987)
Gravity wave drag	Pierrhumbert	Alpert et al (1988)
Vertical Diffusion	Richardson number dependent	
Land model	OSU	Pan and Mahrt (1987)
Land characteristics	USGS	
Direct evaporation	NCAR	Chen et al. (1996)
Topography	Smoothed mean from USGS GTOPO30	

Both short- and long-wave radiation schemes are taken from M.-D. Chou (Chou and Suarez 1994; Chou and Lee 1996). The CO_2 concentration is fixed at 348 parts per million (ppm) throughout the 50-plus years of integration. The effect of aerosol is included, but a fixed seasonal climatological value by Koepke et al. (1997) is used. As will be mentioned later in Section 2.3, since area average temperature and moisture in the regional domain is forced to match those of the Reanalysis by Scale Selective Bias Correction, the effects of CO_2 and aerosol on free atmosphere in the downscaled analysis of these variables will be minimal, but the surface fluxes will certainly be affected. Thus the CO_2 concentration will probably change the surface temperature, evaporation and sensible heat, and eventually impact the land states, such as soil moisture and snow. This is one of several simplifications made in this downscaling and caution needs to be exercised when the downscaled products are used for diagnostics and application.

Cloudiness is computed from relative humidity and vertical motion, as well as from marine boundary layer depth and intensity (Slingo 1987). These clouds interact with the radiation scheme.

The physical parameterization schemes used in RSM are fully tested in global model with ensemble Atmospheric Model Intercomparison Project (AMIP)-type runs. The skill of the simulation is reasonable and comparable to many other global models (Robertson et al. 2004). For the application of the model to high-resolution regional downscaling, no explicit tunings of the physical processes are performed. The results of this lack of the tuning will be seen in some of the biases which appear in the simulation.

2.2. Model Domain and Topography

The model domain is shown in Figure 1. The Mercator projection true at 60N is used in this study. The domain covers the area from 29.466N to 45.719N, and 128.203W to 111.563W. The model coastline and surface elevation are also shown in Figure 1. This domain is selected to focus on the State of California and the neighboring states, but it also incorporates requests from the ocean research community. Note that the major limiting factor of the domain size is computer resource availability. Unfortunately, the choice of the domain affected simulation of winds and precipitation associated with the summertime southwest monsoon in the southeastern part of the domain, due to the lateral boundary placed just at the northern end of the Gulf of California (as shown later). It should also be noted that the lateral boundary nudging zone extends to approximately 20–25 grid points from the boundary, further reducing the useable domain. These limitations will hopefully be remedied in the simulations over a much wider area, currently in progress in collaboration with the Earth Simulator Center in Japan.

2.3. Scale Selective Bias Correction

The accuracy of the dynamically downscaled analysis depends on two factors: (1) the assumption of one-way interaction, and (2) the accuracy of the regional model itself. The former is a fundamental assumption in dynamical downscaling, which sets the theoretical limit to the methodology. The latter factor consists of inaccuracies due to numerics (accuracy of the discretization method, and the treatment of the time evolving lateral boundary conditions) and inaccuracies of the physical processes. These

inaccuracies can be reduced in principle by improving each component, but this requires diligent and continuous efforts, as seen from the fact that many operational numerical forecast centers are spending most of their resources for this sole purpose.

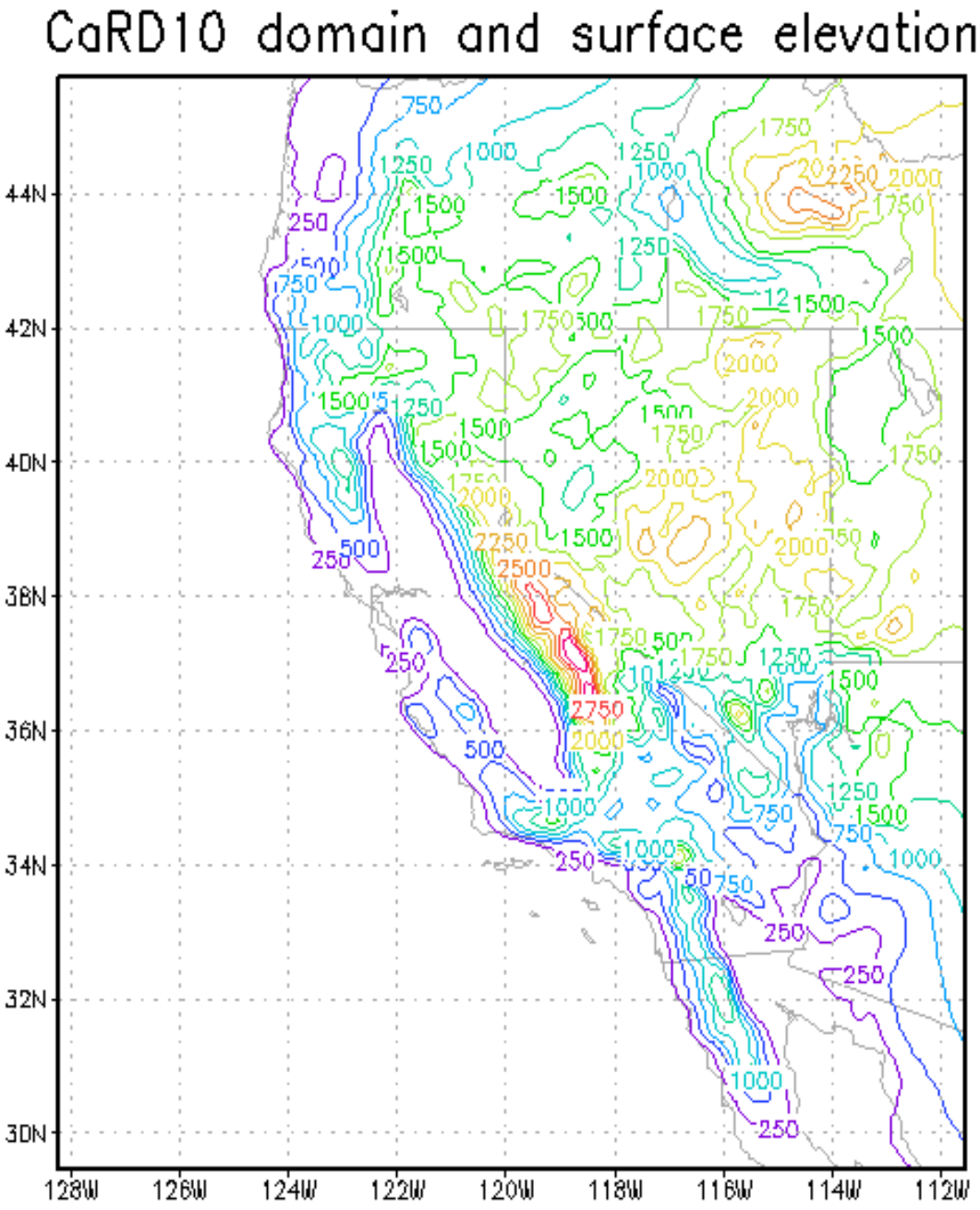

Figure 1. CaRD10 domain and surface elevation

In an attempt to reduce the model error, the research team supposed that the growth of *large scale error* spanning the regional domain is the major cause of inaccuracies in the

dynamical downscaling procedure, because large scale has large spatial and temporal variance. For example, the large-scale error would appear as errors in the phase and amplitude of large-scale features, such as the location and strength of a synoptic scale trough. The error in this scale causes significant error in the large-scale part of the mesoscale features (such as the location of the front). Several studies have noted poor accuracy of dynamically downscaled analysis (e.g., Roads et al. 2003), which this study's authors consider to be due mostly to the large-scale error.

An alternative to reducing the error in the regional model is to "nudge" the regional solution to "truth." This requires knowledge of "truth," and for the downscaling of global analysis, the truth is known on spatial scales for which the global data assimilation system provides accurate analysis (more precisely, the analysis with error small enough to be within the error of observations). This scale is a function of the average distance of the observation stations, observational error of various observation systems used in assimilation, and the resolution of the data assimilation model and analysis system. Considering that the average distance of sounding observation in the United States is approximately 250 km (Archer and Jacobson 2003), the scale for which the global analysis is accurate over the United States is considered to be 300–400 km. In the present study, since the domain includes ocean area, and since radiosonde observation density is less in the early 1950s, 1000 km is chosen as the scale for which reanalysis is considered to be "true."

The research team specifically designed a scale selective bias correction scheme (SSBC), which effectively reduces the error of scales larger than 1000 km (Kanamaru and Kanamitsu 2006). The scheme consists of three components: (1) nudging of the large-scale part of the wind error (deviation) towards zero, which is accomplished by adding a term in the momentum equation to reduce the tendency of the large scale part of the perturbation, (2) removal of the area average deviation of temperature and moisture at every model level, and (3) adjusting the logarithm of surface pressure to the corresponding pressure difference between the global and regional topography. The combination of these procedures reduces the large-scale error and improves the simulation of precipitation, and the downscaling becomes insensitive to the model domain (Kanamaru and Kanamitsu 2006). As an additional merit, the lateral boundary nudging can be considerably reduced.

It should be mentioned here that the reduction of the large-scale error in the regional domain can be achieved by reinitializing the regional model frequently, such that the large-scale error does not fully develop during the downscaling integration (Qian et al. 2003). The weakness of the method is the time required for the regional detail to spin-up, which may take up to 48 hours of integration. Another shortcoming is the discontinuity generated by the frequent start-up. The evolution of the land parameters also causes problems, because fine-resolution observed land initial condition is not available and the land condition needs to be spun-up every time the integration starts.

Note that in case of the downscaling global forecast or simulations (such as global warming), the error in the lateral boundary forcing will become another source of error, but use of global analysis eliminates this problem.

2.4. Lateral Forcing, SST and Land Characteristics

The lateral forcing is taken from NCEP/NCAR[1] 50-year reanalysis (Kalnay et al. 1996), which is the only reanalysis that goes back to the late 1940s. The 6-hourly reanalysis at model sigma levels is used to force the regional model. The RSM model levels are chosen to match the Reanalysis model levels, such that vertical interpolation is avoided. The tendency of the global field is assumed to be constant during the 6 hours.

The European Centre for Medium-Range Weather Forecasts (ECMWF) 40-year Reanalysis Sea Surface Temperature (SST) is used in the downscaling. This SST (Fiorino 2004) is a combination of the SST analysis from the United Kingdom Meteorological Office (monthly mean HaDISST, prior to and including 1981) and the U.S. National Centers for Environmental Prediction (weekly NCEP 2DVAR SST, after 1982 inclusive) cleaned up at the ice edges and interpolated to daily analysis using the mean conserving interpolation scheme (Taylor et al. 2000).

Land characteristics—namely vegetation, cover, and soil types—are taken from the United States Geophysical Survey compilation. The original 10-min resolution data were resampled to 30 min resolution to reduce the data volume size and were then utilized in the downscaling. The Oregon State University Land Model used in this study recognizes 12 types of vegetation:

1. mixed farming tall grassland
2. tall/medium grassland, shrubland
3. short grassland meadow and shrubland
4. tundra
5. sandy desert
6. rocky desert
7. tropical evergreen broadleaved forest
8. evergreen forest, needle-leaved forest
9. medium grassland, woodland
10. deciduous forest
11. mixed deciduous and evergreen forest
12. ice

[1] National Centers for Environmental Prediction/ National Center for Atmospheric Research

It also recognizes 16 types of soil:

1. sand
2. loamy sand
3. sandy loam
4. silt loam
5. silt
6. loam
7. sandy clay loam
8. silty clay loam
9. clay loam
10. sandy clay
11. silty clay
12. clay
13. organic materials
14. water
15. bedrock
16. other (land-ice)

For the vegetation cover, seasonally varying climatology is used. The vegetation type, soil type and vegetation cover in summer are shown in Figure 2 through Figure 4.

Soil moisture and soil temperature are predicted by the model during the nesting period of six hours. These predicted values are carried to the next nesting period, thus they evolve with time during the entire period of downscaling and interact with near surface atmosphere. No attempt to prevent the land state from drifting to its own climatology was made. As shown later, no apparent drift was observed during the 50 years of downscaling.

The topography is taken from the GTOPO30 global digital elevation model and interpolated directly to the model grid. The variance of topography used in the gravity wave drag parameterization (Alpert 1988) is computed as a variance of 30 minute topography within the regional model grid of 10 km.

2.5. Integration Procedure

The downscaling is performed in three streams: 1948–1969, 1968–1989, and 1988–2005. The initial condition of the atmosphere and land is taken from the global Reanalysis at 00UTC on January 1, 1948, linearly interpolated to a regional model grid. In order to avoid spin-up of soil moisture, the three streams overlap over two years: 1968–1969 and 1988–1989. The discontinuity in soil moisture after the two-year overlap becomes small. The research team compared several grid point values of volumetric soil moisture in the layer 10–200 cm between the long continuous RSM run and the NCEP/NCAR Reanalysis interpolated to regional grid, which is as large as 0.25, but the discontinuity between restart and continuous runs reduced to 0.005 or less after two years.

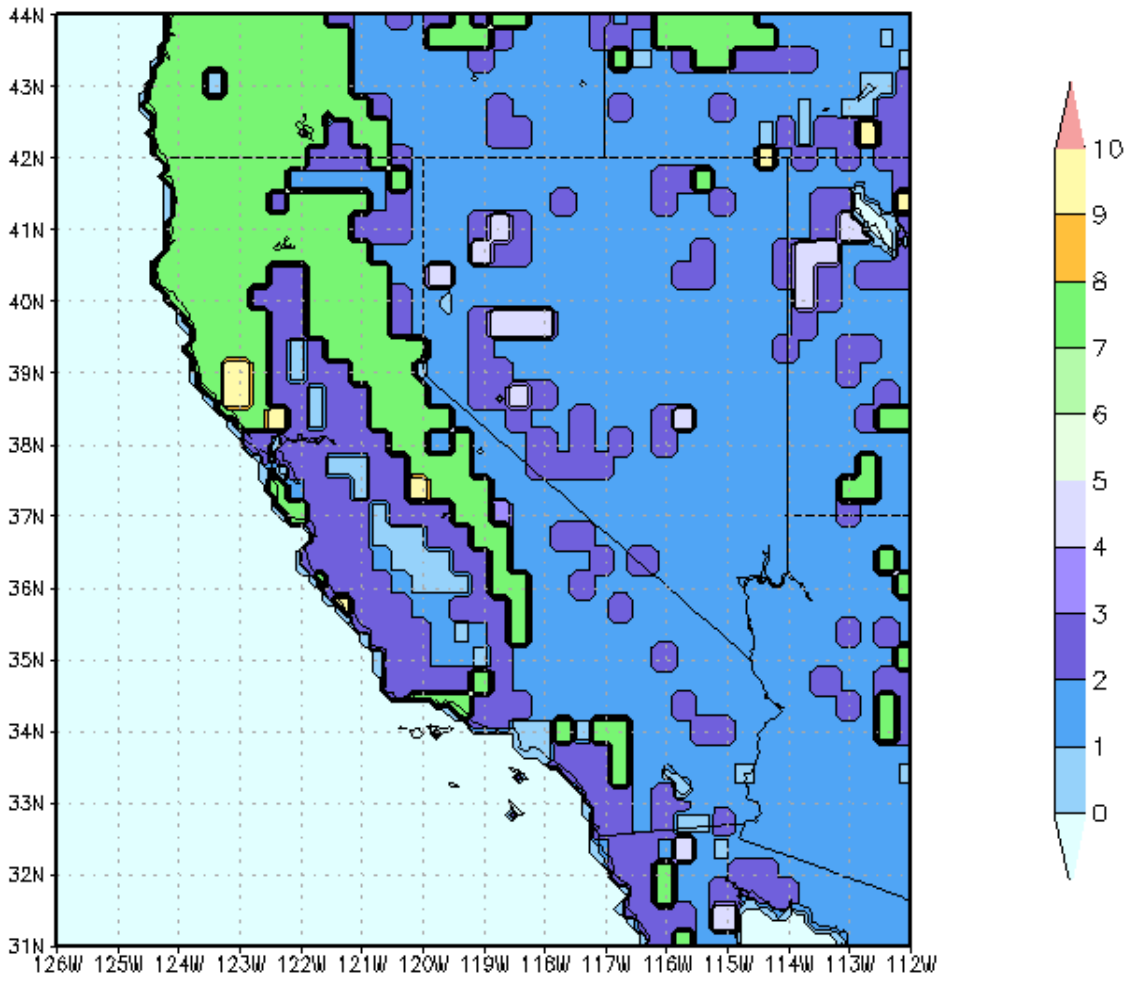

Figure 2. Vegetation type used in the downscaling. The color below the numbers on the color bar differentiate the vegetation classification (for example, classification number 10 as light yellow). See text for vegetation classification.

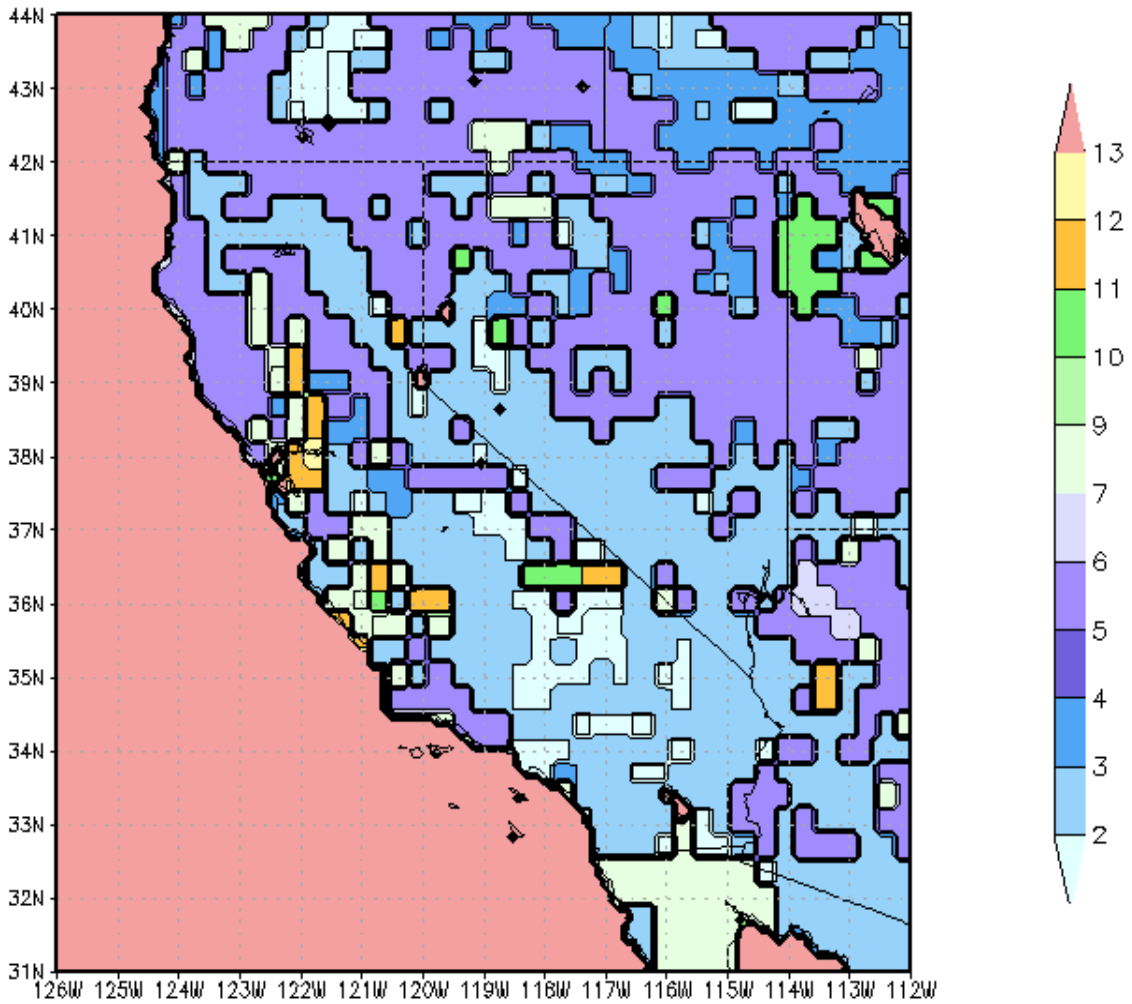

Figure 3. Soil type used in the downscaling. The color below the numbers on the color bar differentiate the soil type classification (for example, classification number 13 as light yellow). See text for soil type classification.

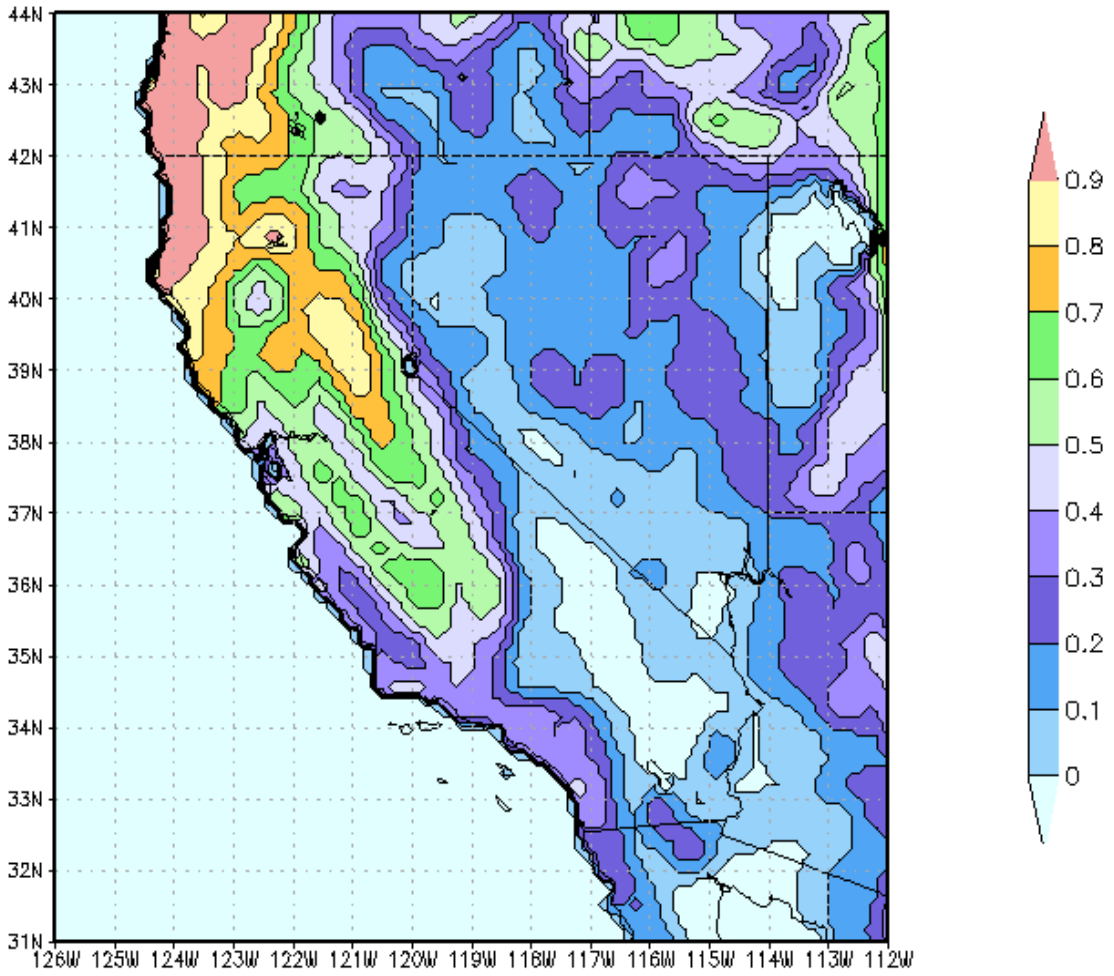

Figure 4. An example of vegetation cover used in downscaling (August). The color bar indicates vegetation cover in fraction.

3.0 Validation of the Downscaled Analysis Against Station Observations

The key to the success of the downscaling is to demonstrate that the downscaled analysis fits better with observation than the coarse resolution global analysis, particularly with near surface observation in a regional scale. Since the accuracy of the downscaled analysis is expected to vary with the time scale, which is an important consideration for climate study, the research team performed the validation against surface observations by separating the time scale to hourly, daily, monthly, seasonal, and decadal, including long-term trend. The station observation locations are plotted in Figure 5 and listed in Table 2. There are three types of station observations: (1) Fifteen hourly buoy observations (courtesy of Steve Taylor; names start with *b*), (2) stations from the United States Historical Climatology Network[2] for monthly and daily means (three coast locations, *c*, six valley locations, *v*, and two mountain locations, *m*), and (3) 12 daily airport station observations from the National Climatic Data Center (NCDC) (three-letter abbreviations).

3.1. Daily Scale

3.1.1. Wind over coastal ocean

The research team computed the normalized wind vector anomaly correlation (Breaker et al. 1994) and vector Root Mean Square Error (RMSE) of three daily analyses—NARR, CaRD10, and R1 (NCEP NCAR Reanalysis)—against fifteen buoy observations during January and August, 2000. These are shown in Figure 6. This validation is of particular interest because the effect of local geography on coastal ocean wind is probably much simpler than that over land. Figure 5 shows the locations of the buoys used in this comparison. Note that the NARR should fit the buoy observations best, since it uses these buoy wind observations in its data assimilation. In other words, this is not an independent validation for the NARR. The figure clearly shows that for almost all the stations, CaRD10 has a higher correlation and lower RMSE than R1 and sometimes the downscaling fits even better than the NARR. The improvement is large for the buoy b25, which is located at the south of the Point Conception, an area characterized by weaker winds with more temporal and spatial variability. This location is also known as the place where the Catalina Eddy forms (see Section 3.3 on synoptic examples). The fit of the downscaled analysis became slightly worse than the R1 at some buoys, but it is not consistent between January and August nor is it systematic, and the differences between CaRD10 and R1 are probably not statistically significant. The average vector correlation and RMSE for all the buoys compared here are shown in Table 3. Compared to R1, the improvement of the RMSE in the downscaling is impressive. Overall, CaRD10 is much closer to NARR (which utilized these buoys) than to R1.

[2] See http://cdiac.ornl.gov/epubs/ndp/ushcn/newushcn.html.

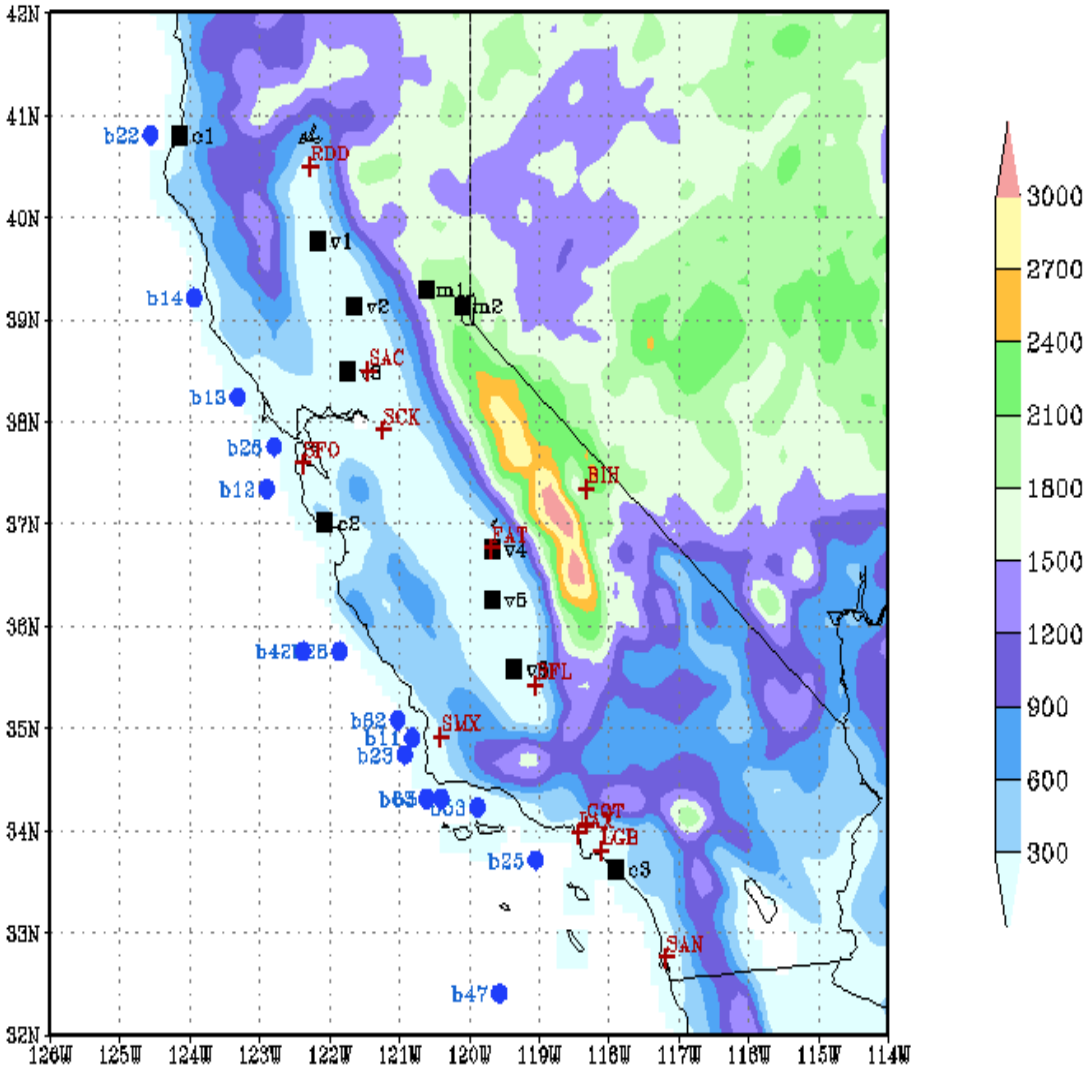

Figure 5. Observation station locations used in downscaling validation. The stations in blue with circles are buoy observation (names begin with *b*; courtesy of Steve Taylor). The stations in black with square mark are the USHCN stations (names begin with *c, v, or m*) and the stations in brown with plus signs are from NCDC (three-letter abbreviation). The color bar indicates altitude in meters.

Table 2.a Buoy station locations

WMO ID	Sign	Location	Latitude	Longitude
46011	b11	Santa Maria	34.88 N	120.87 W
46012	b12	Half Moon Bay	37.36 N	122.88 W
46013	b13	Bodega Bay	38.23 N	123.32 W
46014	b14	Pt. Arena	39.22 N	123.97 W
46022	b22	Eel River	40.78 N	124.54 W
46023	b23	Pt. Arguello	34.71 N	120.97 W
46025	b25	Santa Monica Basin	33.75 N	119.08 W
46026	b26	San Francisco	37.75 N	122.82 W
46028	b28	Cape San Martin	35.74 N	121.89 W
46042	b42	Monterey	36.75 N	122.42 W
46047	b47	Tanner Banks	32.43 N	119.53 W
46053	b53	Santa Barbara E	34.24 N	119.85 W
46054	b54	Santa Barbara W	34.27 N	120.45 W
46062	b62	Pt. San Luis	35.10 N	121.01 W
46063	b63	Pt. Conception	34.27 N	120.66 W

Table 2.b Stations for monthly analysis (data obtained from United States Historical Climatology Network)

COOP ID	Sign	Location	Latitude	Longitude
042910	c1	Eureka WSO	40.80 N	124.17 W
047916	c2	Santa Cruz	36.98 N	122.02 W
046175	c3	Newport Beach Harbor	33.60 N	117.88 W
046506	v1	Orland	39.75 N	122.20 W
045385	v2	Marysville	39.15 N	121.60 W
042294	v3	Davis Exp Farm	38.53 N	121.77 W
043257	v4	Fresno WSO AP	36.78 N	119.72 W
043747	v5	Hanford	36.30 N	119.65 W
049452	v6	Wasco	35.60 N	119.33 W
044713	m1	Lake Spaulding	39.32 N	120.63 W
048758	m2	Tahoe City	39.17 N	120.13 W

Table 2.c Airport stations for daily analysis (data obtained from NCDC)

COOP ID	Sign	Location	Latitude	Longitude
040442	BFL	Bakersfield	35.43 N	119.05 W
040822	BIH	Bishop	37.37 N	118.35 W
045115	CQT	Los Angeles USC	34.02 N	118.28 W
043257	FAT	Fresno	36.77 N	119.72 W
045114	LAX	Los Angeles	33.93 N	118.40 W
045085	LGB	Long Beach	33.82 N	118.15 W
047304	RDD	Redding	40.50 N	122.30 W
047630	SAC	Sacramento	38.50 N	121.48 W
047740	SAN	San Diego	32.73 N	117.17 W
048558	SCK	Stockton	37.88 N	121.23 W
047769	SFO	San Francisco	37.62 N	122.38 W
047946	SMX	Santa Maria	34.90 N	120.45W

Table 3. Mean vector anomaly correlation and RMSE of winds of three analyses and fifteen buoy observations during 2000

	Correlation			RMSE		
	R1	CaRD10	NARR	R1	CaRD10	NARR
January	0.77	0.82	0.86	3.50	2.94	2.17
August	0.66	0.68	0.70	2.52	1.83	1.70

3.1.2. Wind over Land

The research team performed similar comparisons on wind over land, using the 12 airport stations shown in Figure 5. The station locations are shown in red and crosshair marks in Figure 5. Overall, the fit of the three analyses to the land stations are much worse than those over the ocean. This is expected, since the more complex surface topography on land produces a stronger influence on winds. The differences in fit between the three analyses are more diverse, but CaRD10 seems to be consistently better than R1 and NARR, both in terms of correlation and RMSE. The average correlation and RMSE for all the stations are shown in Table 4. The CaRD10 fits best, due to the detailed 10 km resolution topography in CaRD10 compared to 32 km in NARR. Although the surface wind observations are assimilated in NARR, its information content over land seems to be masked by the coarse resolution topography.

Table 4. Mean vector anomaly correlation and RMSE of winds of three analyses and twelve land station observations during 2000

	Correlation			RMSE		
	R1	CaRD10	NARR	R1	CaRD10	NARR
January	0.49	0.56	0.39	3.90	3.24	3.92
August	0.39	0.46	0.41	2.62	2.29	2.47

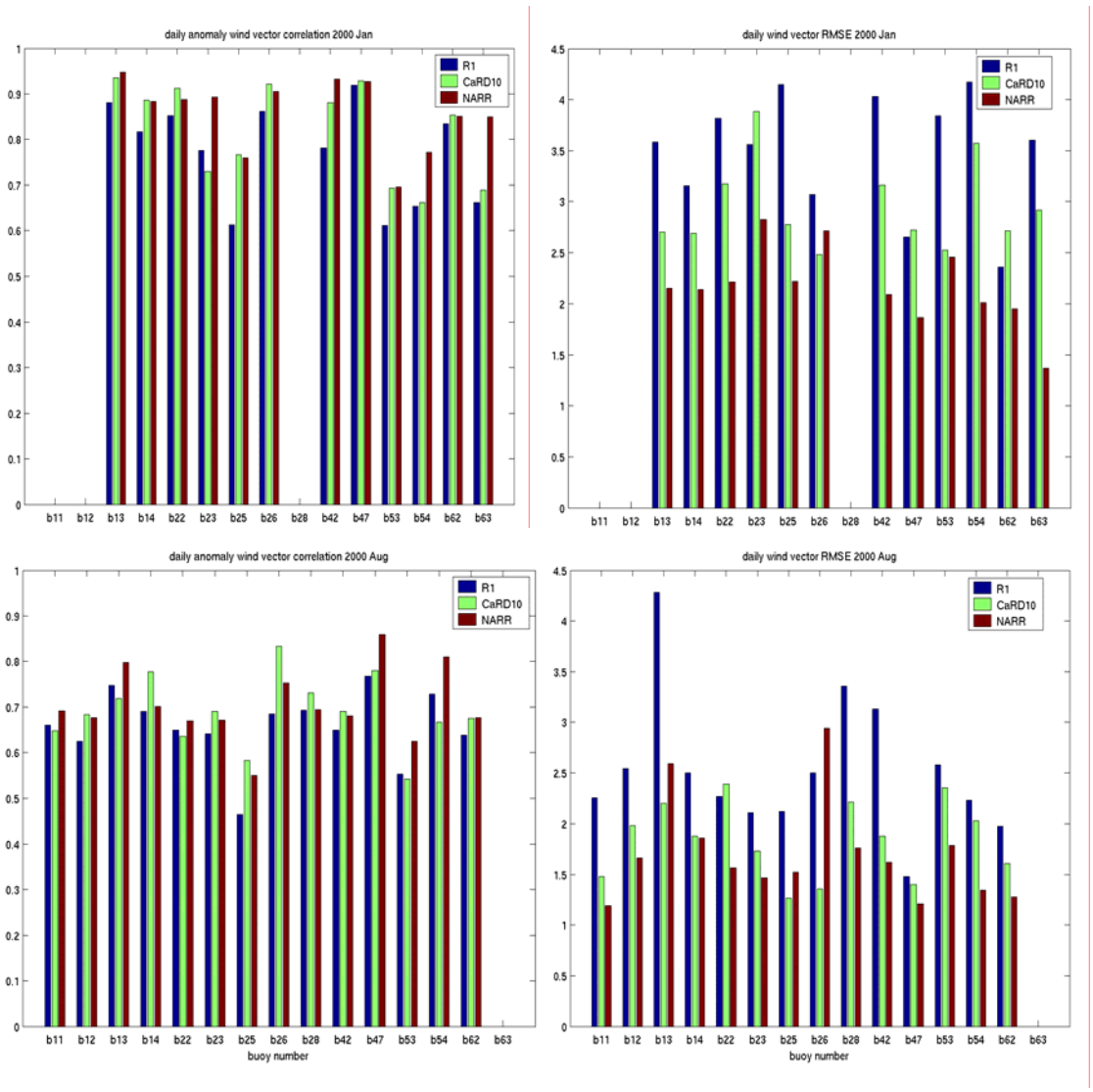

Figure 6. Comparisons of the vector correlation on the left panels and vector root mean square error (RMSE) on the right panels of daily near surface wind analysis with buoy observations, for January (upper panels) and August (lower panels) of 2000. Note the significant increase (decrease) in the correlation (RMSE) from R1 (blue) to CaRD10 (green).

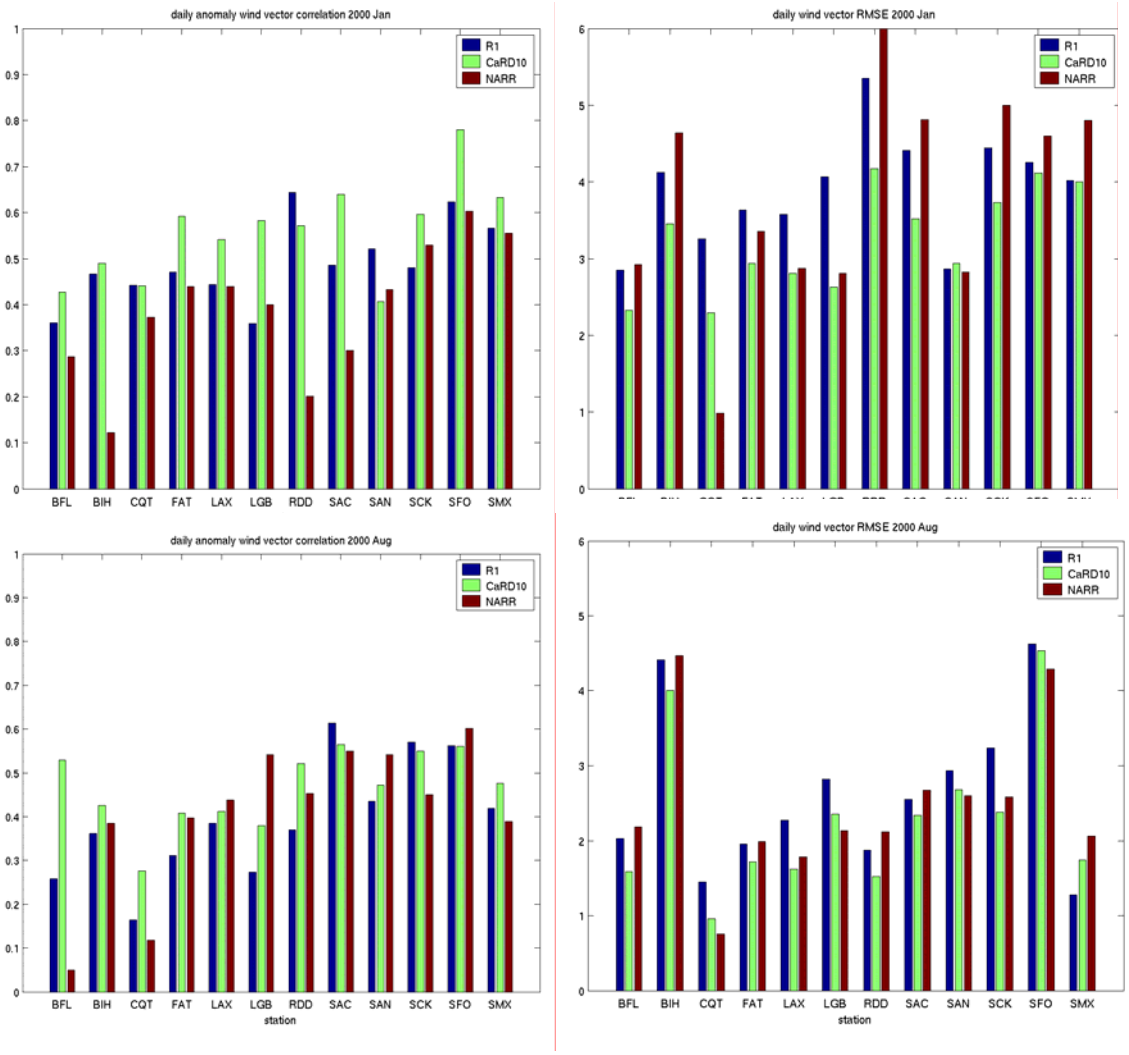

Figure 7. Same as Figure 6, but for land stations

3.1.3. Daily Mean and Max/Min Temperature over Land

Figure 8 is the comparison of correlation of daily mean temperature at 12 land stations in California for January and August, 2000 (the same stations as those used for the wind verification over land). The CaRD10 correlation ranges from 0.5 to over 0.9. During January, the result is mixed (R1 is best at 5 stations, CaRD10 is best at 6 stations, and NARR is best at 1 station). During August, CaRD10 is best for 6 stations, NARR is best for 5 stations, and R1 is best at 1 station. In terms of mean bias removed RMS, the result is about equal for R1, CaRD10 and NARR in January. NARR is the best for 3 stations and CaRD10 is best for 6 stations, and in August, NARR is best for 9 stations and CaRD10 is best for 3 stations.

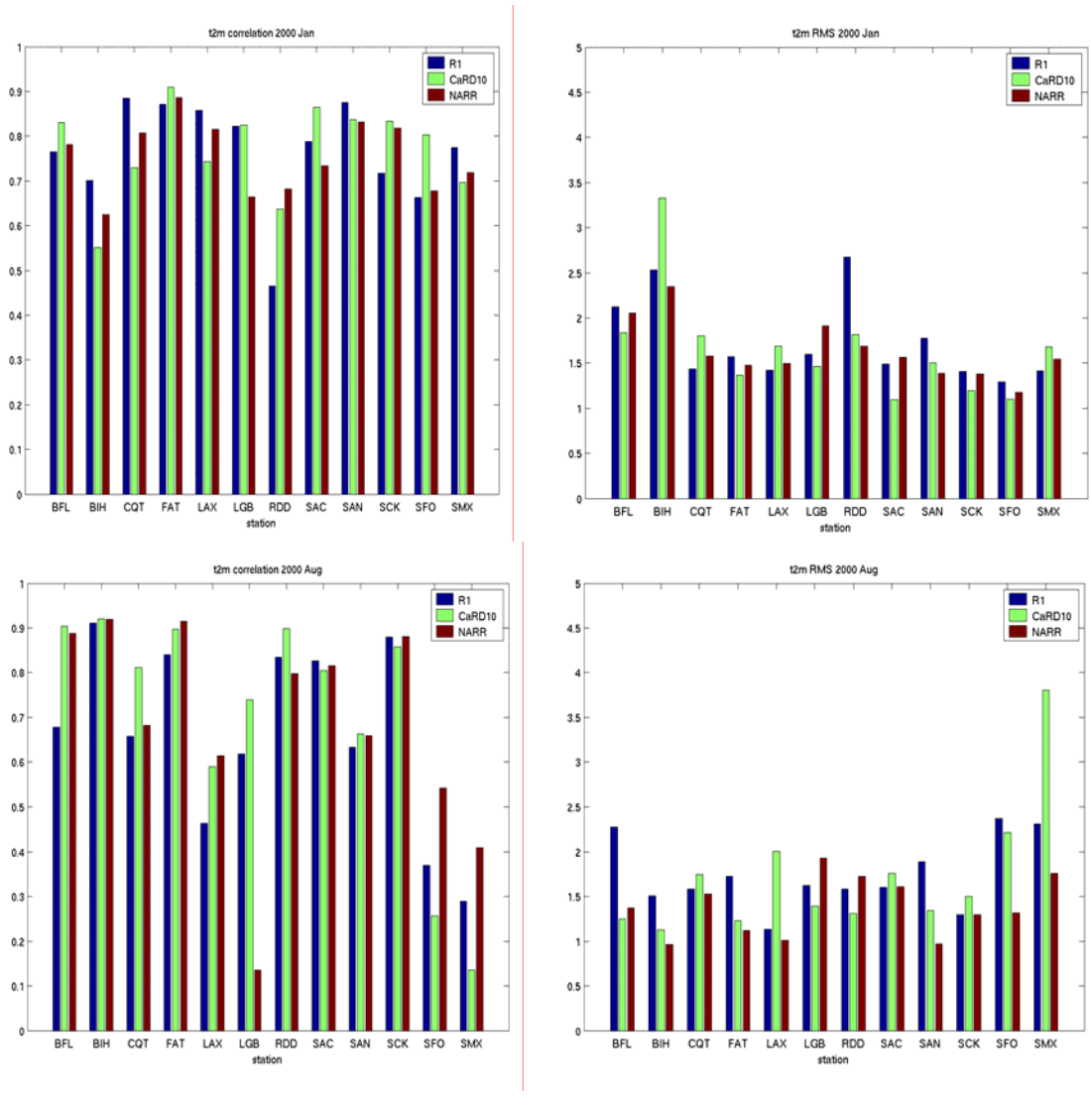

Figure 8. Comparisons of the correlation (left panels) and root mean square error (RMSE) (right panels) of CaRD10 daily near surface temperature with station observations in January (upper panels) and August (lower panels) during 2000

The correlations of daily max/min temperature with observation for R1 and CaRD10 are shown in Figures 9 and 10. The correlation for NARR is not available for this comparison. Daily maximum and minimum temperature correlations and RMS for CaRD10 are mixed. CaRD10 at station BIH is worse at both max and min temperatures than it is at R1, but is better than R1 in terms of mean temperature. The improvement of CaRD10 over R1 is not impressive, but noticeable.

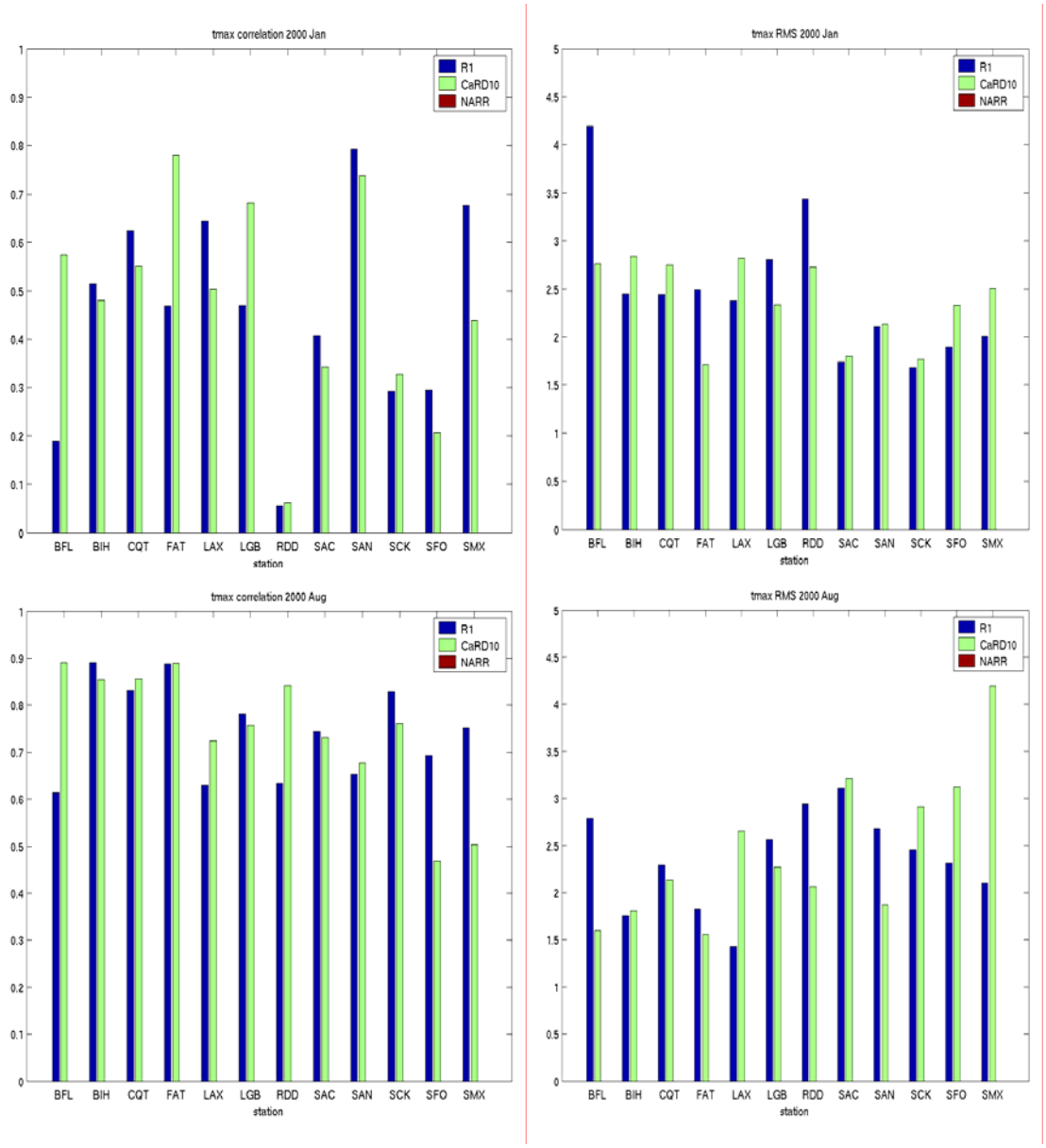

Figure 9. Same as Figure 8, but for daily maximum temperature

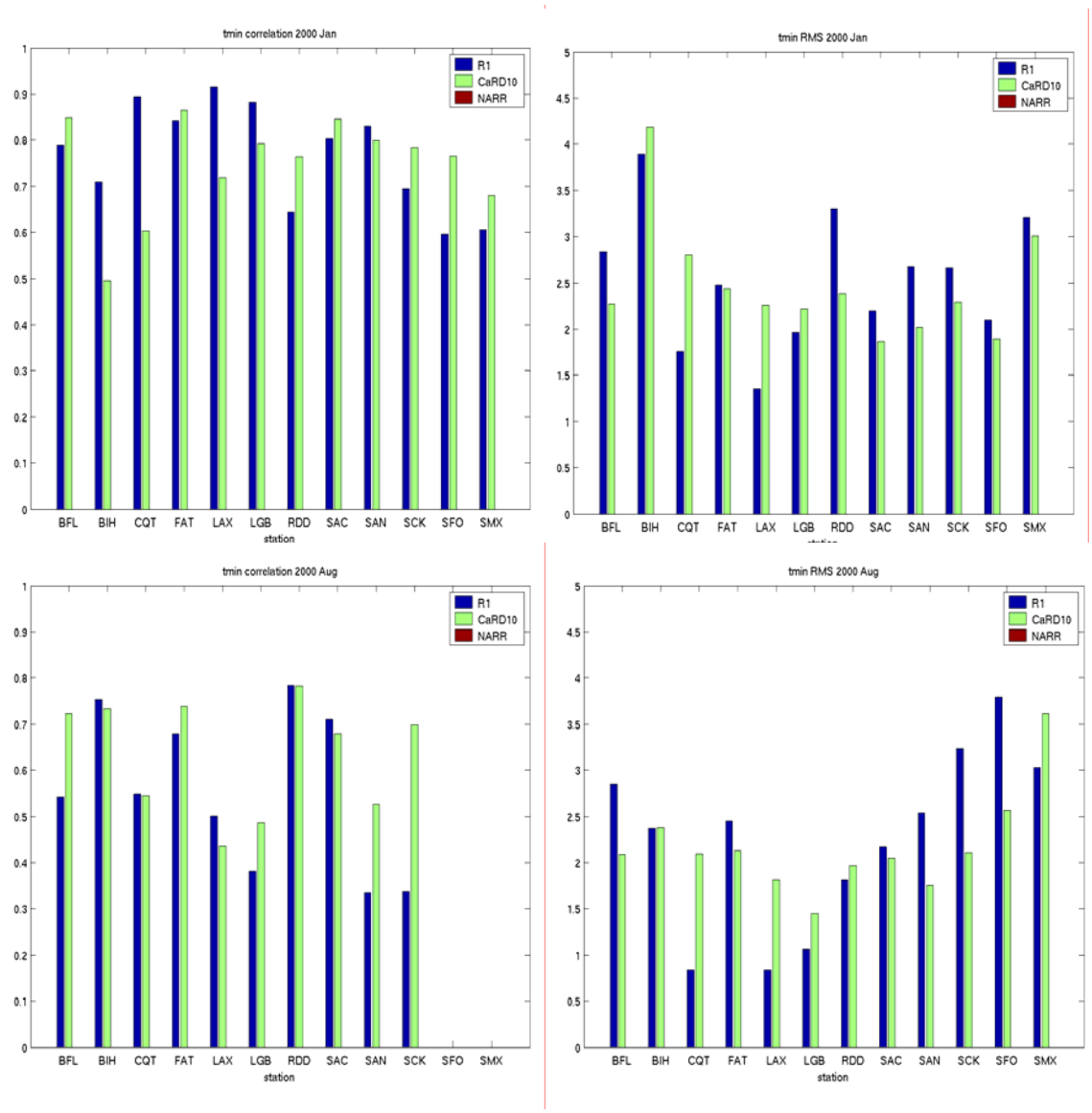

Figure 10. Same as Figure 8, but for daily minimum temperature

Table 5 compares correlation and RMS averaged over all the land observation stations. The correlation of CaRD10 is almost always higher than that of R1, except for the daily minimum temperature in January. The CaRD10 correlation is apparently better than that of the NARR. The RMS of CaRD10 is always less than that of R1 (except for the daily max temperature in August), but NARR has less RMS error for daily mean temperature both in January and August.

Table 6 presents the mean bias. The CaRD10 tends to have smaller bias than R1 and NARR, particularly in winter. This is probably because the surface topography of CaRD10 is much closer to the real topography. The bias of daily mean and daily max/min temperatures at individual airport stations are shown in Figure 11.

Table 5. Mean correlation and RMSE of daily mean temperature and max/min temperature of three analyses and twelve land station observations during 2000

		Correlation			RMSE		
		R1	CaRD10	NARR	R1	CaRD10	NARR
Mean T	January	0.77	0.77	0.75	1.73	1.66	1.63
	August	0.67	0.71	0.69	1.74	1.73	1.38
Tmax	January	0.45	0.47	-	2.47	2.37	-
	August	0.75	0.75	-	2.35	2.45	-
Tmin	January	0.77	0.75	-	2.53	2.47	-
	August	0.40	0.49	-	2.25	2.17	-

Table 6. Mean bias of daily mean temperature and max/min temperature of three analyses and twelve land station observations during 2000

		Bias		
		R1	CaRD10	NARR
Mean T	January	-2.82	-0.63	-0.85
	August	-1.70	-1.40	-0.44
Tmax	January	-3.09	-0.68	-
	August	-0.69	0.70	-
Tmin	January	-1.45	1.54	-
	August	-4.04	-1.98	-

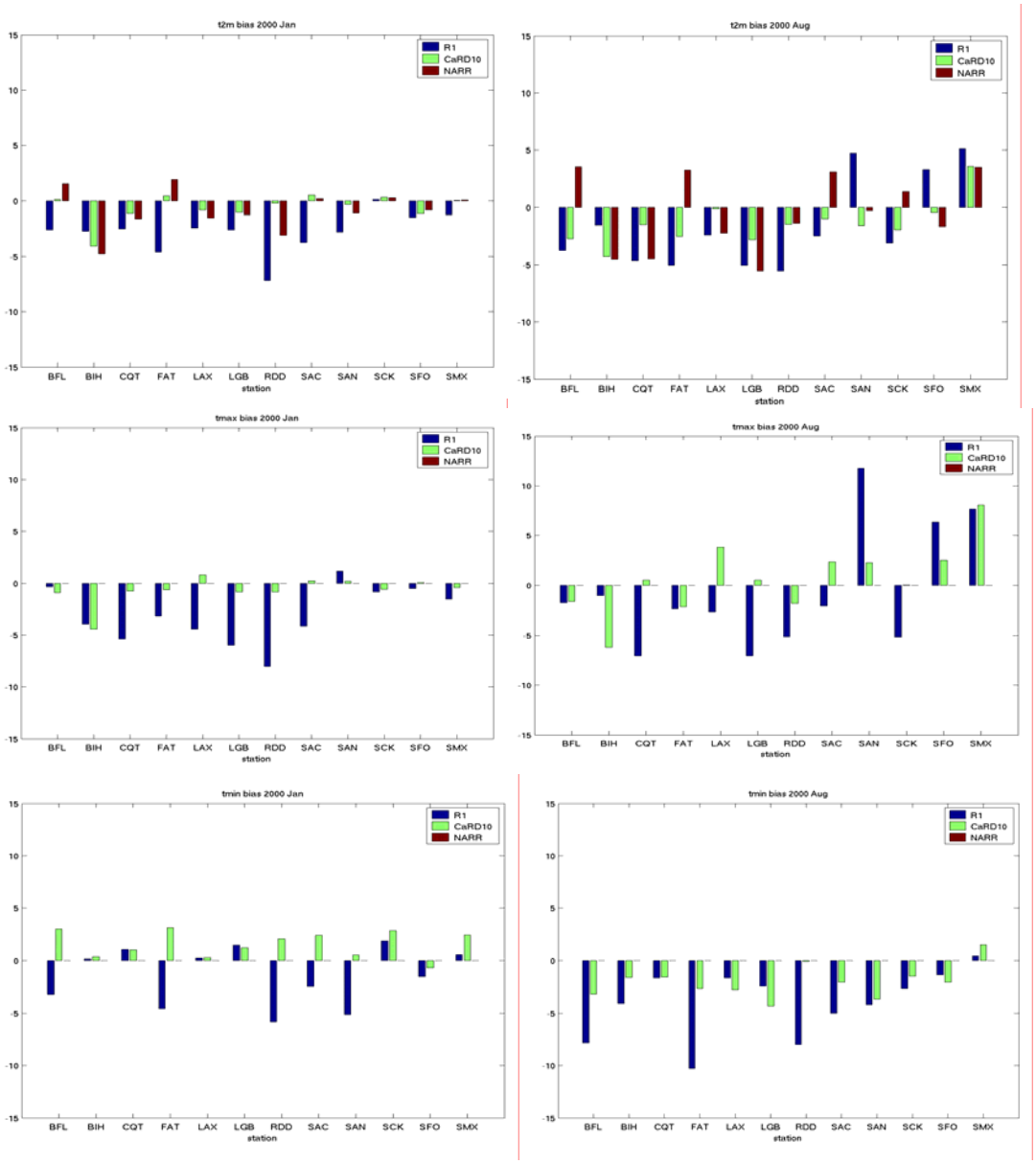

Figure 11. CaRD10 bias of near surface daily mean (top), daily maximum (middle), and daily minimum (bottom) temperature at various observation stations for January (left) and Aug (right) during 2000. Station locations are shown in Figure 5. Note that max/min temperature information was not available for NARR

The CaRD10 bias is smaller than that of R1 and NARR. The sign of daily mean temperature bias tends to be negative (cold bias), For the maximum temperature in January, CaRD10 tends to have negative or no bias, while an almost uniform positive bias is found in the minimum temperature for the same month, which results in reduction of the daily temperature range. In August, although it is not very uniform, minimum temperature has a negative bias but the maximum temperature bias is mixed.

Finally, the daily temperature ranges in summer and winter are compared with a large number of land stations in 1996 and are shown in Figure 12 (courtesy of Mary Tyree).

The geographical patterns look fairly reasonable for both January and July but CaRD10 tends to underestimate the temperature range, particularly in January.

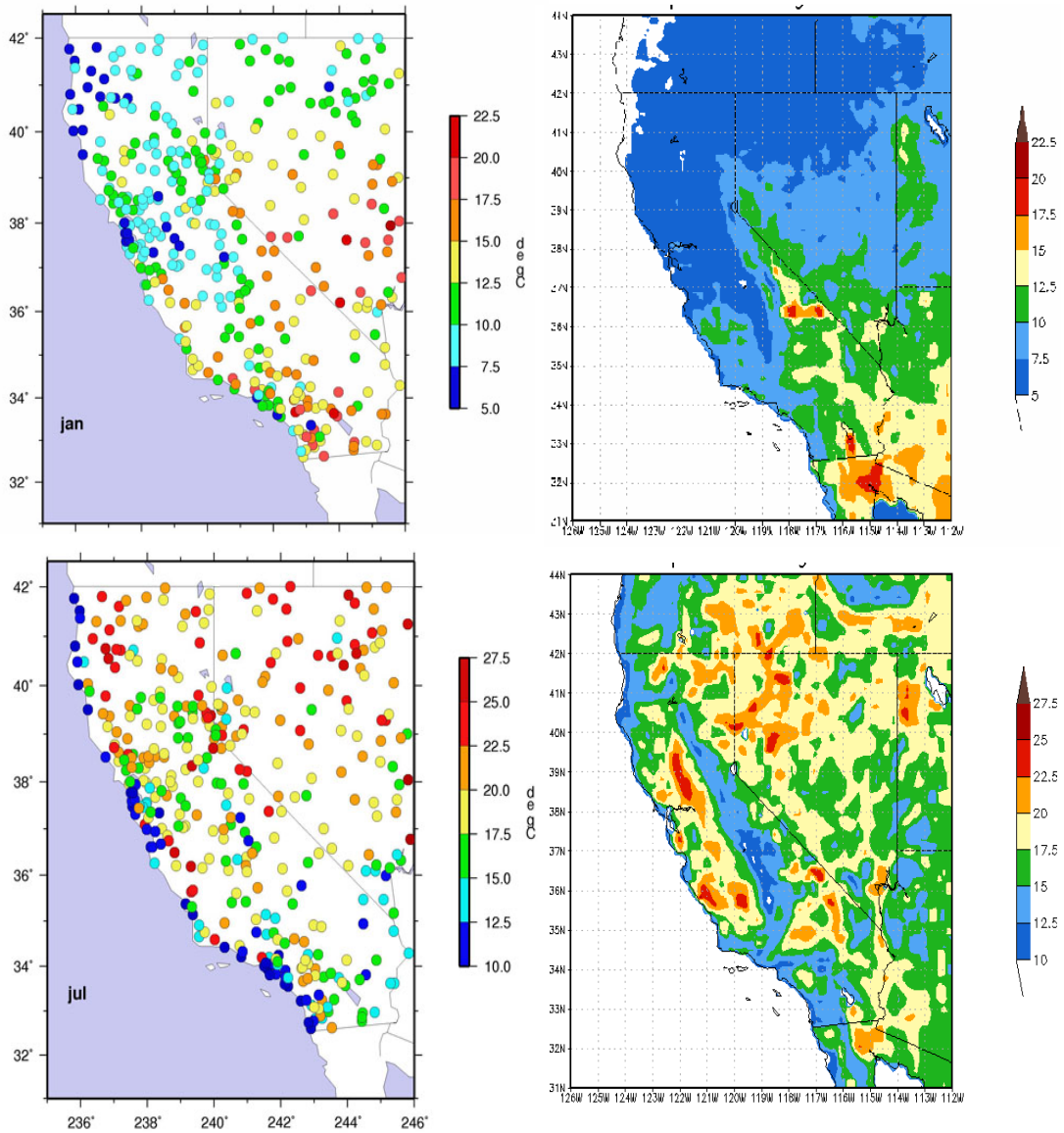

Figure 12. Comparison of daily temperature range for January (upper panels) and July (lower panels) 1996. Left observation (courtesy of Mary Tyree), and right CaRD10.

3.1.4. Precipitation Over Land

The correlation of daily precipitation in August is low (Table 7), but this is due to infrequent precipitation events. In January, the correlation is above 0.6, except for one station. The bias is quite large, and that bias will be discussed in more detail later.

Table 7. Correlation and bias (in mm/day) between CaRD10 and daily station observation of precipitation for 6 selected stations in California in January and August for the period 1948–2003

	January		August	
Station	Corr.	Bias	Corr.	Bias
c2	0.68	1.00	0.50	0.08
c3	0.66	1.33	0.12	-0.02
v1	0.60	3.54	0.33	0.05
v3	0.60	2.43	0.14	0.06
v6	0.43	2.01	0.03	0.01
m1	0.84	1.04	0.40	0.10

In general, the correlation between station observation and CaRD10 is reasonable but not necessarily excellent. Due to the non-Gaussian nature of the precipitation events, as well as to the instrumental error and the spatial representativeness of station observations, validation of daily precipitation against station observation is problematic, and further work is necessary.

3.2. Hourly Scale

Simple correlation of available hourly buoy wind speed observations during the entire two years showed slightly lower correlation than that of the daily observed wind speed but it is not clear how reasonably the hourly variations are reproduced in CaRD10. Instead, this study validated the hourly scale by compositing the monthly diurnal variation from two years of data. Figure 13 through 20 show the comparison of wind speed and wind vector. We see that the agreement with observation is reasonably good, amazingly so at some locations, such as the buoy b42 in April and May and buoy b47 in September. At buoy b25 and b42, the dynamical downscaling tends to give larger diurnal amplitude, but phase is reasonable. The agreement is better for station b47. At station b63, the amplitude is reasonable, but the peak is shifted by 4–5 hours during April to September.

Another example of the composite of the diurnal variation of winds is shown in Figure 21. This is the one month CaRD10 wind time-height composite compared with the observed composite taken from the special observation at Piedras Blancas (Ralph et al., 2000, the particular figure used here is provided courtesy of Paul Neiman). The observation is based on the hourly wind profiling radar deployed by National Oceanic

and Atmospheric Administration (NOAA). The timing of the diurnal variation of low level wind speed is very well represented by CaRD10, although the variability tends to be less (6.5 meters per second (m/s) in observation versus 4.5 m/s in CaRD10). The variation of CaRD10 wind direction is fairly reasonable at around 1000 m above ground, but tends to vary too much close the surface.

Overall, diurnal variation is fairly reasonably reproduced by the downscaling, although the detail and accuracy may need further study.

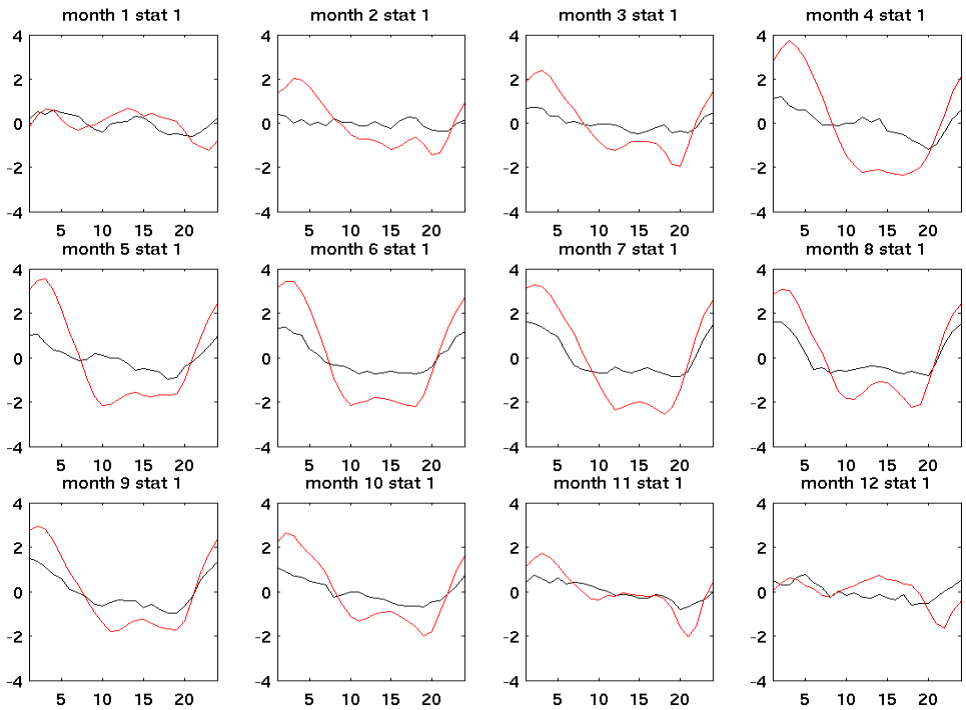

Figure 13. Comparison of the monthly composited diurnal variation of near surface winds for each month in 2000 and 2001 at buoy station b25. Black lines are observation and red lines are CaRD10

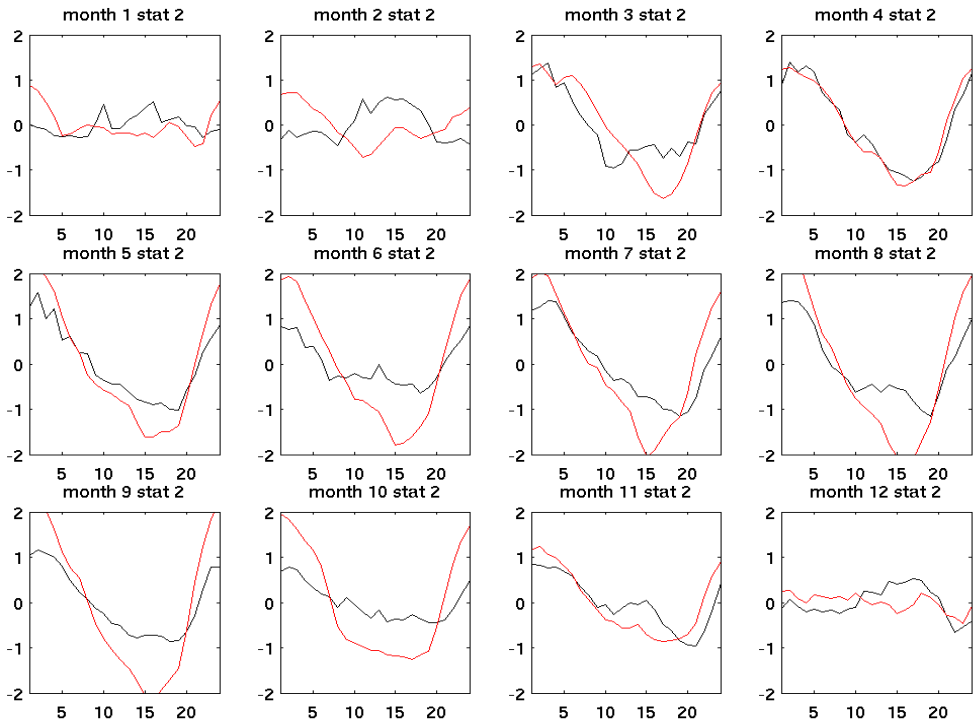

Figure 14. Same as Figure 13 but for buoy b42

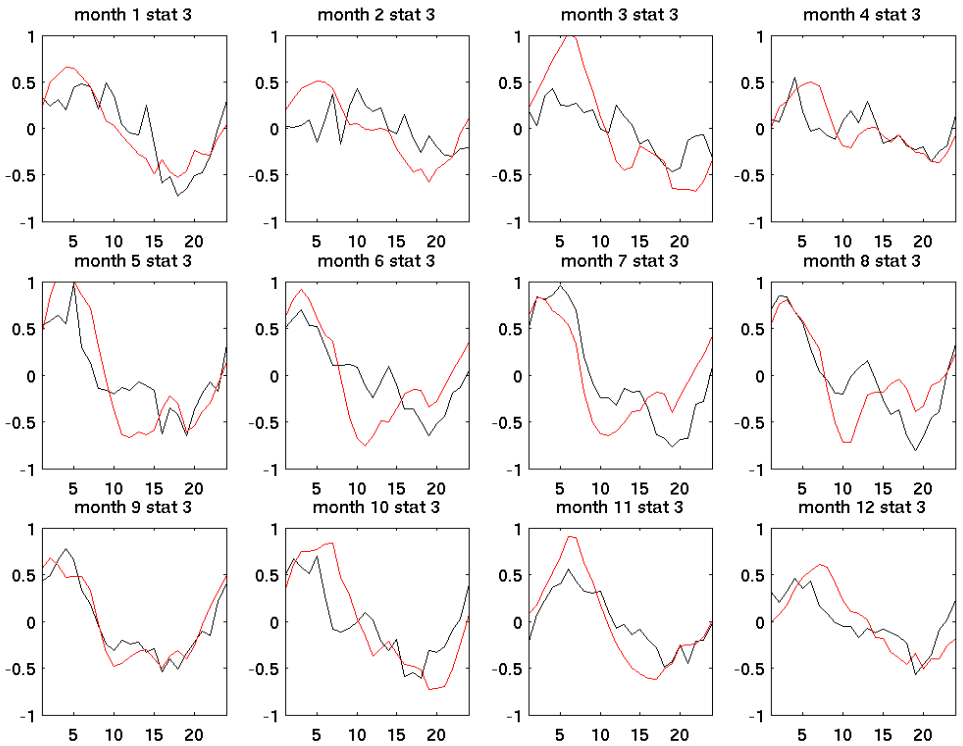

Figure 15. Same as Figure 13, but for buoy b47

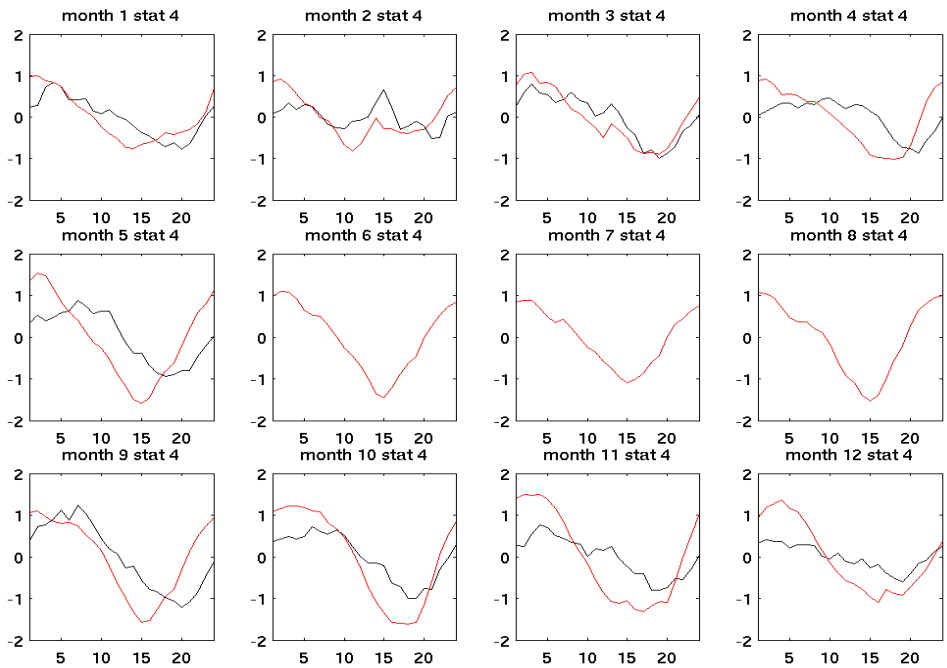

Figure 16. Same as Figure 13, but for buoy b63

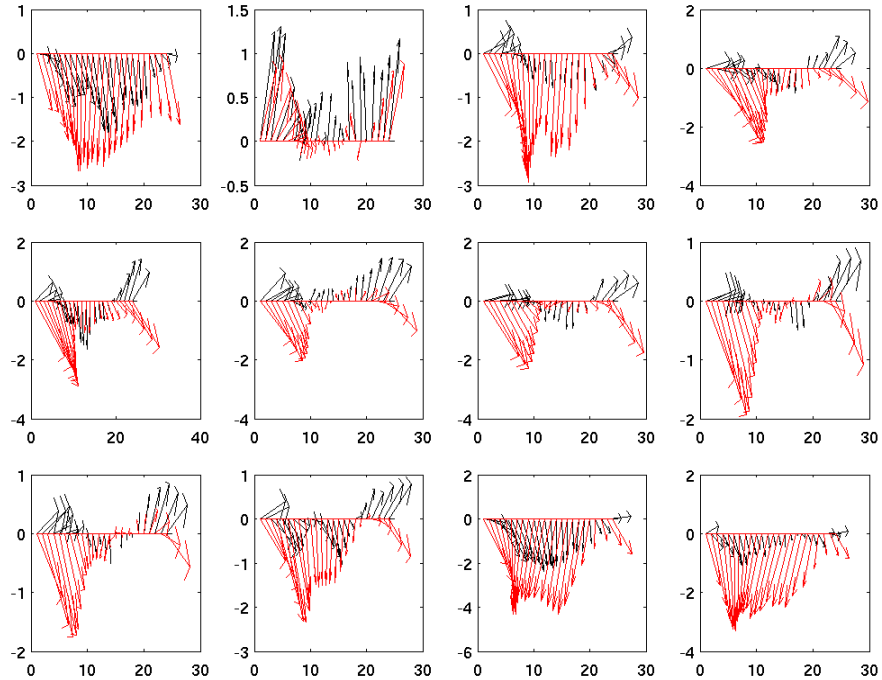

Figure 17. Comparison of the monthly composited diurnal variation of near surface wind vector for each month in 2000 at buoy station b25. Black arrows are observation and red arrows are CaRD10.

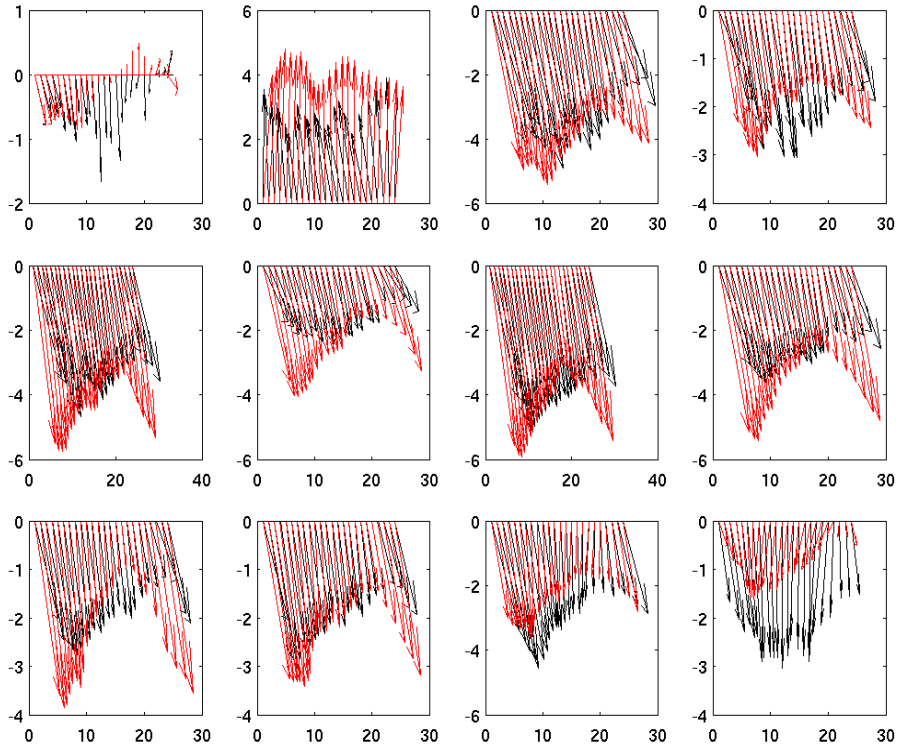

Figure 18. Same as Figure 17, but for buoy b42

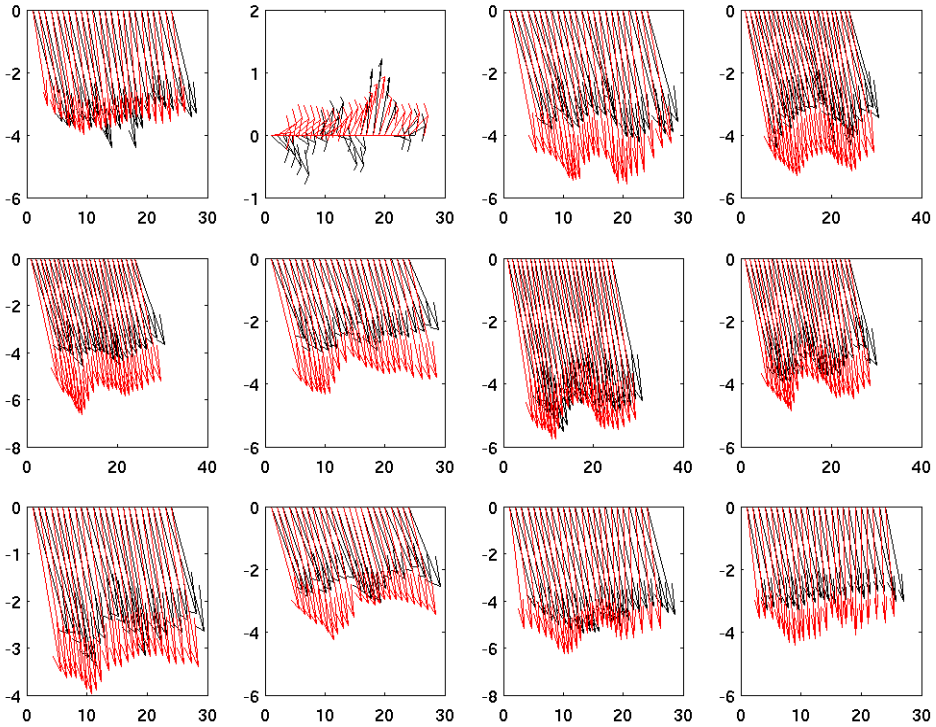

Figure 19. Same as Figure 17, but for buoy b47

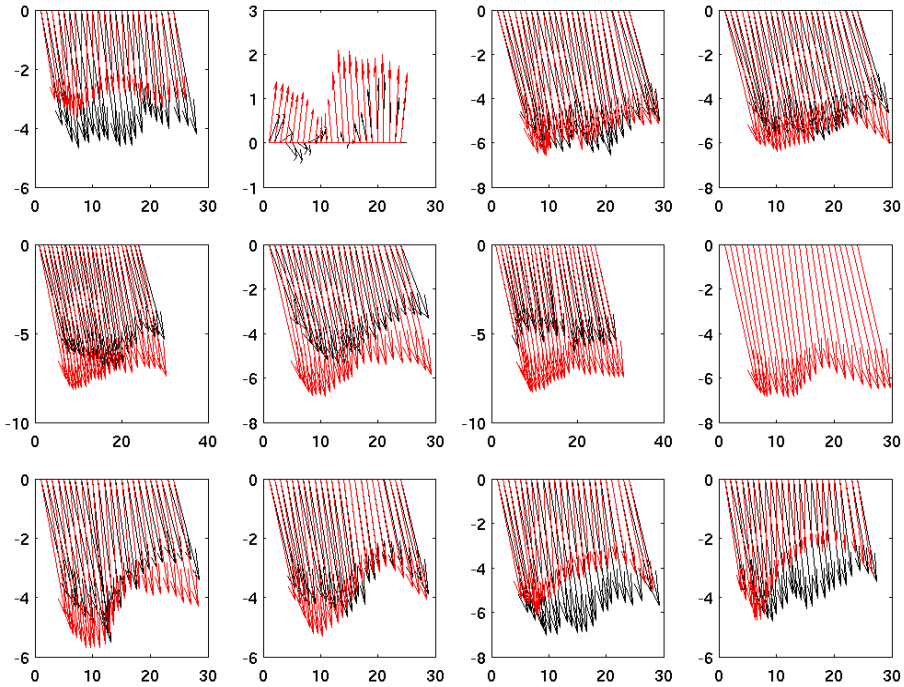

Figure 20. Same as Figure 17, but for buoy b63

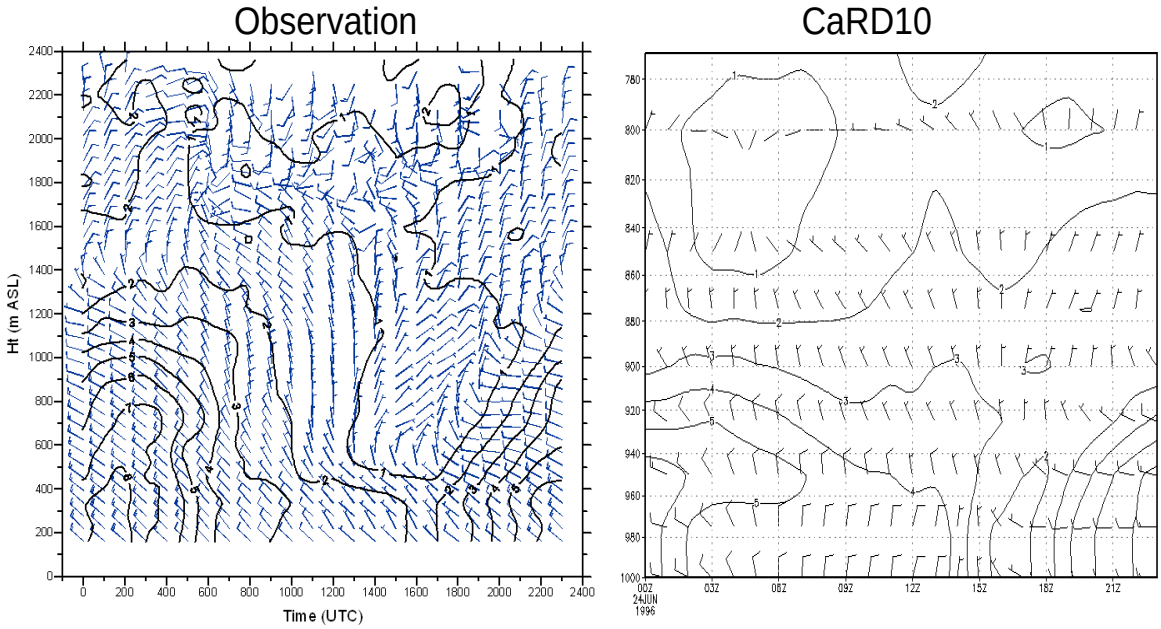

Figure 21. Validation of composite diurnal variation of wind and wind speed at Piedras Blancas (35N, 121.3W)

3.3. Synoptic Examples

Comparison of the dynamically downscaled analysis with station observation in terms of correlation, root mean square and bias errors is not sufficient to demonstrate the meteorological quality of the downscaled analysis. The integrity of CaRD10 can be more clearly demonstrated by showing examples of synoptic events. This section presents three typical mesoscale examples of Catalina Eddy, coastally trapped wind reversal (CTWR), and Santa Ana events.

The Catalina Eddy is well documented by Wakimoto (1987) and Mass and Albright (1989). The research team took a typical case from Mass and Albright (their Figure 2a) and examined the surface wind field from CaRD10. As shown in Figure 22, the dynamically downscaled analysis detects the eddy at a reasonable location, demonstrating the capability of the dynamical downscaling. Two discontinuity-like features in wind—one starting at Point Conception and the other extending from the south central region of the eddy toward the west-south-west direction—are undocumented and worth further study.

A comprehensive review of CTWR is found in Nuss et al. (2000). The present study examined a typical case to see whether dynamical downscaling can reproduce evolution of such small scale detail without local observations. As shown in Figure 23, the dynamical downscaling provides excellent reproduction of the time evolution of the phenomena, which has a relatively short time scale of 24 hours or less.

An example of a Santa Ana event is taken from the downscaled analysis on October 26, 2003. This date is well known for the strong Santa Ana which is associated with a large wildfire (the Cedar fire) in Southern California (Keely et al. 2004). Figure 24 shows typical strong offshore wind with very warm temperatures along the southern California coast.

Although these are limited examples, it is clear that dynamical downscaling is capable of reproducing synoptically consistent small scale details over ocean and land.

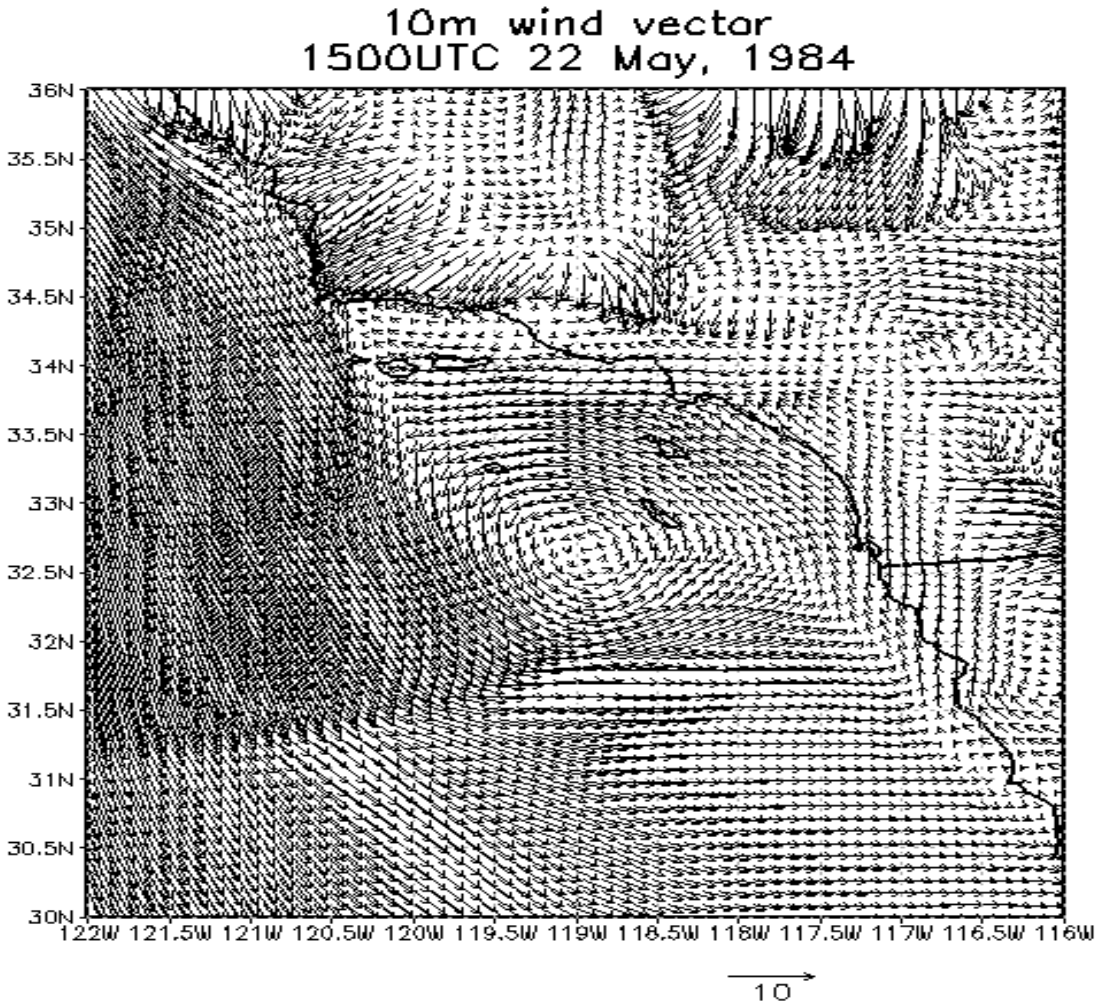

Figure 22. An example of the Catalina Eddy appeared in the CaRD10 at 1500UTC on May 22, 1984

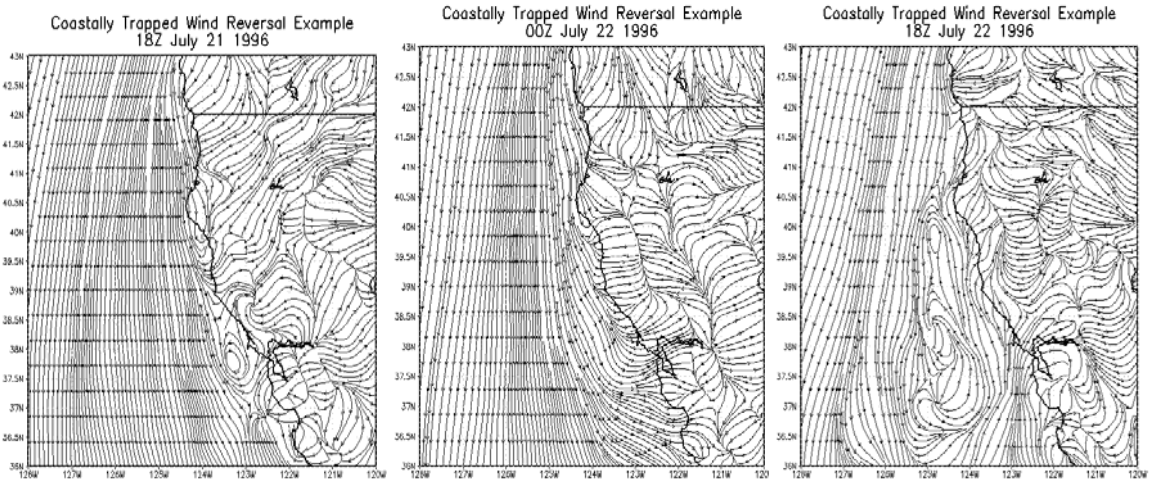

Figure 23. An example of the evolution of Coastally Trapped Wind Reversal on July 21 to 22, 1996

3.4. Monthly Averages

Validation of monthly average daily mean and maximum temperature and precipitation over land was performed using about 80 land stations during 1984–1996. The monthly average data are more easily available than the daily data, and thus there are more observations available for comparison. Figures 25 and Figure 26 show the fit of CaRD10 to these observations in January and August. The monthly mean 2-meter temperature in January correlates very well, above 0.7 over the entire domain except 3 stations. The correlation is good along southern coast of California as well as in Nevada and Northeastern California. The correlation tends to be better along the southern coast of than toward inland. On the average, the correlation in August is lower by 0.1, compared to January. In August the correlation tends to be lower along the coast and becomes better toward inland. The correlation stays above 0.6 over the entire domain. The reason for this particular distribution of the skill is not entirely clear, but some influence from ocean temperature is suspected. Our preliminary investigation showed that the CaRD10 temperature for coastal land in summer correlates more weakly with coastal SST than observed. This dominant local response may be responsible for the poorer fit. This problem may be due to the overestimated effect of land surface atmosphere interaction in the model. For the daily maximum temperature (Figure 26) during January, correlation is mostly over 0.7. The lowest correlation occurs in the Central Valley area where the value is in the 0.6 range or lower, but other areas have very high correlations. During August, the correlation tends to be lower, particularly in the southern half of the domain.

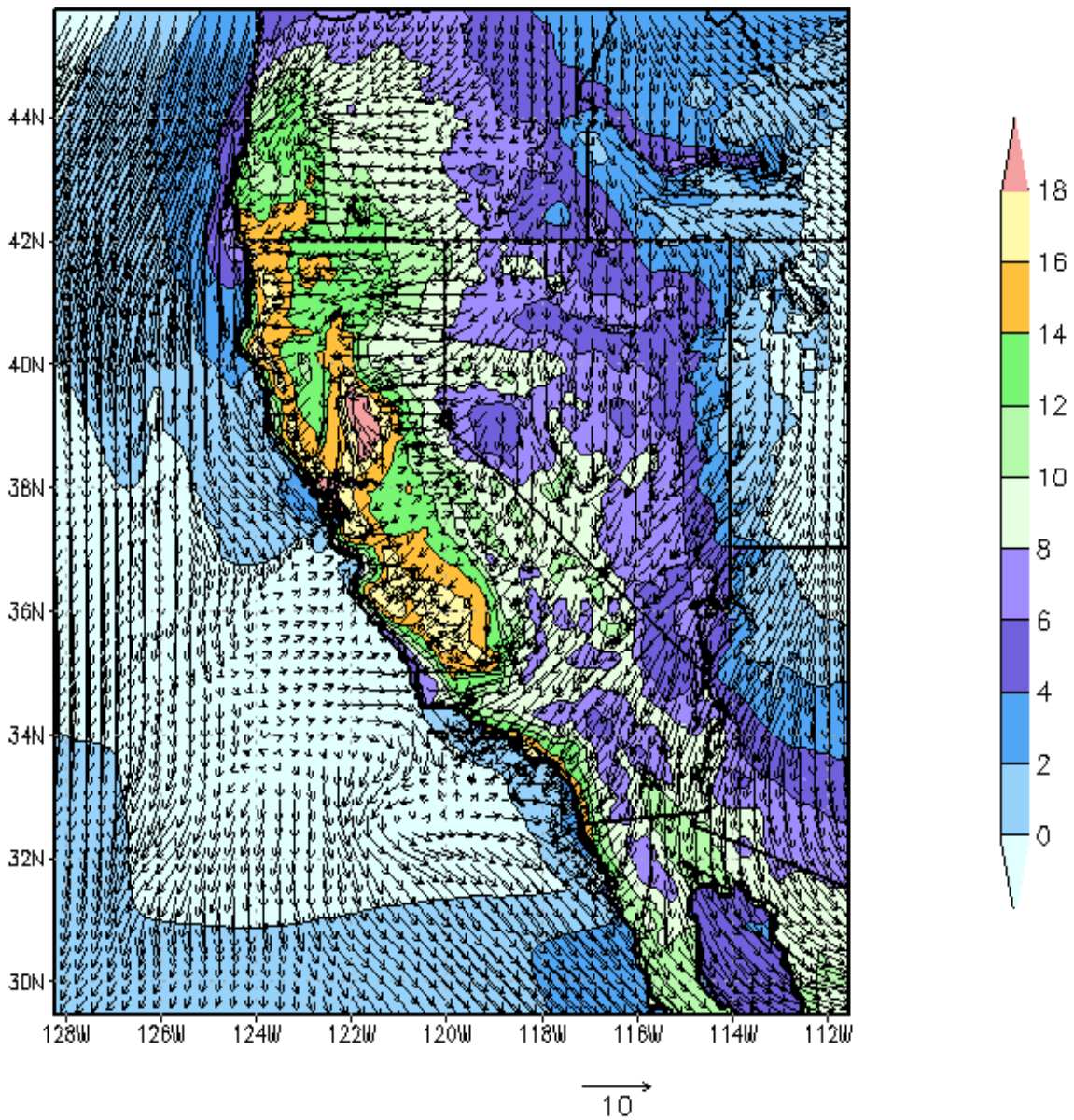

Figure 24. An example of Santa Ana events, 00Z October 26, 2003

The correlations of monthly average precipitation are shown in Figure 27. During January, the correlation is fairly high in most of California, while it is lower in Nevada where less precipitation occurs. During summertime, the correlation is much lower (less than 0.6) over most of the domain. This is partly due to the lack of precipitation during this season.

Temporal correlation of monthly mean 2m T with observations

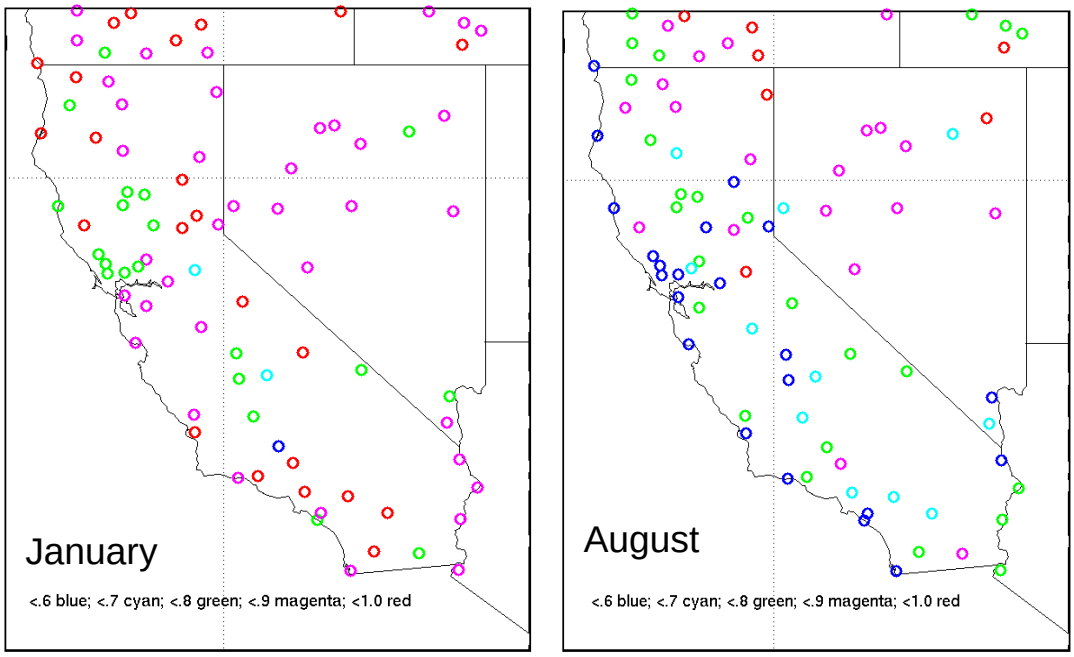

Figure 25. Correlation of monthly mean daily mean temperature with observation for the period 1948–1996

Temporal correlation of monthly daily max temperature with obs.

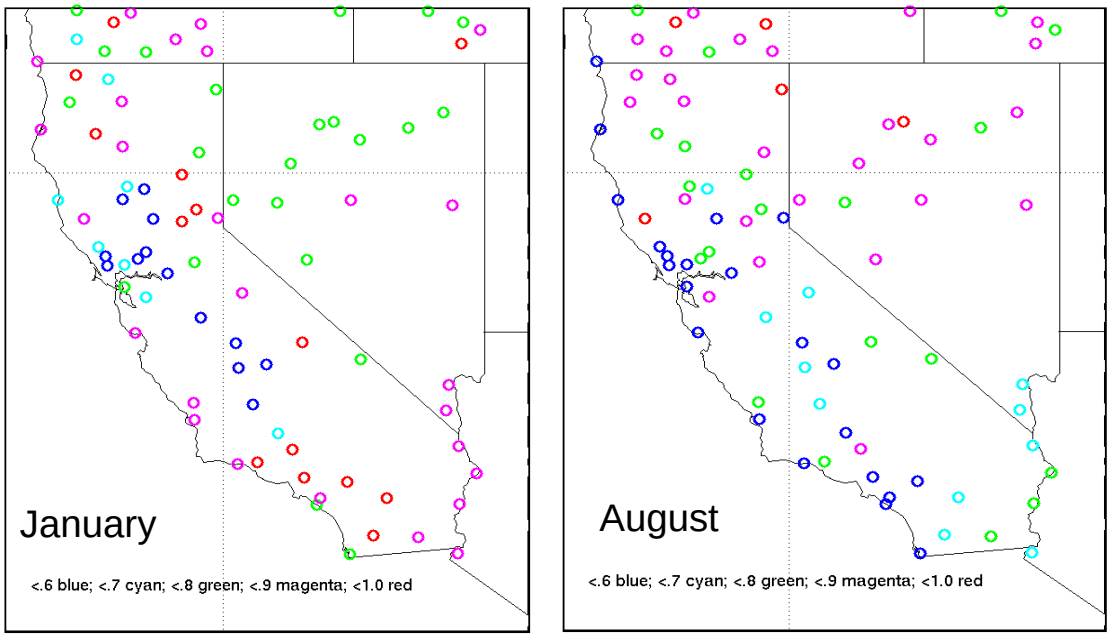

Figure 26. Correlation of monthly mean daily maximum temperature with observation for the period 1948–1996

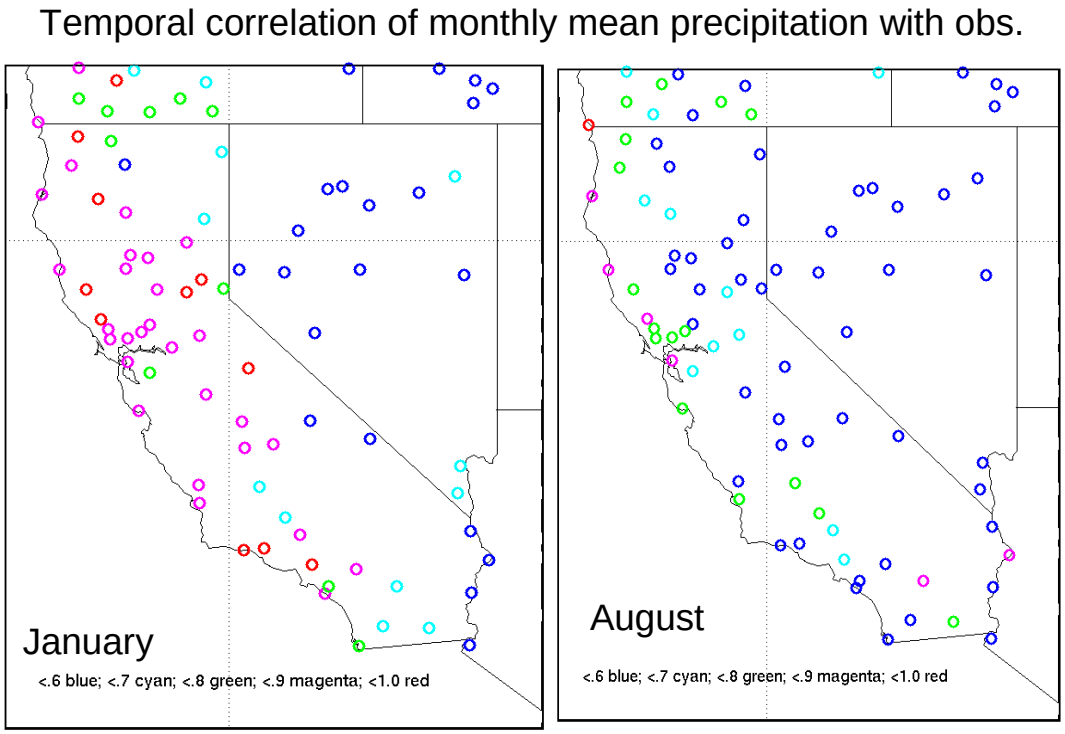

Figure 27. Correlation of monthly mean precipitation with observation for the period 1948–1996

The monthly variation of correlation at selected coastal (3 stations), valley (6 stations) and mountain (2 stations) locations is shown in Figures 28 though 30. The mean 2-meter temperature (Figure 28) has high correlation in winter months and drops during the summer months. Somehow, the coastal station displays very poor correlation during the summer. For the stations in the Central Valley, correlation is high in spring and fall, and drops down again in summer. Mountain station skill is mixed. The correlation of max temperature (Figure 29) is about the same as the mean temperature. The peak skill in spring and fall over valley stations is more pronounced for this variable. For the monthly mean precipitation (Figure 30), the correlation is better in winter and worse in summer, again reflecting small precipitation events in summer.

3.5. Trend

For validation of longer time scales, this study examined the trends for the 1950–1996 periods at several selected stations (see Figure 5 for the station locations: 3 coastal stations, 6 valley stations, and 2 mountain stations, denoted as c1-3, v1-6 and m1-2, respectively). Table 8 shows the comparison for the January and August trends. In January, the CaRD10 and observation trends agree fairly well, although the magnitude of the trend in the CaRD10 is consistently smaller (except for Mountain station m1). All the trends in the observation are positive, while CaRD10 shows a small negative trend in the valley at some stations. In August, the CaRD10 trend does not agree with observation at all. Observed trends are all positive (except at one valley station, v6), while CaRD10 trends are all negative, with the exception of the mountain stations.

Table 8. Comparison of 1950–1996 trend in monthly mean near surface temperature between observation and CaRD10

	Station	January		August	
		Obs.	CaRD10	Obs.	CaRD10
Coast	c1	+0.04	+0.02	+0.04	-0.04
	c2	+0.05	+0.02	+0.03	-0.05
	c3	+0.04	+0.02	+0.02	-0.02
Valley	v1	+0.04	+0.01	+0.00	-0.04
	v2	+0.02	+0.00	+0.02	-0.04
	v3	+0.00	-0.00	+0.01	-0.03
	v4	+0.03	+0.01	+0.05	-0.05
	v5	+0.01	-0.00	+0.02	-0.05
	v6	+0.01	-0.00	-0.00	-0.05
Mountain	m1	+0.03	+0.05	+0.03	+0.00
	m2	+0.05	+0.00	+0.04	+0.12

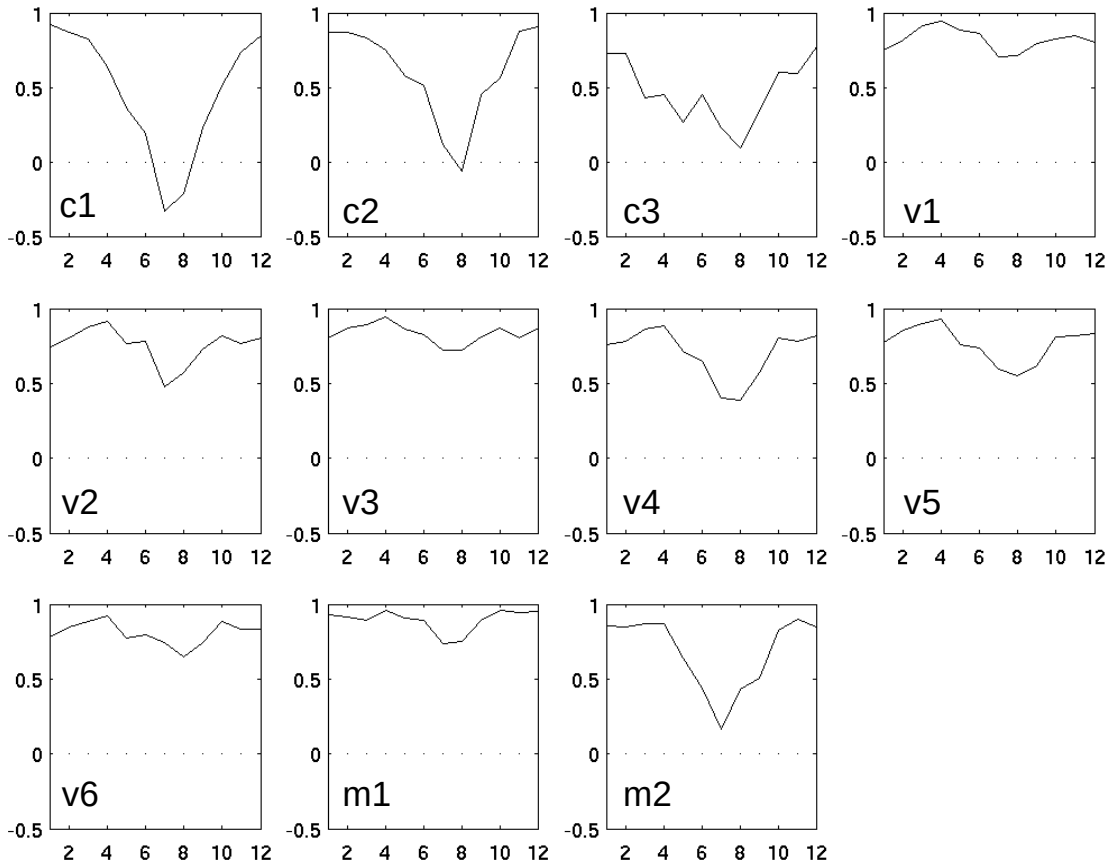

Figure 28. Variation of correlation of monthly mean temperature with observation for the period 1948–1996 at coastal (c1 to c3), central valley (v1 to v6), and mountain (m1 and m2) stations

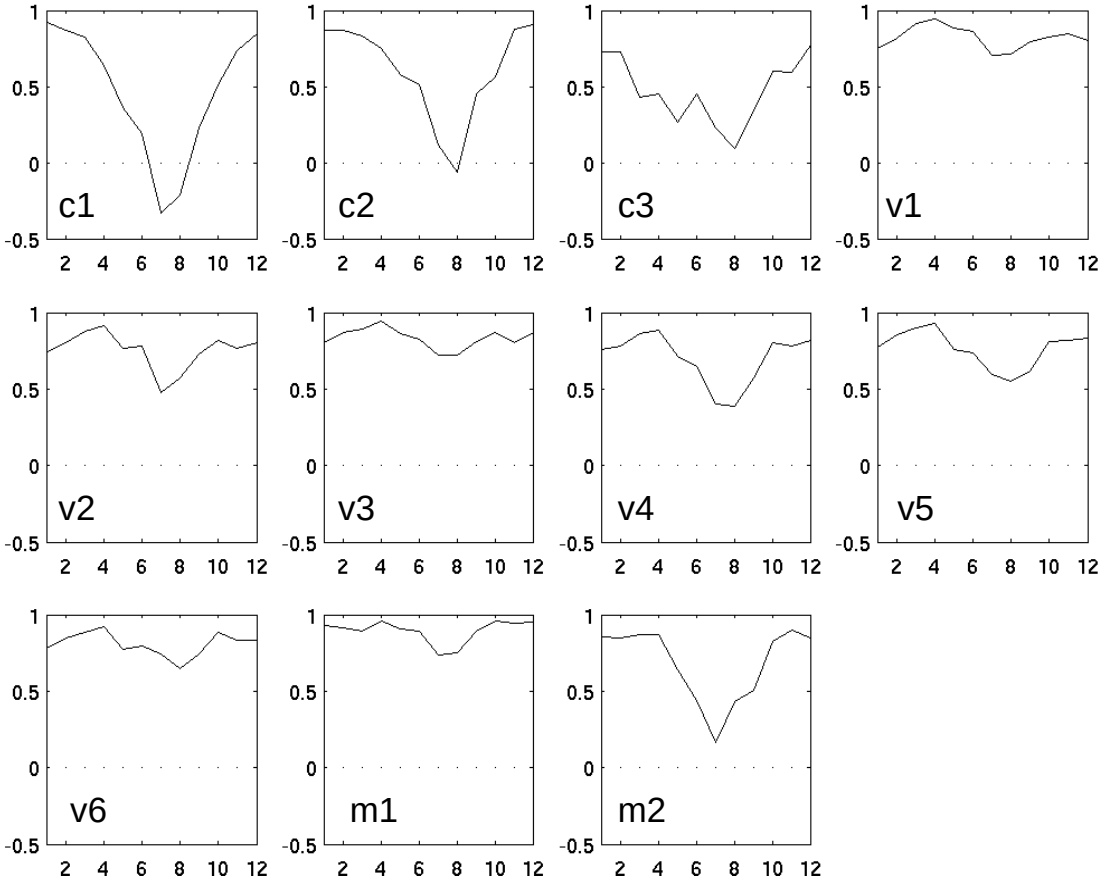

Figure 29. Variation of correlation of monthly mean daily max temperature with observation for the period 1948–1996 at coastal (c1 to c3), central valley (v1 to v6), and mountain (m1 and m2) stations

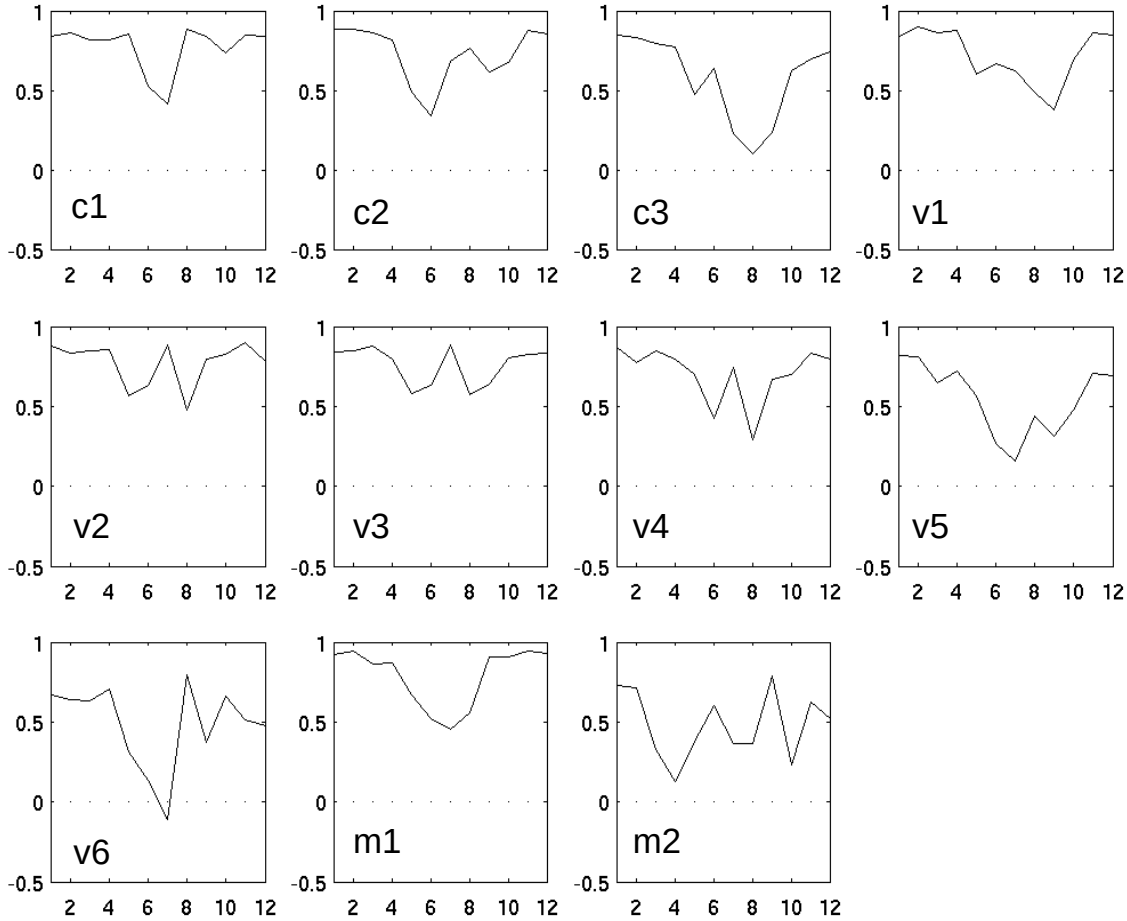

Figure 30. Variation of correlation of monthly mean precipitation with observation for the period 1948–1996 at coastal (c1 to c3), central valley (v1 to v6), and mountain (m1 and m2) stations

These conflicting results of CaRD10 need to be examined in detail. Preliminary research suggests several causes. One is that the current downscaling does not take into account changes in land use, irrigation, and urbanization, or changes in greenhouse gases and aerosol. The second is that the land surface processes affect near surface temperature too strongly in the model. A third possible reason is the effect of poorly analyzed coastal sea surface temperature with a cooling trend affecting the long-term temperature trend over land.

Figure 31 shows the geographical distribution of trends in CaRD10 for January and July. In January, the warm trend is apparent over most of the land region. The positive trend is greatest over the Sierra Nevada and Northern California/Oregon, as well as large part of Nevada. The Central Valley displays weak or no trend. During July, most of the area shows a negative trend with a slight positive over Nevada and part of Oregon. There is a strong cold trend in coastal ocean surface temperature, which seems to have some influence on the negative trend in the Central Valley. The impact of coastal SST on

California is not well documented. Further study of the possible problem of SST used in CaRD10 is warranted.

Figure 32 compares the trend of near surface temperature between CaRD10 and R1. There is very little resemblance between the two figures in January, but the two tend to agree better with slight cooling in the valley and warming at other places in August. The trend in downscaling at or near the surface may not be controlled by the lateral boundary forcing, but by some other mechanism—namely the regional model land surface physics and detailed topography. The seasonal variability of this regional model's response—and accordingly the accuracy of the trend in CaRD10—still requires more detailed analysis and validation.

As the last demonstration of the validation of decadal variability, the seasonal variation of monthly mean precipitation at 11 coastal, central, and mountain stations were compared between two 25 year periods: 1950–1974 and 1975–1996. The research team observed a clear shift in the maximum precipitation month from the December-January 1950–1974 period to the January–March,1975–1996 period (Figure 33a). Similar shifts were found in the observations (Figure 33b). Although this is just a simple demonstration, the CaRD10 is capable of reproducing decadal variability in the precipitation.

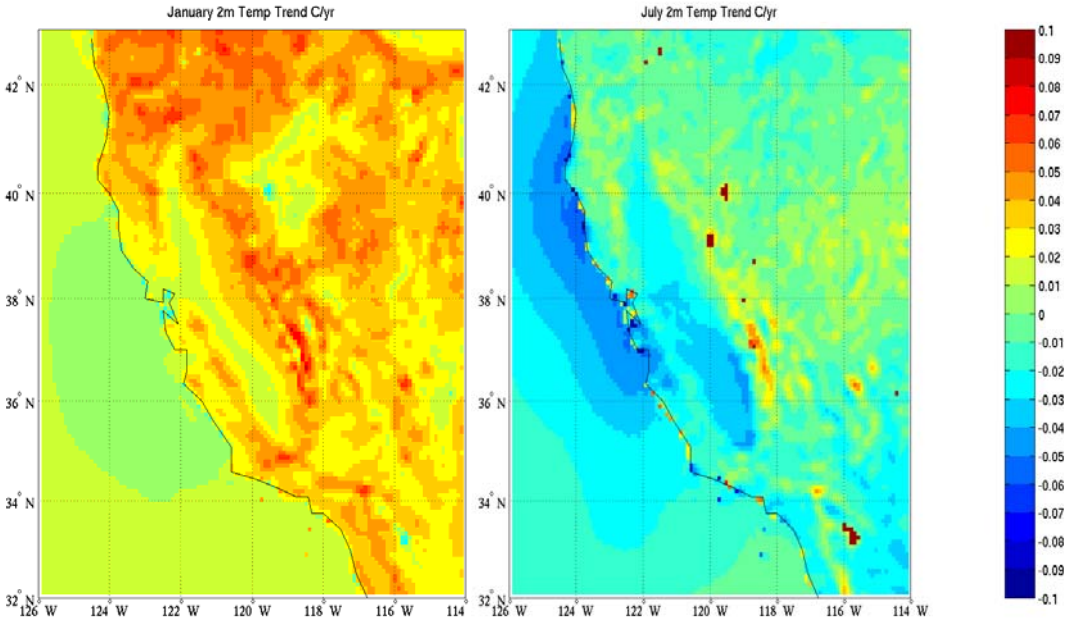

Figure. 31. CaRD10 1950–1996 trend of 2-meter temperature for January (left) and July (right)

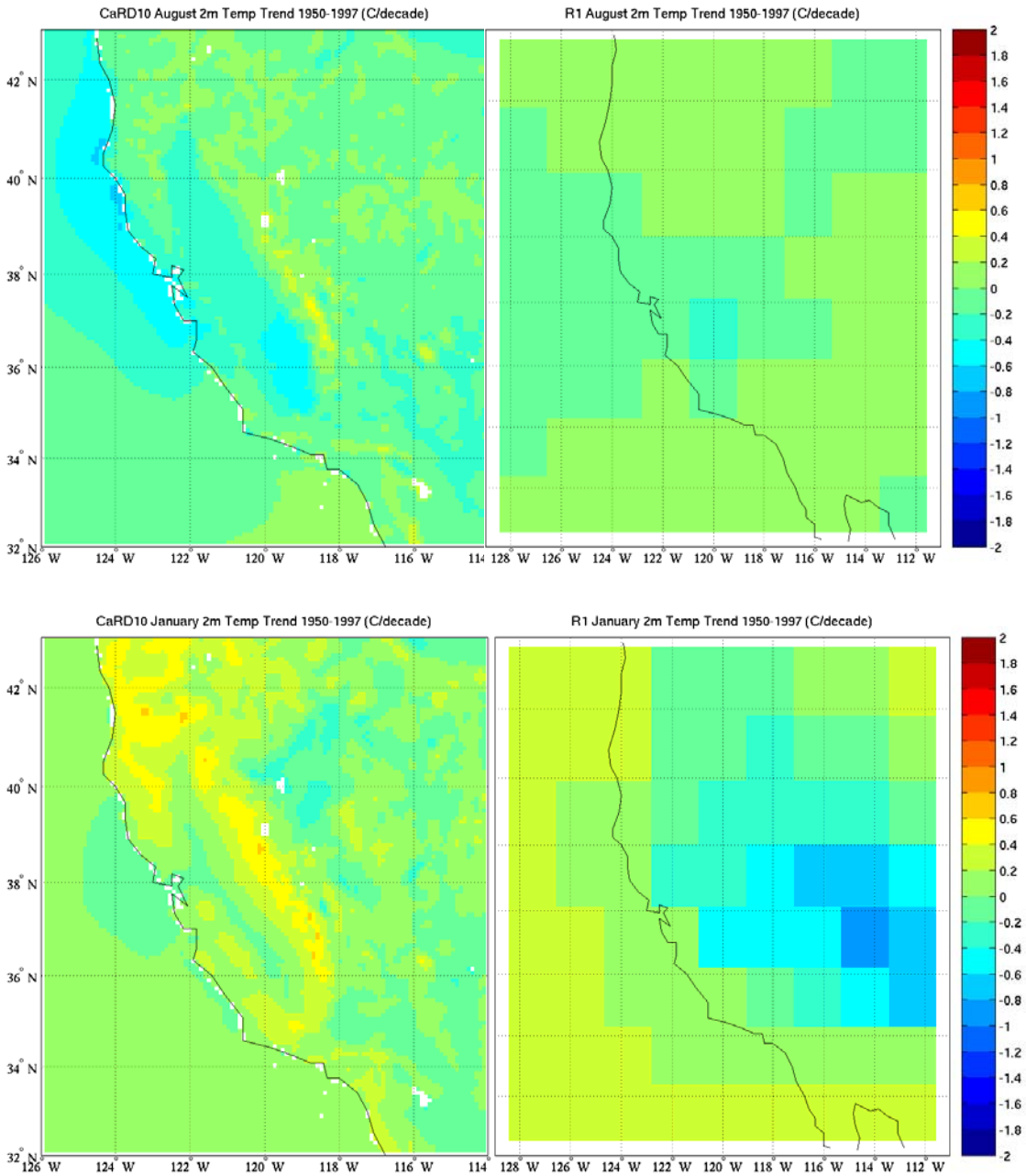

Figure 32. Comparison of 1950–1997 trend of near surface temperature between CaRD10 (left) and R1 (right) for January (bottom) and August (top)

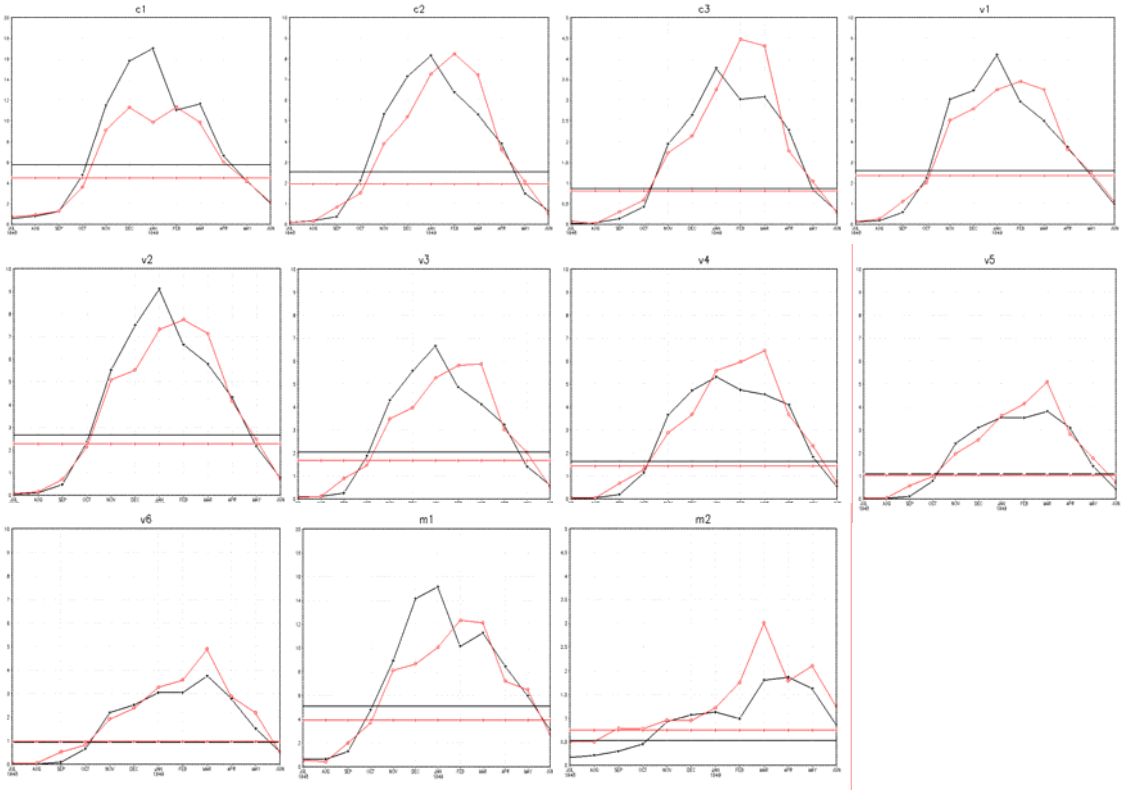

Figure 33a. Seasonal variation of monthly averaged precipitation in CaRD10 at 11 selected observation locations. Black lines are for the period 1950–1974 and red lines for 1975–1996. The horizontal lines are the annual averages.

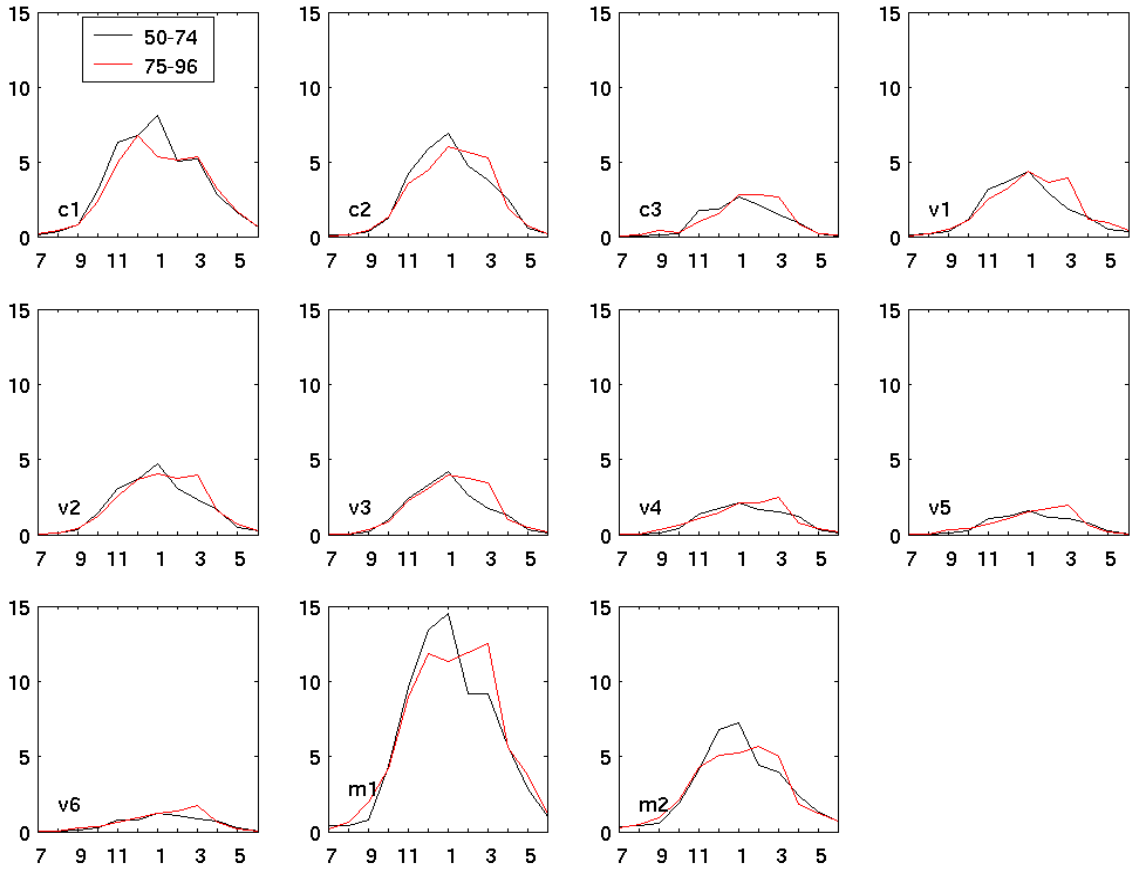

Figure 33b. Same as Figure 332a, but from station observation

4.0 Comparison with North American Regional Reanalysis

Although there are several differences in the observations used between R1 and NARR (for example, satellite-retrieved temperature versus direct use of radiance), when the dynamical downscaling is compared with NARR, the large-scale components of the two analyses are not expected to be too different. The major difference should appear in the regional scale, since NARR utilizes a dense surface observation network. It is, however, noted that the NARR does not utilize 2-meter temperature observation over land, and it is also noted that although near-surface winds and humidity are used, their impact on the analysis is found to be "marginal" (Mesinger et al. 2006). Thus, the only small scale observation that significantly impacted NARR was the surface pressure, but how much the small-scale surface pressure observations affect the analysis of other variables is not very clear. In addition to conventional surface observations, NARR utilizes observed precipitation in the data assimilation. This distinguishes NARR from other global reanalyses and makes it a unique product. The observed precipitation will add small scale information provided by the precipitation analysis to the resulting analysis.

The downscaling technique used in CaRD10 is less accurate than the data assimilation analysis, because it does not utilize regional, small-scale observations. However, as was shown in the comparison of the analyses with station observations, the CaRD10 is not necessarily worse than NARR, which is probably due to its finer horizontal resolution. Since there is no apparent reason to assume that NARR is closer to the observation, as shown in the previous section (with the exception of precipitation), the comparison of CaRD10 and NARR is simply a demonstration of how two analyses are similar and/or different, and does not provide the quality of the analysis. The exception is precipitation, since NARR utilized observed precipitation analysis.

Figure 34a, b compares January and July mean 2-meter temperature. The geographical patterns are very similar between the two panels, but with more regional detail in CaRD10. NARR is generally warmer than CaRD10 due to the smoother topography used in NARR. Figure 35a, b compares 10-meter winds in January and July. Again, during January, the patterns are very similar, but with more small scale detail in CaRD10. Note the difference in wind vector in the Southern California coast where CaRD10 shows much stronger offshore winds than NARR. During July, the patterns are similar over most of California and the northern part of the domain, but a large difference exists over the northern end of the Gulf of California and along the eastern boundary, where strong southerly monsoon flow (Mo et al. 2005) is almost entirely lacking in the CaRD10. The southwesterly flow from over the southern half of Nevada is also very weak in CaRD10. This lack of monsoonal southerly jet is due to the placement of the lateral boundary, where R1 did not resolve the small-scale monsoonal jet due to its coarse horizontal resolution (Mo et al. 2005).

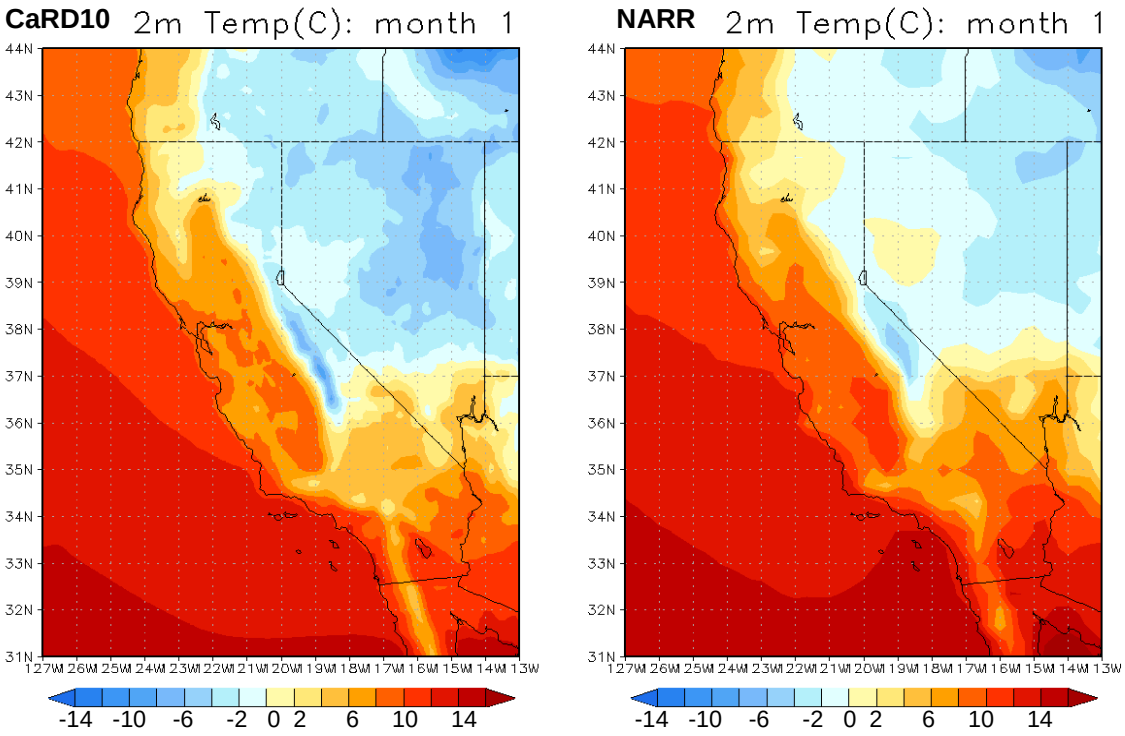

Figure 34a. Comparison of January mean 2-meter temperature between CaRD10 (left) and NARR (right)

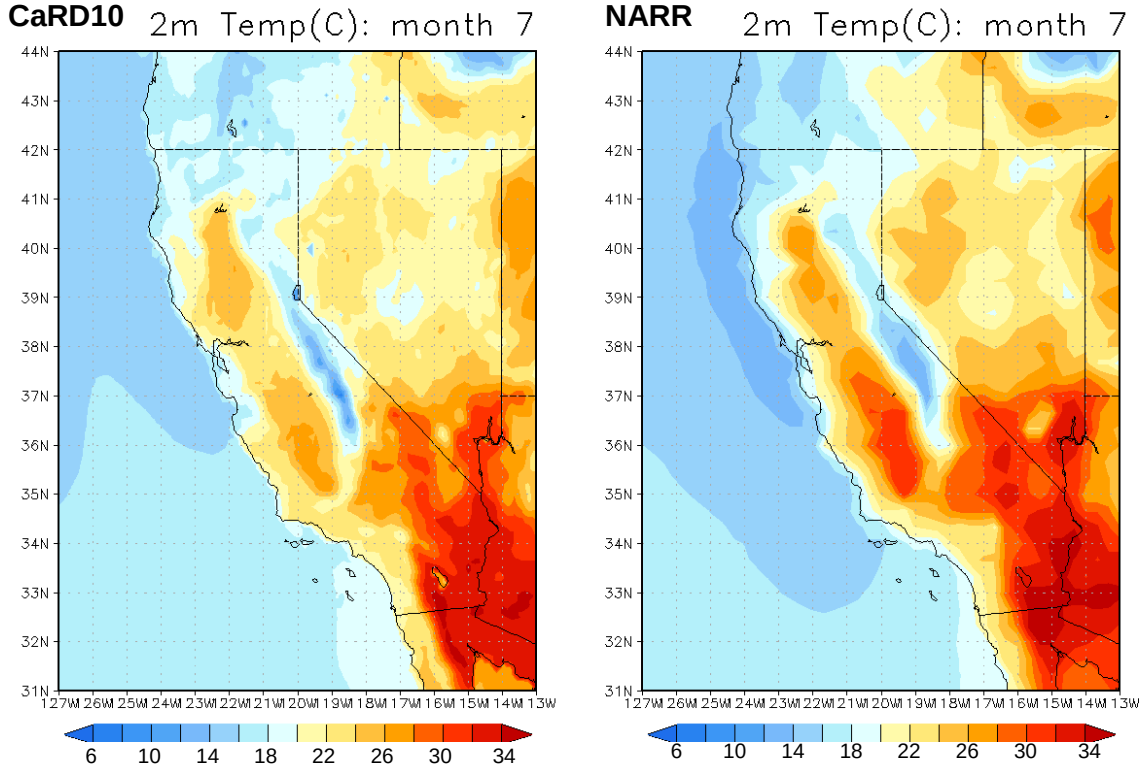

Figure 34b. Same as Figure 34a, but for July

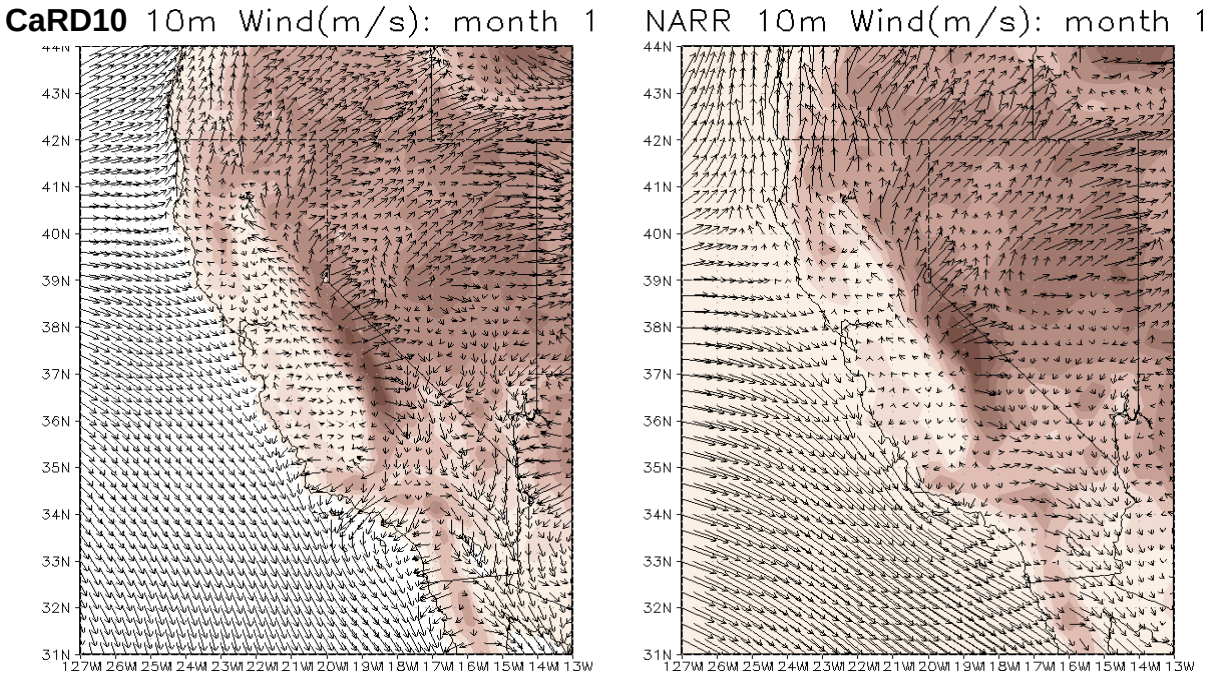

Figure 35a. Comparison of January mean 10-meter wind vector between CaRD10 (left) and NARR (right)

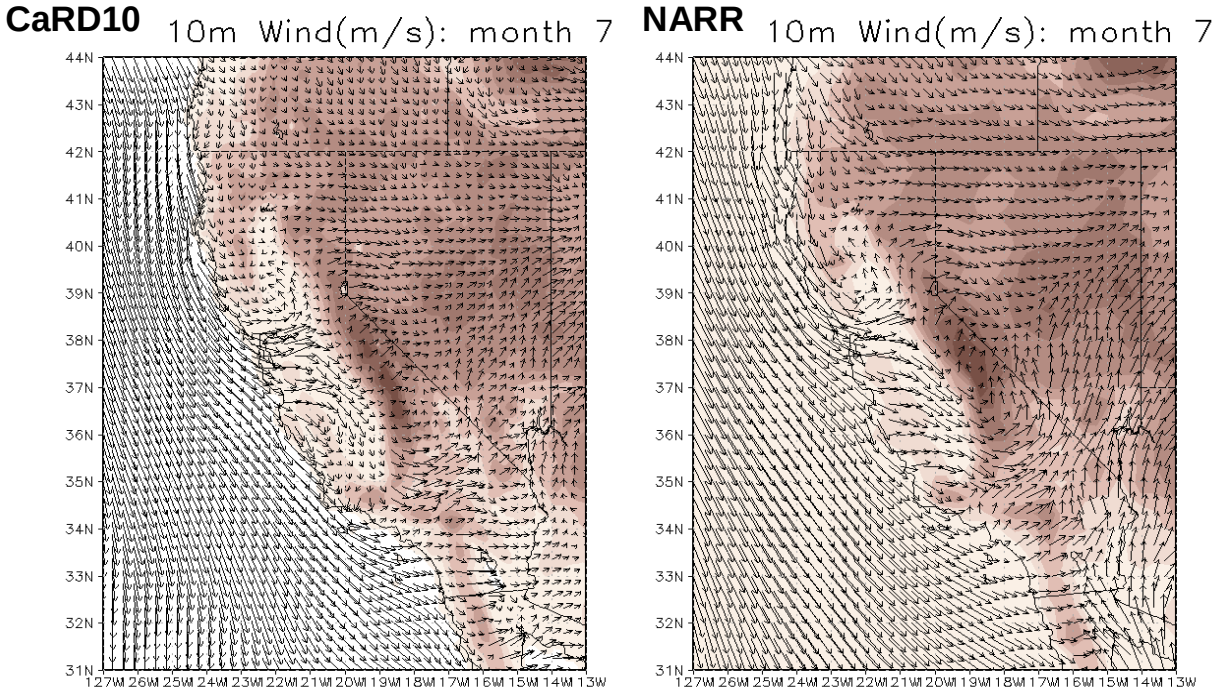

Figure 35b. Same as Figure 35a, but for July

Figure 36a, b compares January and July mean precipitation. Note that the precipitation in NARR is based on independent analysis of precipitation (Higgins et al. 2000) and not on the model produced precipitation. The patterns are very similar, but the CaRD10 precipitation amount is much greater, by nearly a factor of two, both in January and July. This overestimation of precipitation was also suggested in the comparison with station observation detailed in Section 3. In addition, during July, the monsoonal precipitation maximum over Arizona is missing in CaRD10, probably due to the lateral boundary placement that weakened the southerly jet over the Gulf of California.

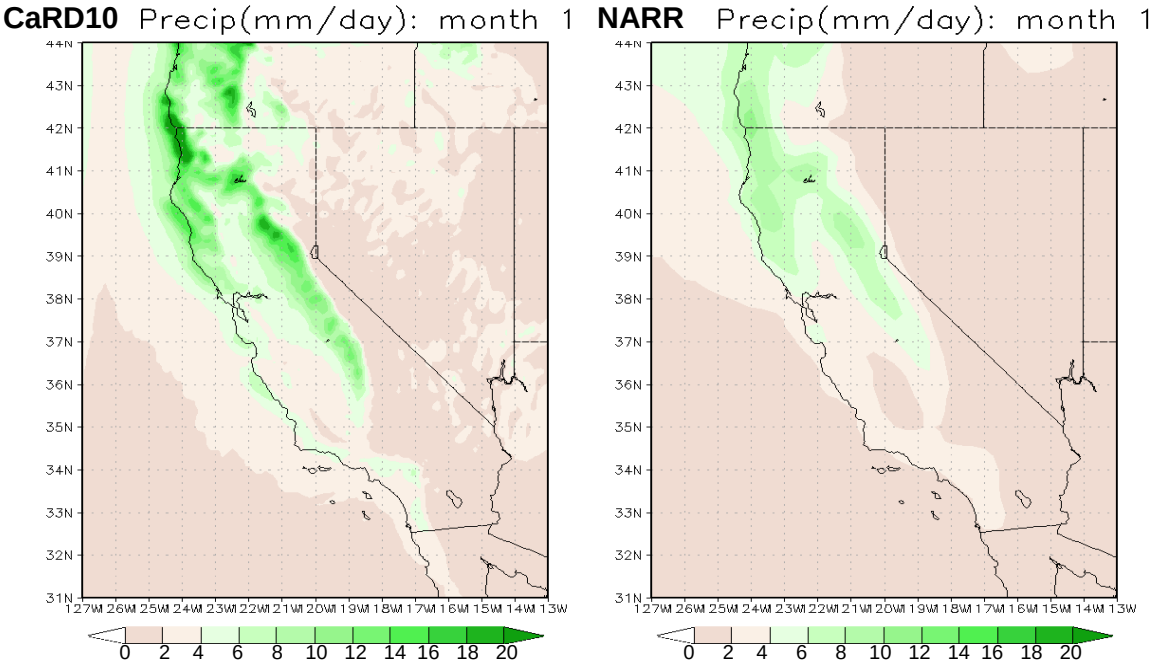

Figure 36a. Comparison of January mean precipitation between CaRD10 (left) and NARR (right)

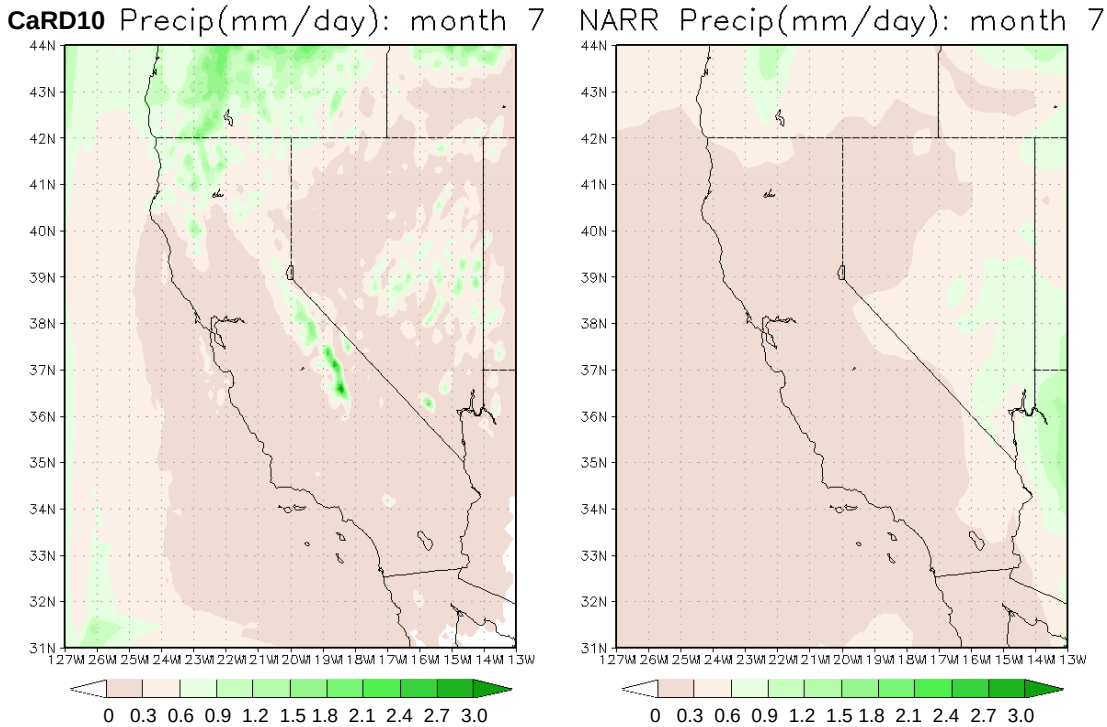

Figure 36b. Same as Figure 36a, but for July

Figure 37a, b compares soil moisture in the layer 10–200 cm underground. The patterns are not very similar in both January and July, reflecting the difference both in precipitation and land model between CaRD10 and NARR (OSU scheme versus NOAH scheme). The NARR lacks small-scale detail in soil moisture, due to coarser resolution and also to the resolution of the observed precipitation. Without observation of soil moisture, it is difficult to judge the quality of this field. However, the use of observed precipitation and an improved land scheme might possibly give an advantage to NARR.

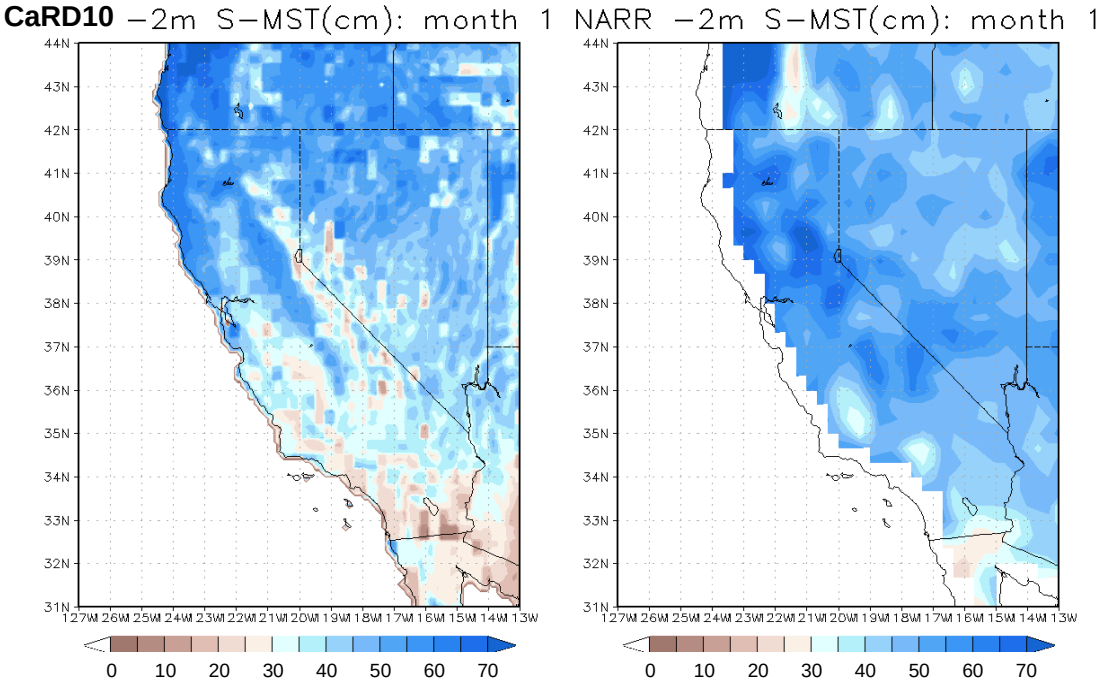

Figure 37a. Comparison of January mean soil moisture between CaRD10 (left) and NARR (right)

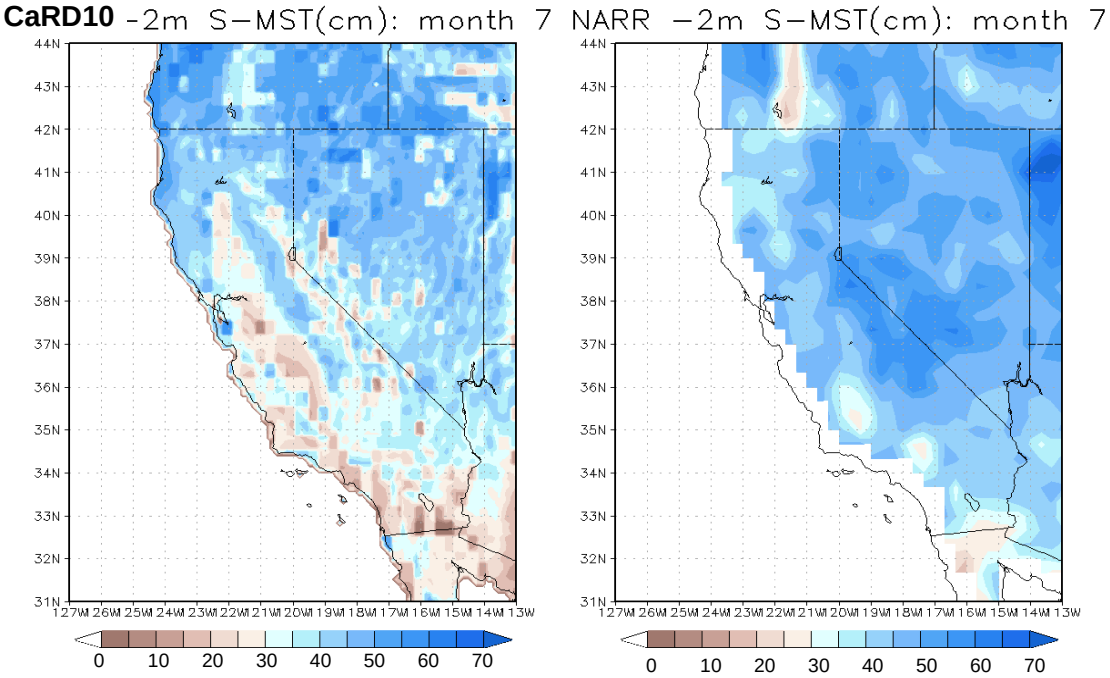

Figure 37b. Same as Figure 37a, but for July

Figure 38a, b compares climatology of surface evaporation between CaRD10 and NARR. The patterns are different, but some similarity exists. In January, the increased evaporation over Sierra can be seen on both analyses, but it is much stronger in CaRD10. The enhanced evaporation over the ocean just north of Los Angeles, which is not observed in NARR, is worthy of note. The area is characterized by the strong offshore flow as shown in Figure 34a (left), which is not so clear in NARR, although there are some weak indications. This strong offshore wind is responsible for enhanced evaporation in CaRD10.

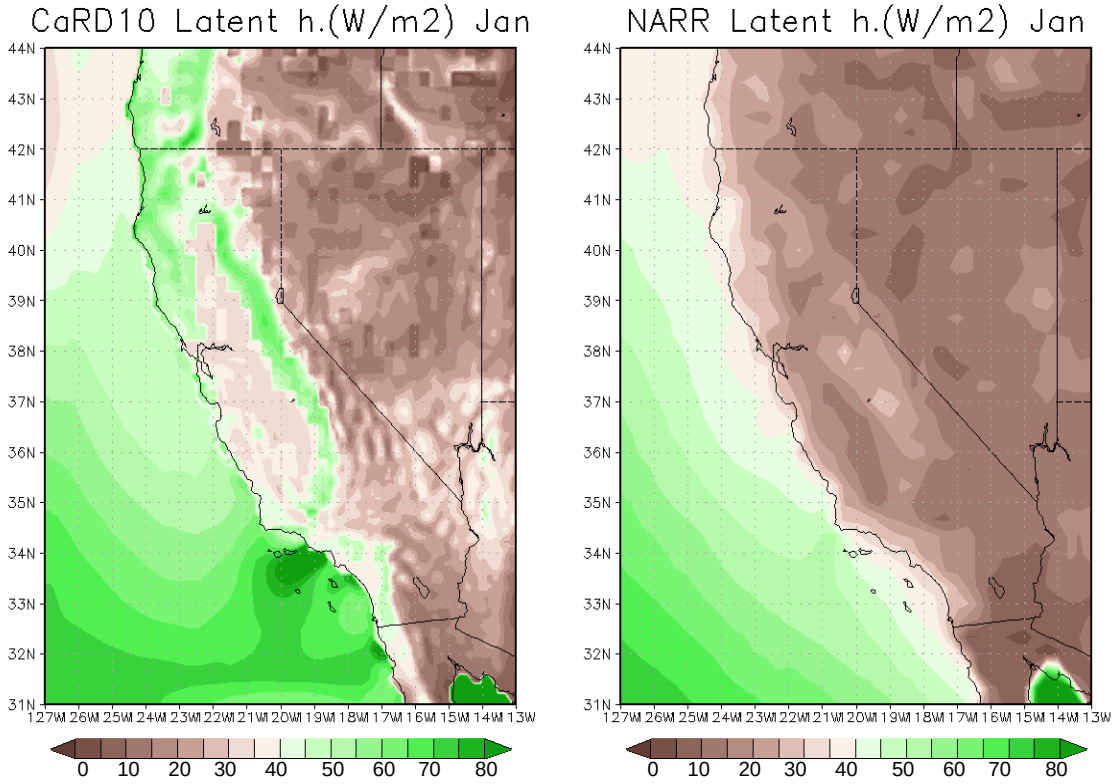

Figure 38a. Comparison of surface evaporation (January) between CaRD10 (left) and NARR (right)

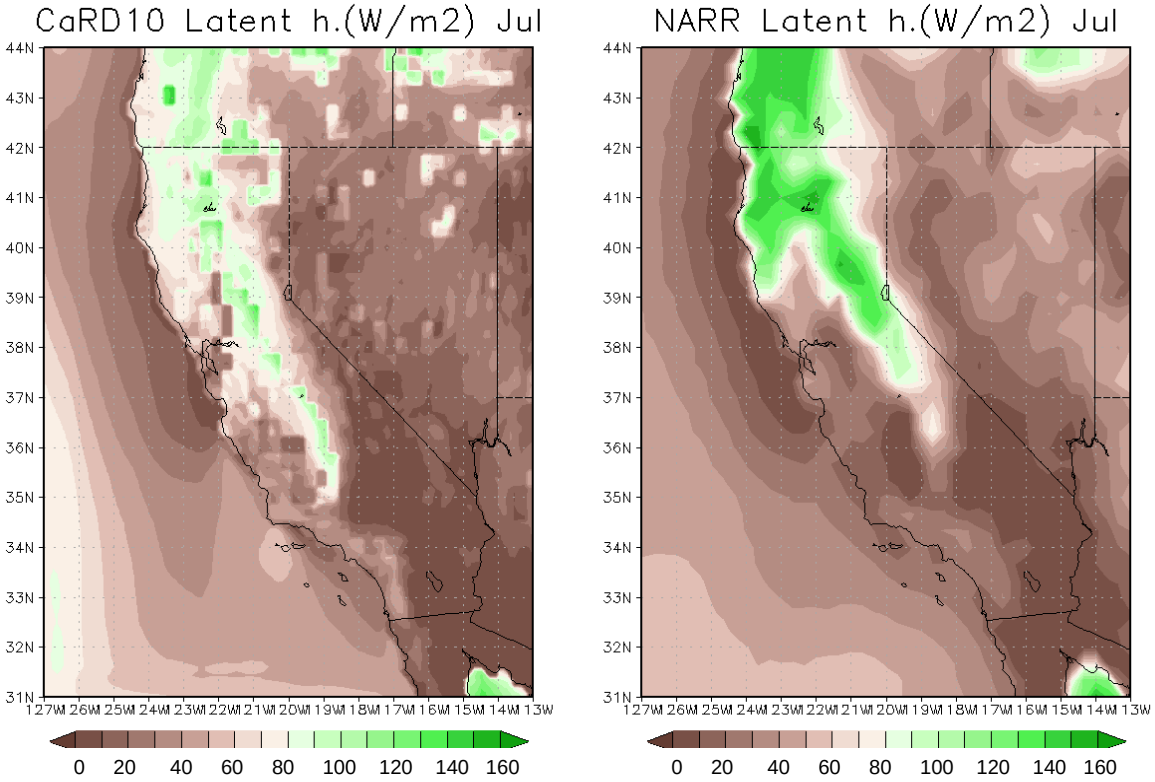

Figure 38b. Same as Figure 38a, but for July

Figure 39 compares the climatology of the diurnal variation of near-surface temperature. Since NARR is available 3-hourly, the output of the same interval from CaRD10 is used for comparison. In general, the two analyses agree very well. Interesting features to be noted are the strong inflow of oceanic air into the Central Valley through the San Francisco Bay Area, branching north and southwards as the flow hits the terrain. This flow feature has large diurnal variation. The other noteworthy feature is the large-scale southerly flow which develops over the entire state of Nevada at UTC 18–21.

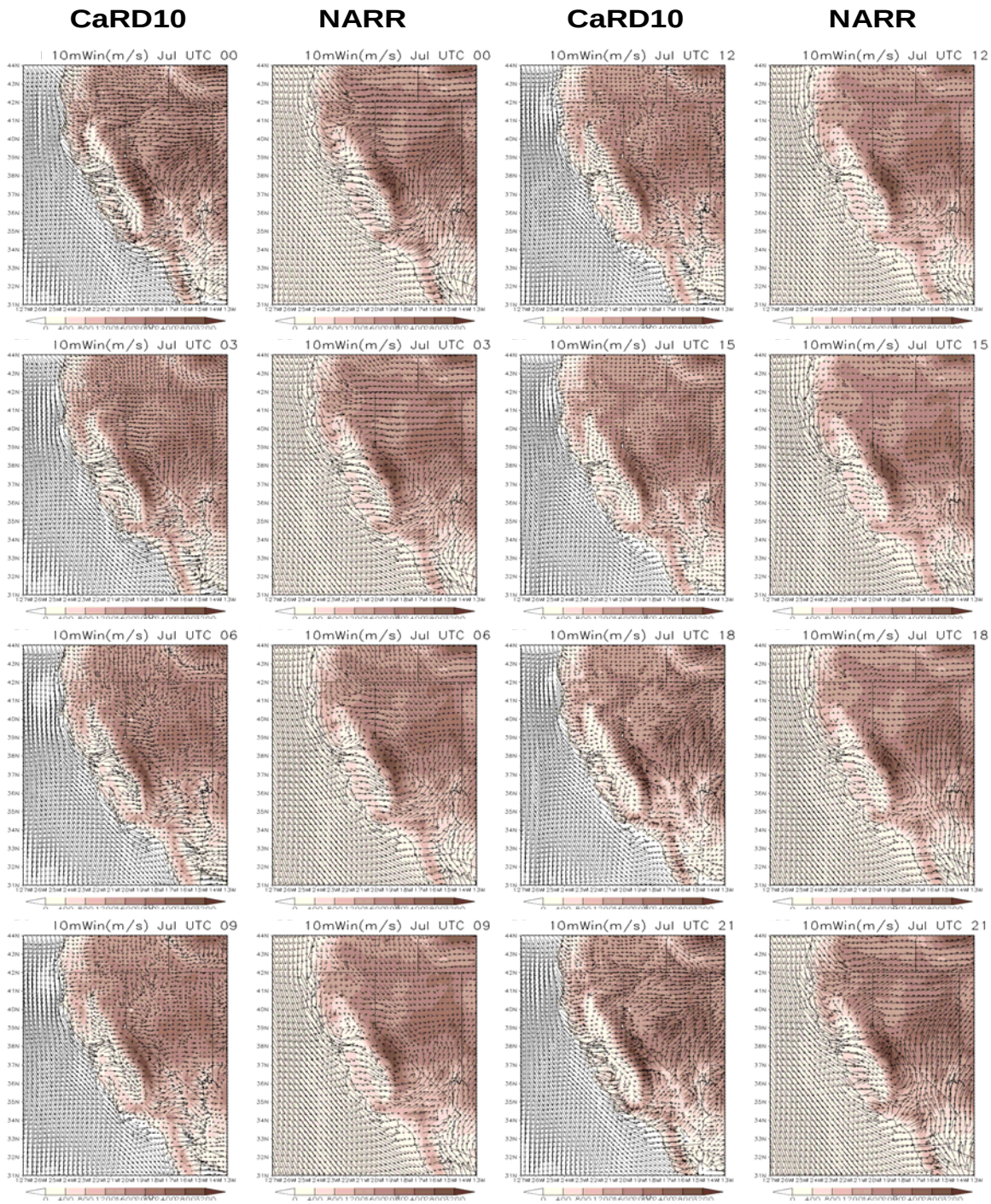

Figure 39. Comparison of mean diurnal variation of near surface winds in July between CaRD10 (left) and NARR (right)

Figure 40 a, b compares the trends of the January and July near-surface temperature during 1979–2002 (when the NARR is available). In January, overall warming in the eastern part of the domain is common to all three analyses, while many small-scale details in the CaRD10 and NARR do not agree. Over the state of California, the weak cooling trend over Sierra Nevada and warming in the valley, as well as a strong warming in Northern Nevada can be seen on both CaRD10 and NARR, but does not appear in R1. In August (Figure 40b), the trends in CaRD10 and NARR agree better, although the trend is much larger in CaRD10. The pattern of the trend in R1 seems to agree with NARR, although it lacks detail.

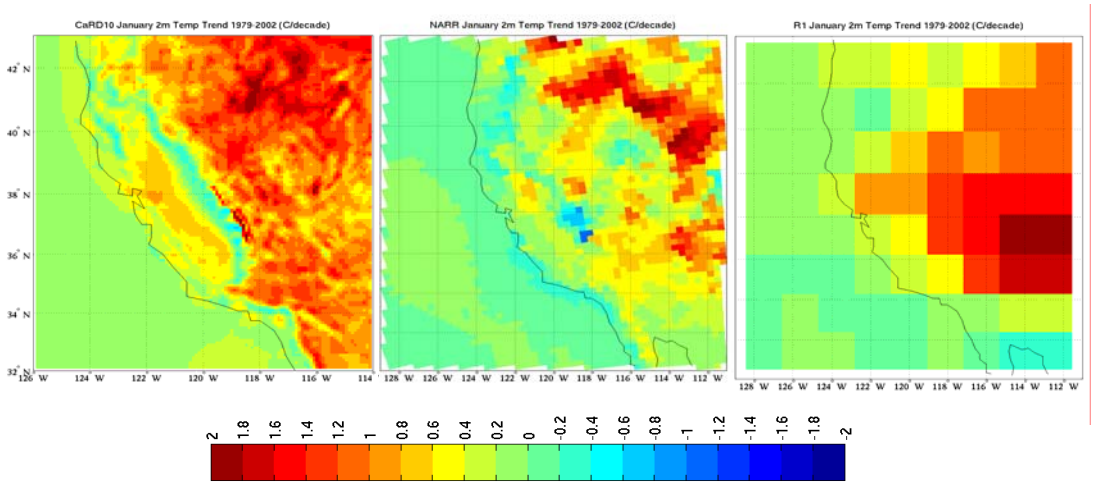

Figure 40a. Comparison of 1979–2002 trend between CaRD10 (left), NARR (center) and R1 (right) in January

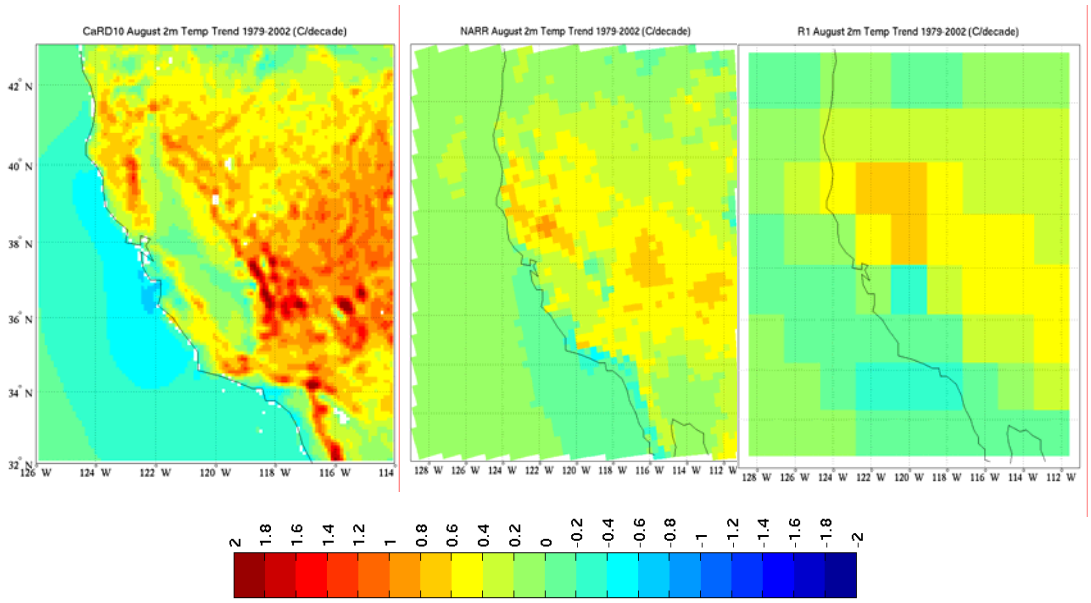

Figure 40b. Same as Figure 40a, but for August

5.0 Comparison of Precipitation with Gridded Analysis

The validation of precipitation against station observation is problematic due to measurement error and representativeness of the observation. The research team tried to overcome this problem by using high-resolution gridded precipitation analysis. The team utilized two products: The Parameter-elevation Regression on Independent Slopes Model (PRISM), and the Higgins analysis. PRISM (Daly et al. 1994, 2001, 2002) is a method to analyze small-scale precipitation distribution over complex topography, by combining various information, such as distance, elevation, cluster, vertical layer, topographic facet, coastal proximity, and effective terrain. For PRISM, only monthly average analyses were available, and the research team used them for validating monthly average and long-term trends. Higgins analysis (Higgins et al. 2000) is based on modified Cressman successive-scan analysis technique, and available daily on a 1/8-degree grid. This analysis is used as observed precipitation in the NARR data assimilation system. The research team utilized this analysis for computing threat and bias scores of the daily CaRD10 precipitation.

Figure 41 compares the bias of monthly climatology (January and August) against the PRISM analysis for CaRD10, NARR, and R1. It is apparent that the bias in CaRD10 is large, exceeding 9 millimeters (mm)/day in some places. The bias is much smaller in NARR due to the use of observed precipitation. This NARR bias is simply the difference of the NARR (Higgins et al. 2000) and PRISM precipitation analyses. It is interesting to note that the patterns of the CaRD10 and NARR biases are very similar, both in winter and summer. Whether this is a problem of PRISM analysis, or the common systematic error of numerical models (RSM and NCEP Eta models) is a subject of future research. It is also noted that the R1 bias is much smaller, but the lack of small-scale detail makes it difficult to judge the quality of the analysis.

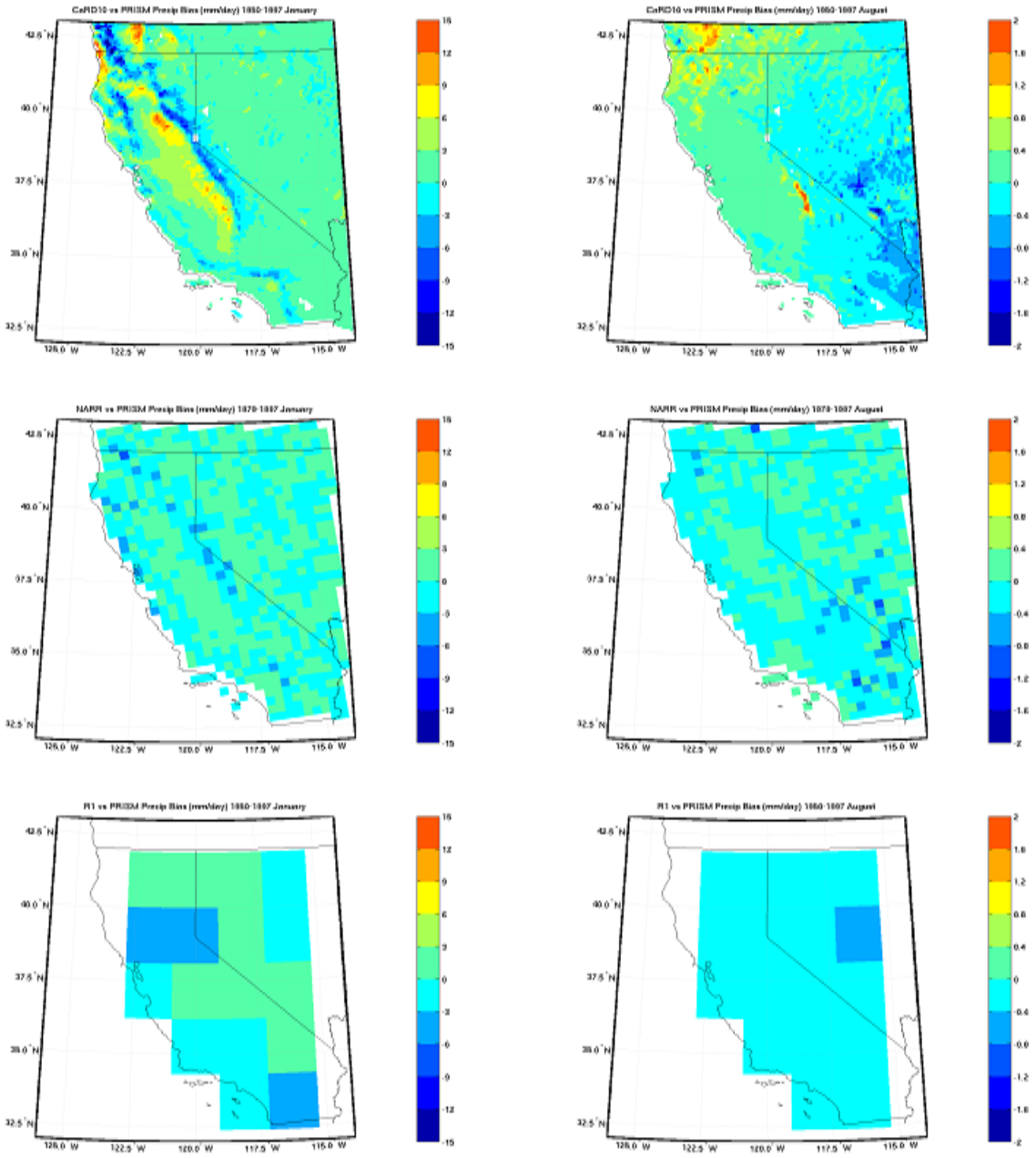

Figure 41. Comparison of the precipitation bias against PRISM analysis for CaRD10 (top), NARR (middle), and NRR (bottom) in January (left column) and August (right column). Unit in mm/day.

Equitable threat scores (Schaefer 1990) and bias scores are good measures of the precipitation skill of the model in terms of its spatial extent. The equitable threat score is defined as:

$$\frac{H - CH}{F + O - H - CH}$$

where F is the number of grid points that forecast more than the precipitation threshold. O is the number of grid points that observe more than the threshold. H is the number of grid points that correctly forecast more than the threshold. CH is the expected number of correct forecasts due to chance (F*O/T), where T is the total number of grid points inside the verification domain. The threat score of zero indicates random predictions and 1 indicates perfect forecast for that particular threshold. The threat score is basically the ratio of the correct forecast area to the total area of the forecast and observed precipitation. The score is penalized for forecasting rain in the wrong place and not forecasting it in the right place. The bias score is defined as F/O. The score does not assess the placement of precipitation but indicates if a model is over- or under-forecasting areas of precipitation. The best score is 1.0. Scores above (below) 1.0 mean wet (dry) bias of precipitation forecast.

Table 9 shows the daily precipitation skill scores of NARR and CaRD10 against Higgins analysis for January and August of 1998. Not surprisingly, NARR threat scores in January are consistently better than those of CaRD10, but CaRD10 scores are still reasonable considering precipitation is not assimilated in CaRD10. The imperfect skill of the NARR is due to the spatial and temporal interpolation of precipitation, as well as to the precipitation assimilation method, which does not reproduce the observed precipitation exactly. Both NARR and CaRD10 show the best skill at the threshold of 2 mm/day. CarD10 bias scores are better than NARR for smaller precipitation thresholds, but a wet bias is apparent in larger precipitation thresholds. These scores suggest that CaRD10 precipitation in January covers reasonable areas of precipitation as a whole, but the area is too wide and too much precipitation occurs in the wrong places. August precipitation is small, and CaRD10 shows no skill in the threat score; while NARR shows some skill, although the scores are considerably lower than January. Bias scores suggest that CaRD10 is too dry in August.

Table 9. Daily precipitation skill scores of NARR and CaRD10 in January and August of 1998 against Higgins analysis

	January				August			
Threshold	Threat		Bias		Threat		Bias	
(mm/day)	NARR	CaRD10	NARR	CaRD10	NARR	CaRD10	NARR	CaRD10
0.05	0.25	0.19	0.75	0.96	0.24	0.03	0.50	0.44
0.1	0.34	0.20	0.82	1.04	0.27	0.03	0.71	0.56
0.2	0.40	0.22	0.89	1.09	0.27	0.03	1.09	0.59
0.5	0.48	0.27	0.99	1.13	0.25	0.02	1.66	0.70
1	0.52	0.30	1.01	1.14	-	-	-	-
2	0.53	0.32	1.06	1.15	-	-	-	-
5	0.47	0.30	1.20	1.27	-	-	-	-
10	0.37	0.24	1.42	1.65	-	-	-	-

Figure 42 is the comparison of the temporal correlation of monthly averaged precipitation against the PRISM analysis in January and August, computed for the 1979–2002 period. It is very clear that the NARR has extremely high correlation, since it used observed precipitation. While the correlation in CaRD10 is lower, particularly in August, since there are very few rain events in the region during August, this low correlation in summer may not be surprising. The CaRD10 correlation in winter over the State of California is generally above 0.7, which agrees with the correlation against station observation shown in Figure 27. The correlation is particularly low on the lee side of the Sierra Nevada. This may be likely due to the lack of cloud water prediction in this version of the model, which prevents advection of cloud water to the lee side of the mountains, causing difficulties in reproducing precipitation spreading to the east of the high mountain ranges. The correlation of precipitation in the R1 in winter is quite respectable, considering its coarse horizontal resolution. The summer correlation is much lower, although precipitation events are very scarce in this season.

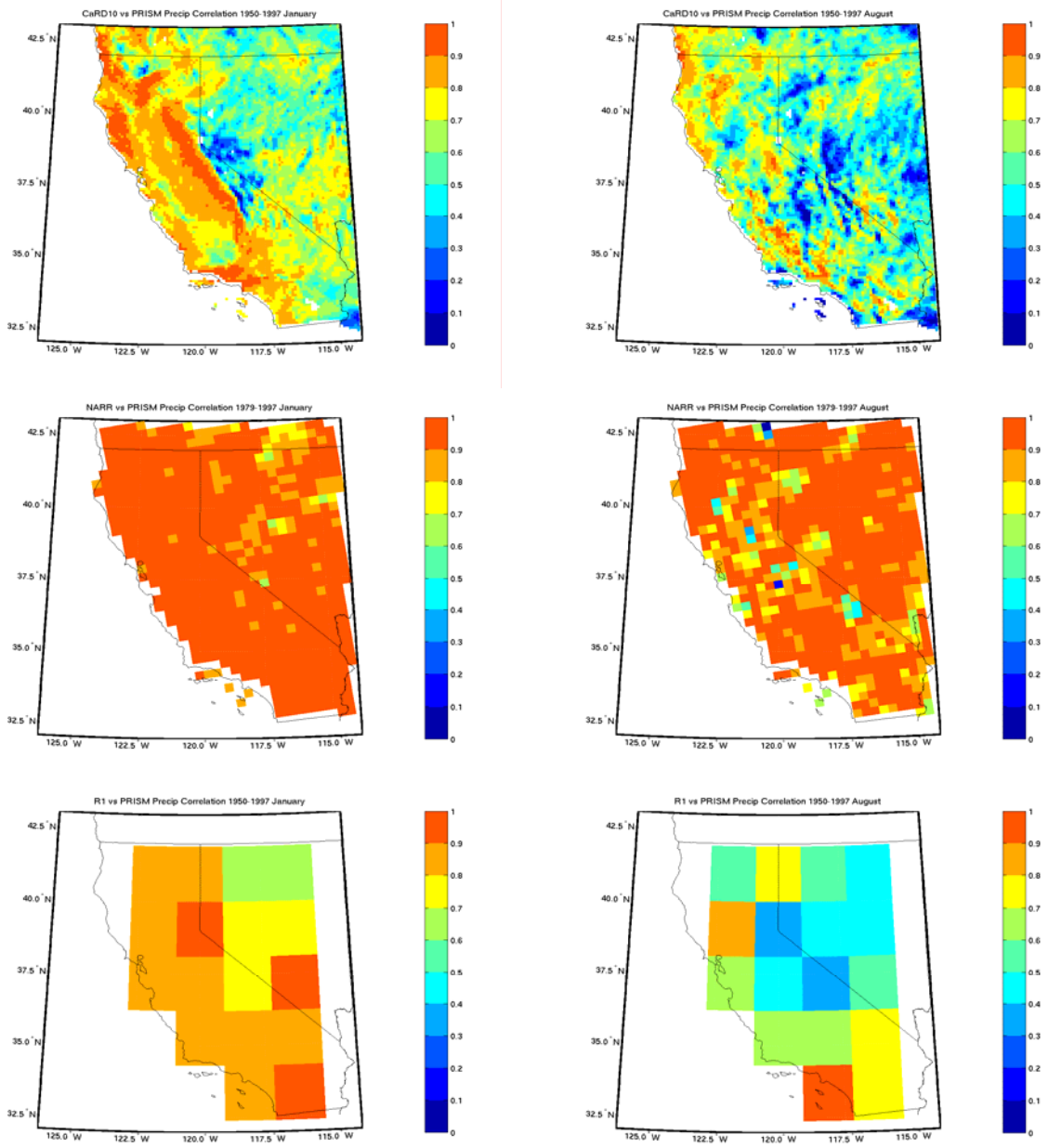

Figure 42. Comparison of the temporal correlations of monthly mean precipitation against PRISM analysis in January (left column) and August (right column) for CaRD10 (top), NARR (middle), and NRR (bottom) computed for 1979–2002 period

Figure 43 compares bias–removed root mean square difference of precipitation from PRISM analysis. NARR again fits best with PRISM for both months, but some difference is apparent along the Sierra Nevada, which also shows up in the CaRD10. This may most likely point to the uncertainties in the observed precipitation over high elevations.

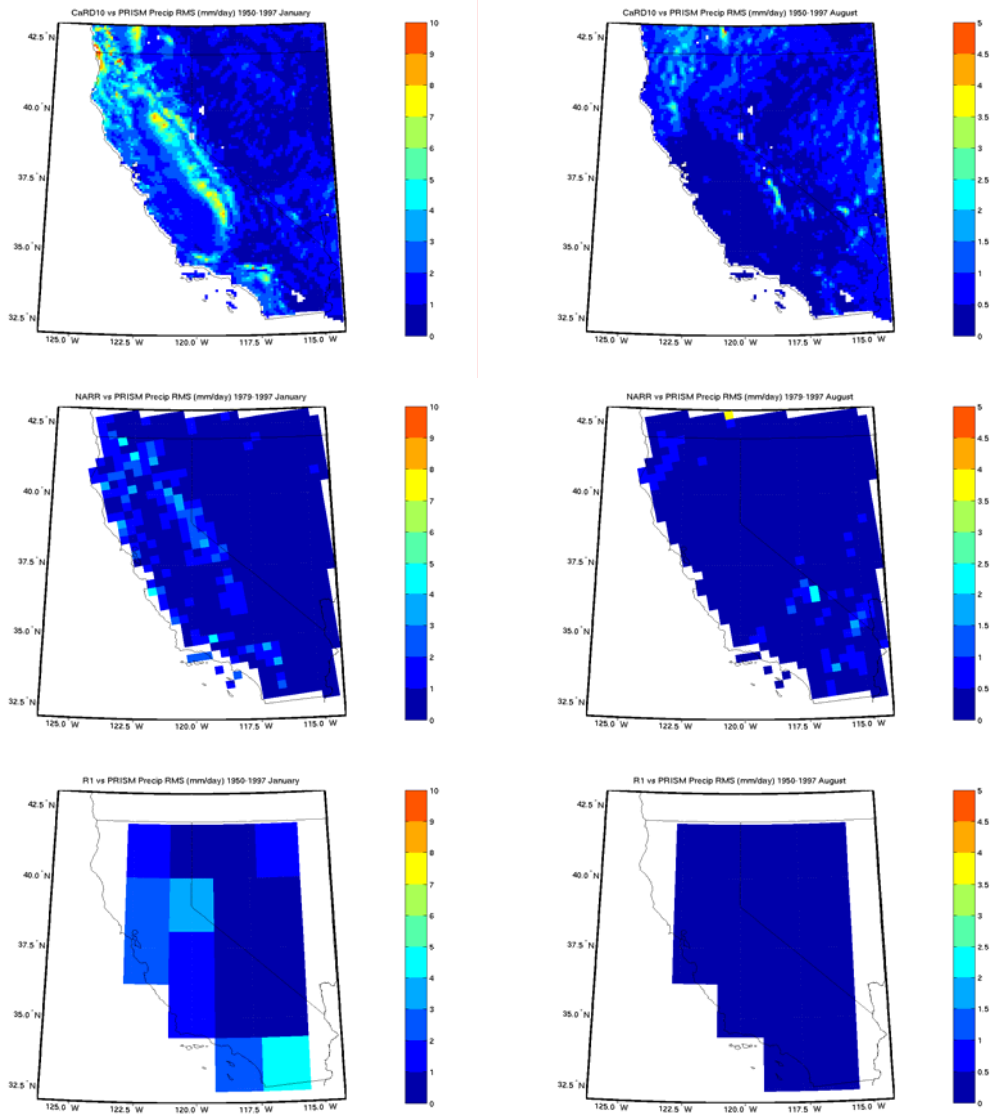

Figure 43. RMS difference of monthly average precipitation between CaRD10 (top), NARR (middle), and R1 (bottom) with PRISM analysis. Left column is for January and right column is for August.

Finally, the 1950–1997 trend in precipitation is compared between PRISM and CaRD10, as shown in Figure 44. Both patterns agree quite well, with much more small-scale detail in CaRD10. The tendency of increased precipitation in the south and reduced precipitation along the northern California/Oregon coast stands out. The negative tendency along the high Sierra Nevada is very clear in CaRD10, but some hint of it is seen in PRISM.

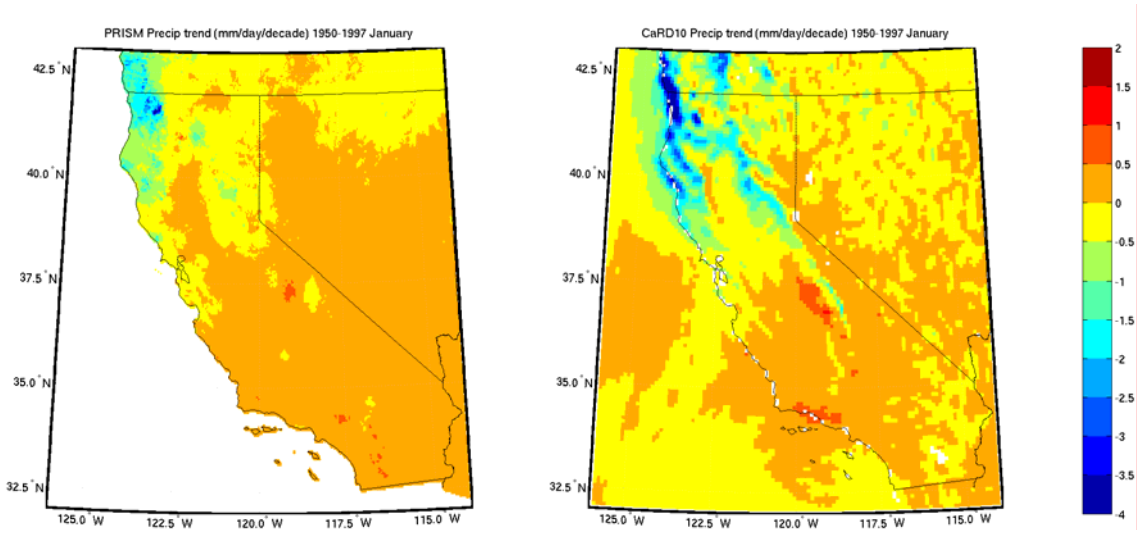

Figure 44. Comparison of 1950–1997 trend in January mean precipitation rate, PRISM (left), and CaRD10 (right). Unit is in mm/day/decade.

In summary, the comparison with PRISM precipitation analysis indicated that the CaRD10 is reasonable in reproducing year-to-year variation of monthly mean precipitation, as well as its long-term trend. However, the absolute amount of precipitation has a significant positive bias. These conclusions agree well with the CaRD10 comparison with station observations. The NARR precipitation agrees nearly perfectly with PRISM, since it utilizes observed precipitation. There is some difference in the precipitation analysis used by NARR and PRISM, particularly over high altitude, where both analyses show some degree of difference.

6.0 Conclusions

The dynamical downscaling of NCEP/NCAR 50-year Reanalysis was performed over the State of California and the neighboring states and ocean. The horizontal resolution of the regional model is 10 km and the output is produced every hour. The integration period covers 57 years, from 1948 to 2005. The Scale Selective Bias Correction (Kanamaru and Kanamitsu 2006) is applied to reduce the error of the scale greater than 1000 km.

Comprehensive validation of the downscaled analyses was performed using available buoy observation over coastal ocean and various land stations. The analyses were also compared with large-scale boundary forcing (R1) to make sure that the regional downscaling does provide regional-scale information more accurately than the large-scale forcing field. In addition, comparison was made with the NARR and with the PRISM precipitation analysis to further ensure the quality of the product. These validations were separately performed for hourly, daily, monthly, and decadal trends.

In general, the quality of the downscaled product is high. The product is definitely better than the coarse-resolution R1, and even better than NARR for some fields. There is a large difference in the quality between winter and summer; winter being better and summer being more problematic. The winds over coastal ocean are much improved by downscaling, but NARR is better, due to the use of the buoy observation in the data assimilation. Over land, the accuracy of CaRD10 near-surface winds and temperature frequently outperforms NARR, due to the finer topography resolved by the CaRD10. The examination of typical mesoscale events, namely the Catalina eddy, Coastally Trapped Wind Reversal, and Santa Ana showed that the downscaling is reproducing characteristic features very well. There are some differences in the skill of the CaRD10 for daily and monthly mean time scales. The monthly mean skill is generally much higher, and seasonal dependency is also different. The long-term trend of near-surface temperature obtained from 1950–1996 agrees fairly well with station observations during winter, but the trend is underestimated. During the summer season, the trend is negative over a large part of the domain in CaRD10, while it is positive in the station observations. This discrepancy is likely the result of poor representation of land process in the model, as well as of the inaccuracies in the coastal sea surface temperature used in the CaRD10.

The precipitation skill showed that the correlation is of the order of 0.5 to 0.6 for daily scale and 0.6–0.8 in the monthly scale, which is reasonably good. However, there is a noticeable positive bias in large precipitation events. Comparison with Higgins analysis revealed that the CaRD10 precipitation is more than 1.5 times that of the observed when the precipitation exceeds 10 mm per day. Although the Higgins analysis may not be fully trusted, particularly over complex terrain, the overestimation of the CaRD10 is most likely. The 1950–1997 trend agrees very well between the CaRD10 and PRISM. These precipitation validations seem to suggest that although the absolute magnitude of the precipitation may be problematic in some cases, the long-term trend, year-to-year variation, and probably day-to-day variation are reasonably good and can be used for climate research if researchers are sufficiently cautious.

A comparison of the monthly climatology of CaRD10 with NARR showed that the CaRD10 near-surface temperature and winds are very similar to NARR with more regional detail, especially in winter. During the summer, CaRD10 winds associated with the South West Monsoon and the Gulf of California low-level jet is poorly simulated by CaRD10, due to the placement of the lateral boundary. The comparison of soil moisture revealed that the two are not very similar. This is due to the difference in precipitation (observed in NARR, and model produced in CaRD10) and to the difference in land process parameterization. The latent heat flux and sensible heat flux are a little more similar between the two.

In summary, the downscaled analysis is useful as additional material for observational global change study, but users need to be aware of its strengths and weaknesses before applying it to their own objectives.

Future work will concentrate on the refinement of the downscaling products. The bias in precipitation will be reduced by the use of different convective parameterization. The inclusion of cloud water prediction is also considered. The refinement in snow modeling is desirable and will be forcefully pursued. Another ambitious plan is to perform downscaling with a coupled regional ocean model, which will drastically improve small scale features over ocean. The research team is targeting the second version of the downscaling over California, starting sometime in 2007.

7.0 Data Archive and Availability

The CaRD10 dataset consists of an hourly GRIB (GRIdded Binary) file. The total amount of data is about 5 terabytes (TB) and the data are stored on local raid disks at Scripps, as well as in the file server at the San Diego Supercomputer Center. In addition, daily, monthly, seasonal, and climatological averages are produced. Some frequently used variables are extracted and stored separately as time series files. The GRIB is a machine-independent standard file format used internationally by operational weather forecast centers. Various utility programs to read, process, and convert the file to other formats are available on the Internet.[3]

The variables in the output file are classified into two groups: (1) Standard pressure level fields, and (2) two-dimensional fields. Actual variables appearing in these two groups of fields are listed in Table 10 and 12, respectively. Table 11 provides a list of pressure levels. The volume of various types of data is listed in Table 13.

The data are currently available in-house at Scripps online. They can also be obtained by writing to kana@ucsd.edu or hkanamaru@ucsd.edu. Web access of the entire dataset is now in progress (http://cec.sdsc.edu), and should be complete in mid-summer 2006.

Table 10. List of pressure level variables in the output file

	Variable name	Field description and unit
1	HGTprs	Geopotential height (gpm)
2	UGRDprs	East-west wind component (m/s)
3	VGRDprs	North-south wind component (m/s)
4	TMPprs	Temperature (K)
5	VVEL	Pressure vertical velocity (Pa/sec)
6	RHprs	Relative humidity (%)
7	SPFHprs	Specific humidity (Kg/Kg)
8	ABSV	Absolute vorticity (1/sec)

[3] For example, see the following websites: National Weather Service Climate Prediction Center (www.cpc.ncep.noaa.gov/products/wesley/wgrib.html), NCAR Command Language (NCL) (www.ncl.ucar.edu), and Grid Analysis and Display System (GrADS) (http://grads.iges.org/grads/grads.html).

Table 11. List of pressure levels

#	Pressure levels (hPa)
1	1000
2	925
3	850
4	700
5	600
6	500
7	400
8	300
9	250
10	200
11	150
12	100
13	70
14	50
15	30
16	20
17	10

Table 12. List of non-pressure level variables in the output file

	Name	Field description and unit
1	PRESsfc	Surface Pressure (Pa)
2	PTEND	Surface Pressure tendency (Pa/s)
3	PWAT	Precipitable water (Kg/m**2)
4	RHclm	Column integrated relative humidity (%)
5	TMPtrp	Temperature at tropopause (K)
6	PREStrp	Pressure at tropopause (Pa)
7	UGRDtrp	u-wind at tropopause (m/sec)
8	UGRDtrp	v-wind at tropopause (m/sec)
9	VSSH	Vertical speed at tropopause (1/sec)
10	LFTX	Surface lifted index
11	LFTXB	Best (4-layer) lifted index
12	TMPmwl	Temperature at max wind level (K)
13	PRESmwl	Pressure at max wind level (Pa)
14	UGRDmwl	u wind at max wind level (m/sec)
15	VGRDmwl	v wind at max wind level (m/sec)
16	HGTsfc	Surface elevation (m)
17	PRMSL	Pressure reduced to MSL (Pa)
18	UFLX	Zonal component of momentum flux (N/m**2)
19	VFLX	Meridional component of momentum flux (N/m**2)
20	SHTFL	Sensible heat flux (W/m**2)
21	LHTFL	Latent heat flux (W/m**2)
22	TMPsfc	Sfc skin Temperature (K)
23	SOILW1	Volumetric soil moisture content layer (0-10cm)
24	SOILW2	Volumetric soil moisture content layer (10-200cm)
25	TMPdlr1	Soil temperature layer (0-10cm)
26	TMPdlr2	Soil temperature layer (10-200cm)
27	WEASD	Water equivalent of accumulated snow depth (kg/m**2)
28	DLWRF	Sfc Downward long wave radiation flux (W/m**2)
29	ULWRFsfc	Sfc Upward long wave radiation flux (W/m**2)
30	ULWRFtoa	Toa Upward long wave radiation flux (W/m**2)

Table 12. (continued)

31	USWRFtoa	Toa Upward solar radiation flux (W/m**2)
32	USWRFsfc	Sfc Upward solar radiation flux (W/m**2)
33	DSWRFsfc	Sfc Downward solar radiation flux (W/m**2)
34	TCDChcl	High cloud Total cloud cover (percent)
35	PREShct	Pressure high cloud top (Pa)
36	PREShcb	Pressure high cloud bottom (Pa)
37	TMPhct	Temperature high cloud top (K)
38	TCDCmcl	Middle cloud Total cloud cover (percent)
39	PRESmct	Pressure middle cloud top (Pa)
40	PRESmcb	Pressure middle cloud bottom (Pa)
41	TMPmct	Temperature middle cloud top (K)
42	TCDClcl	Low cloud Total cloud cover (percent)
43	PRESlct	Pressure low cloud top (Pa)
44	PREScb	Pressure low cloud bottom (Pa)
45	TMPlct	Temperature low cloud top (K)
46	PRATE	Precipitation rate (kg/m**2/s)
47	CPRAT	Convective precipitation rate (kg/m**2/s)
48	GFLUX	Ground heat flux (W/m**2)
49	LAND	Land-sea mask (1=land; 0=sea) (integer)
50	ICEC	Ice concentration (ice=1; no ice=0) (1/0)
51	UGRDhag	u wind at 10m (m/s)
52	VGRDhag	v wind at 10m (m/s)
53	TMPhag	Temperature at 2m (K)
54	SPFHhag	Specific humidity at 2m (kg/kg)
55	TMAX	Maximum temperature at 2m (K)
56	TMIN	Minimum temperature at 2m (K)
57	RUNOF	Runoff (kg/m**2)
58	PEVPR	Potential evaporation rate (w/m**2)
59	UGWD	Zonal gravity wave stress (N/m**2)
60	VGWD	Meridional gravity wave stress (N/m**2)
61	HPBL	PBL height (m)
62	SRWEQ	Snowfall rate water equivalent (kg/m**2/s)

Table 12. (continued)

63	SNOEV	Snow sublimation heat flux (W/m**2)
64	SNOHF	Snow melt heat flux (W/m**2)
65	QUFLX	Column integrated moisture u-flux (m/s)
66	QVFLX	Column integrated moisture v-flux (m/s)
67	CWAT	Plant canopy surface water (kg/m**2)
68	DSWRFtoa	Toa Downward solar radiation flux (W/m**2)
69	TCDCclm	Total cloud cover (percent)
70	ALBDO	Albedo (percent)
71	SFCR	Surface roughness (m)
72	VGTYP	Vegetation type (nondim)
73	VEG	Vegetation cover (percent)
74	SLTY	Soil type (nondim)
75	ALHTF	Alternate latent hflux (W/m**2)
76	ECPY	Canopy evaporation (w/m**2)
77	BGRUN	Baseflow-groundwater runoff (kg/m**2)

Table 13. Data volumes for various types of outputs

Types of data	Data volume
57-year hourly data	5 TB
1-year hourly data	86 GB
57-year daily data	250 GB
57-year daily one variable	1.3 GB
Monthly averages	8 GB
Monthly hourly averages	220 GB

8.0 References

Alpert, J. C., M. Kanamitsu, P. M. Caplan, J. G. Sela, G. H. White, and E. Kalnay, 1988: Mountain induced gravity wave drag parameterization in the NMC medium-range model. Preprints of the Eighth Conference on Numerical Weather Prediction, Baltimore, MD, American Meteorological Society, 726–733.

Archer, C. L., and M. Z. Jacobson, 2003: "Spatial and temporal distributions of U.S. winds and wind power at 80m derived from measurements." *J. Geophy. Res.* **108**, 4289, doi:10.1029/2002JD002076.

Breaker, L. C., W. H. Gemmil, and D. S. Crosby, 1994: "The Application of a Technique for Vector Correlation to problems in Meteorology and Oceanography." *J. Appl. Met.* **33**, 1354–1365.

Chen, F. and coauthors, 1996: "Modeling of land surface evaporation by four schemes and comparison with FIFE observations." *J. Geophy. Res.* **101**, 7251–7268

———, and J. Dudhia 2001a: "Coupling an advanced land-surface hydrology model with the Penn States/NCAR MM5 modeling system. Part I: Model implementation and sensitivity." *Mon. Wea. Rev.* **129**, 569–585.

———, and ——— 2001b: "Coupling an advanced land-surface hydrology model with the Penn States/NCAR MM5 modeling system. Part II: Preliminary model validation." *Mon. Wea. Rev.* **129**, 587–604.

Chou, M.-D., and M. J. Suarez, 1994: *An efficient thermal infrared radiation parameterization for use in General Circulation Models.* Technical Report Series on Global Modeling and Data Assimilation, National Aeronautical and Space Administration/TM-1994-104606, 3, 85 pp.

———, and K.-T. Lee, 1996: "Parameterizations for the absorption of solar radiation by water vapor and ozone." *J. Atmos. Sci.* **53**, 1203–1208.

Daly, C., R. P. Neilson, and D. L. Philps, 1994: "A statisticaltopographic model for mapping climatological precipitation over mountainous terrain." *J. Appl. Meteor.* **33**,140–158.

———, Taylor, G. H., W. P. Gibson, T. W. Parzybok, G. L. Johnsonn, and P. Pasteris, 2001: "High-quality spatial climate data sets for the United States and beyond." *Transactions of the American Society of Agricultural Engineers* **43**, 1957–1962.

———, Gibson, W. P., G. H. Taylor, G. L. Johnson, and P. Pasteris, 2002. "A knowledge-based approach to the statistical mapping of climate." *Climate Research* **22**, 99–113.

Fiorino, M., 2004: A Multi-decadal Daily Sea Surface Temperature and Sea Ice Concentration Data Set for the ERA-40 Reanalysis. ERA-40 project Report Series. ECMWF, Shinfield Park, Reading, RG2 9AX, UK. 16pp.

Higgins, R. W., W. Shi, E. Yarosh, and R. Joyce, 2000: Improved United States precipitation Quality control system and analysis. NCEP/Climate Prediction Center Atlas No. 7, U.S. Department of Commerce. [Available at: http://www.cpc.mcep.npoaa.gov/research_papers/ncep_cpc_atlas/7/index.html]

Hong, S.-Y., and H.-L. Pan, 1996: "Nonlocal Boundary Layer Vertical Diffusion in a Medium-Range Forecast Model." *Mon. Wea. Rev.* **124**, 2322–2339.

Juang, H.-M., and M. Kanamitsu, 1994: "The NMC nested regional spectral model." *Mon. Wea. Rev*. **122**, 3–26.

Kalnay, E., and coauthors, 1996: "The NCEP/NCAR 40-year reanalysis project." *Bull. Amer. Met. Soc.* **77**, 437–471.

Kanamaru, H., and M. Kanamitsu, 2006: "Scale Selective Bias Correction in a Downscaling of Global Analysis Using a Regional Model." Accepted for publication in *Monthly Weather Review.*

Kanamitsu, M. and K. Mo, 2003: "Dynamical Effect of Land Surface Processes on Summer precipitation over the Southwestern United States." *J. Climate* 16, 496–509.

———, H. Kanamaru, Y. Cui, and H. Juang. 2005: *Parallel Implementation of the Regional Spectral Atmospheric Model.* CEC-500-2005-014. Available from www.energy.ca.gov/2005publications/CEC-500-2005-014/CEC-500-2005-014.PDF.

Keely, J. E., C. J. Fotheringham, and M. Moritz, 2004: "Lessons from the October 2003. Wildfires in Southern California." *Journal of Forestry* **102**, 26–31.

Koepke, P., M. Hess, I. Schult, and E. P. Shettle, 1997: *Global aerosol data set.* MPI Meteorologie Hamburg Report No. 243, 44 pp.

Mass, C. F., and M. D. Albright, 1989: "Origin of the Catalina Eddy," *Mon. Wea. Rev.* **117**, 2406–2436.

Mesinger, F., G. DiMego, E. Kalnay, K. Mitchell, P. C. Shafran, W. Ebisuzaki, D. Jovic, J. Woollen, E. Rogers, E. H. Berbery, M. B. Ek, Y. Fan, R. Grumbine, W. Higgins, H. Li, Y. Lin, G. Manikin, D. Parrish, and W. Shi, 2006: North American Regional Reanalysis. Submitted to *Bull. Amer. Met. Soc.*

Moorthi, S., and M. J. Suarez, 1992: "Relaxed Arakawa-Schubert: A parameterization of moist convection for general circulation models." *Mon. Wea. Rev.* **120**, 978–1002.

Mo, K. C., M. Chelliah, M. L. Carrera, R. W. Higgins, and W. Ebisuzaki, 2005: "Atmospheric Moisture Transport over the United States and Mexico as Evaluated in the NCEP Regional Reanalysis." *J. Hydromet.* **6**, 710–728.

Nuss, W. A., J,. M. Bane, W. T. Thompson, T. Holt, C. E. Dorman, F. M. Ralph, R. Rotunno, J. B. Klemp, W. C. Skamarock, R. M. Jackson. A. M. Rogerson, C. Reason, and P. Jackson, 2000: "Coastally Trapped Wind Reversals: Progress Toward Understanding." *Bull. Amer. Met. Soc.* 81, 719–743.

Orszag, S. A., 1970: "Transform method for calculation of vector coupled sums: Application to the spectral form of the vorticity equation." *J. Atmos. Sci*. **27**, 890–895.

Pan, H.-L., and L. Mahrt, 1987: "Interaction between soil hydrology and boundary layer developments." *Boundary Layer Meteor.* **38**, 185–202.

Qian, J.-H., A. Seth, and S. Zebiak, 2003: "Reinitialized versus Continuous Simulations for Regional Climate Downscaling." *Mon. Wea. Rev.* **131**, 2857–2874.

Ralph, F. M., P. J. Neiman, P. O. G. Persson, J. M. Bane, M. L. Cancillo, J. M. Wilczak, and W. Nuss. 2000: "Kelvin Waves and Internal Bores in the Marine Boundary Layer Inversion and Their Relationship to Coastally Trapped Wind Reversals." *Mon. Wea. Rev.* **128**, 283–300.

Roads, J. O., S.-C. Chen, and M. Kanamitsu, 2003: U.S. regional cliate simulations and seasonal forecasts. *J. Geophys. Res*. **108**, 8606, doi10.1029/2002JD002232.

Robertson, A. W., U. Lall, S. E. Zebiak, and L. Goddard. 2004: "Improved Combination of Multiple Atmospheric GCM Ensembles for Seasonal Prediction." *Mon. Wea. Rev.* **132,** 2732–2744.

Schaefer, J. T., 1990: "The critical success index as an indicator of warning skill." *Wea. Forecasting* 5, 570–575.

Slingo, J. M., 1987: "The development and verification of a cloud prediction model for the ECMWF model." *Quart. J. Roy. Meteor. Soc*. **113**, 899–927.

Taylor, K. E., D. Williamson, and F. Zwiers, 2000: The sea surface temperature and sea-ice concentration boundary conditions of AMIP II simulations. PCMDI report #60, 20pp.

Tiedtke, M., 1983: The sensitivity of the time-mean large-scale flow to cumulus convection in the ECMWF model. Proceedings of the ECMWF Workshop on Convection in Large-Scale Models, 28 November–1 December 1983, European Centre for Medium-Range Weather Forecasts, Reading, England, 297–316.

von Storch, H., H. Langenberg, and F. Feser, 2000: "A spectral nudging technique for dynamical downscaling purposes." *Mon. Wea. Rev.* **128**, 3664–3673.

Wakimoto, R. M., 1987: "The Catalina Eddy and its Effect on Pollution over Southern California." *Mon. Wea. Rev.* **115**, 837–855.

Williamson, D. L., 2002: "Time-Split versus Process-Split Coupling of Parameterizations and Dynamical Core." *Mon. Wea. Rev.* **130**, 2024–2041.